Deterioration and conservation of rock-hewn sandstone cave-temples in Longdong area, China

Yinghong Wang

School of Geography and the Environment
St Hilda's College
University of Oxford

Submitted for the degree of *Doctor of Philosophy*

In Science and Engineering in Arts, Heritage and Archaeology

2021

ABSTRACT

Cave-temples are multivalent types of immovable cultural heritage which link spiritual values as places for Buddhism rituals, aesthetic values because of the Buddha sculptures, inscriptions and murals they contain, historic values as significant objective evidence of the history of the eastward spread of Buddhism, as well as economic values as tourist attractions. It is, therefore, highly necessary to preserve them in a sustainable manner and pass them on to the next generation.

The Longdong area refers to the area to the east of the Long mountains, i.e. the southern section of the Liupanshan mountain chain, in Gansu Province, China. This region was also the eastern section of the Silk Road connecting the Central Plain in China to western countries. A great number of cave-temples are hewn from outcrops of the widespread sedimentary sandstone units in the region and face severe deterioration problems endangering their values and integrity. Thus, study regarding deterioration process is required in order to understand the impacts of these deterioration risks.

Accordingly, the research presented in this thesis focuses on studying and evaluating the rock deterioration and its impacts aiming to clarify the major weathering mechanisms of these cave-temples. The North Grotto Temple (NGT), situated near Qingyang, is the oldest site representing the highest artistic value of grotto art in the Longdong area, hence, was selected as the study site. The overall research comprised three phases. The first phase involved field investigation and survey of weathering features; the second phase focused on in situ detection, modelling prediction and laboratory characterization of deteriorating salts, and the third phase comprised laboratory simulation of salt weathering at North Grotto Temple and how it affects the rock properties. A range of portable non-destructive devices (including Karsten tube and surface hardness tester (Proceq Equotip® 3 and 550), ultrasonic instrument (Proceq PunditLab) were used in the research, along with a non-invasive method of sampling salts (fiber paper pulp poultices), a range of laboratory analysis and experimental methods (including ion

chromatography and environment cabinet) and modelling software (thermodynamic model - ECOS-RUNSALT).

According to the research, several deterioration patterns, such as granular disintegration, efflorescence, alveolar, were identified on the NGT sandstone façade, which illustrate that salt weathering is probably the leading weathering agent at the site. A mixture of salts was predicted to form in the site, i.e. aphthitalite, bloedite, picromerite, darapskite, mirabilite, hexahydrite, starkeyite, nitromagnesite, halite, niter, and sylvite. Large diurnal variation of humidity in the site enhances the likelihood of salt weathering. Laboratory simulation showed experimentally that the salt mixtures can cause material loss, appearance changes and modify the petrophysical properties of sandstones, which badly affects the integrity of rock.

In sum, this study illustrates that the sandstone cave-temples in the Longdong area are under cumulative damage from salt weathering. Environmental control is a necessary measure in order to manage the risks threatening the on-going preservation of the sandstone cave-temples.

ACKNOWLEGEMENTS

First and foremost, I would like to express my heartiest gratitude to my supervisor, Professor Heather Viles for her insightful guidance and considerable encouragement to complete my doctoral research. She always inspires me in exploring more aspects of possibilities and teaches me how to do good science and be a real researcher.

I would also like to give my deepest appreciation to Dunhuang Research Academy (DRA) for their friendly and supportive assistance during the fieldwork and laboratory work. Thanks to Professor Qinglin Guo, Dr Shanlong Yang, and Dr Zongren Yu, for their kindness help in the arrangement of on-site work and utilization of equipment in the DRA lab. And a special thanks to Mrs Huiping Cui, Mrs Wenhuan Guo, and Mr Zengyang Han for their enthusiastic help in the fieldwork in the North Grotto Temple.

I would like to acknowledge the financial support from the Engineering and Physical Research Council Doctoral Training Centre for Science and Engineering in Art Heritage and Archaeology (SEAHA).

My earnest thanks to Mrs Hong Zhang and Dr Mona Edwards for providing technical support during my laboratory work in the Oxford Resilient Building and Landscape Lab (OxRBL).

Last but not least, the utmost gratitude and appreciation to my parents for their understanding and unreserved support.

TABLE OF CONTENTS

LIST OF FIGURES

LIST OF TABLES

1. BACKGROUND

1.1. What are rock-hewn cave-temples and their history in China?

Cave-temples, also called grottoes, are one kind of architecture hewn from rock cliffs in a way that imitates the form of ordinary temples on the ground (Li, 1997). They are used for carrying out a series of Buddhism practices, e.g. meditation and Buddhism rituals (Sun, 2015). They normally comprise rock/clay Buddha sculptures of various sizes, content-rich murals and rock structures, like rock pillars and ceilings. This special form of architecture left invaluable historical materials for studying the introduction and development of Buddhism in China, and is an important element of the cultural heritage along the Silk Road.

Cave-temples originate from ancient India. The earliest construction of cave-temples was approved by the emperor of the Maurya Dynasty, Ashoka the Great (c. 268 to 232 BCE) (Li, 1997). With the prevalence of Buddhism in India, the number of cave temples increased rapidly during ancient times. From previous research, it is known that 1,200 cave-temples were hewn in northern India between 2nd century BCE and 9th century CE (Sun, 2015).

The popularity of Cave-temples in ancient China was a consequential 'product' of the eastward spread of Buddhism (Liu, 1993). According to archaeological findings, Buddhism appeared in China in the first half of the 2nd

century CE. It was the heyday of the ancient powerful empire, Kushan Empire, whose territory spread to encompass the most part of central Asia and South Asia (Wu, 1985). Monks and merchants from this empire travelled together along the Silk Road and entered what is today known as Xinjiang, China via Kashmir to spread Buddhism (Sun, 2015). The oldest cave-temple in China, Kizil cave, is found in Baicheng county, Xinjiang. The earliest construction date of the cave was detected as 310 ± 80 CE based upon ^{14}C dating of branches and wheat straw discovered in gouges and rock walls in the cave (Su, 2019). The inscription found at the site shows that the Kizil cave was probably abandoned in the 8th century CE due to wars occurring in that area (Zhao, 2001). Together, the many rock-hewn cave-temples in China form a significant physical record which documents the history of the spread of Buddhism.

The 5th century CE to 6th century CE is the period in which the construction of rock-hewn temples flourished in China. During this period, a great number of cave-temples of various scales emerged in Gansu Province, Ningxia Hui Autonomous Region, Shaanxi Province, Shanxi Province, Henan Province, Shandong Province, and Inner Mongolia Autonomous Region which are the core regions of the northern area of Central Plain of China (Su, 2019). For example, the five famous UNESCO World Heritage sites, namely Mogao Caves, Maijishan Cave-temple Complex, Bingling Cave-Temple Complex, Yungang Grottoes, and Longmen Grottoes were all initially hewn and constructed during this period (see Figure 1.1). This demonstrates the successful development and rise of Buddhism in China at that time, boosting

Figure 1.1. Map of Chinese cave-temples listed in UNESCO World Heritage Sites

the number of believers including the emperors of the Northern Wei which was the dynasty that ruled northern China during 386-534 CE. And conversely, Buddhism received not only spiritual support but also a huge amount of material support from the monarch, resulting in the rapid ramp-up of the number of the tangible symbols of Buddhism, cave-temples. Some emperors, like Emperor Wencheng, used the religion as a political tool to strengthen his authority and to establish the legitimacy of governance (Su, 1978).

The gradual localization and sinicization is a notable feature in Buddhism's development and evolution in China. The cave-temples provide direct evidence of this evolution. For instance, increasing number of cave ceilings imitating the shape and structure of ancient Chinese timber palaces

appeared in the 6th century CE cave-temples, and constructing a timber pavilion connecting to the façade of cave-temples was very popular in the period of the 9th-10th century CE (Su, 2019), which reflects the influence of ancient Chinese architectural styles on the grottoes. Furthermore, the integration within Buddhism of Chinese native religion and philosophy is perfectly reflected through cave-temples. Caves which embrace Confucianism, Taoism and Buddhism were discovered amongst those hewn in the 11th century CE (Guo, 1989).

According to the result of the Third National General Investigation of Cultural Heritage (2007-2011), there are 24,422 cave-temples and rock inscriptions in China, accounting for 18.45% of the total number of Chinese immovable cultural relics (Chen, 2012). They were constructed during nearly all feudal dynasties in Chinese history. Generally speaking, cave-temples occupy a significant and valuable position both in Chinese cultural heritage categories and world cultural heritage due to their grand scale, widespread distribution, and their complete demonstration of the evolution route of a foreign religion in China (Zhang, 2019).

1.2. What are the major problems affecting the preservation of cave-temples in China?

The problems that cave-temples encounter primarily include the following aspects:

a. The structural instability of the rock mass of cave-temples, i.e. the instability of caves and the whole rock cliff,

b. The decay of the historical remains in caves, e.g. murals and statues,

c. Weathering and breakdown of the rock mass including the facades,

d. Impact of human activities, e.g. tourism and conservation practices.

Cave-temples are hewn from rock cliffs. The stability of rock strata within the cliffs determines the stability of the cave-temples. As bedrock outcrops, those cliffs constantly evolve and are shaped by contact with the Earth's atmosphere, water, and organisms. In addition, construction of cave-temples involves carving of the caves themselves, as well as crafting murals and statues, all of which necessarily break the original supporting relationships between the strata. Readjustments in physical and mechanical properties of the rock in order to restore the equilibrium will occur, which may lead to the development of secondary fissures in the interior of the rock, the dislocation of rock formations and other phenomena damaging the integrity of the rock. When the adjustment exceeds the threshold of the failure tolerance of the rock or where there are strong external forces involved, such as earthquake, heavy precipitation, etc., the unstable rock can easily fail and collapse, which is catastrophic to cave-temples. This was the most urgent issue confronted by almost every Chinese cave-temple between 1960s and 1980s when modern conservation work began. Filling fissures, cracks and holes with a mixture of lime and local earth, laying supporting brick walls and columns, pouring

reinforced concrete support beams, dredging earth from caves, digging drainage ditches, as well as installing waterproof sheets were the common measures applied in cave-temples. These measures effectively temporarily stabilized dilapidated cave-temples (North Grotto Temple Conservation Institute, 2016). An engineering geological measure, anchor reinforcement, was introduced into several grotto conservation projects in the late 1980s in an attempt to solve the instability problem of the rock mass and appears to have been successful. The reinforcement and conservation project carried out in Maijishan Grottoes is the largest and longest project in China. The method called 'reinforcing bar netted chock and netted-shell bolting and shotcrete support' was applied between 1977 and 1984, in which shotcrete was applied on the area of 9,100 square meters, 2,300 anchor rods were installed with a total length of 12,500 meters, moreover, a new steel-concrete 1000-meter half-hanging walkway was erected surround the mountain (Zhang, 2019).

Murals and Buddha sculptures are important elements of cave-temples which have considerable heritage significance in spite of being forgotten and abandoned for a long period of time until re-discovered and re-treasured in the first decades of the 20th century CE. They are not well-preserved due to the long-term erosive impact of weathering agents, such as water and soluble salts. Deterioration patterns, like crusting, discoloration, flaking etc., are found both in pigmented layers and supporting layers (soil & plant fibre layers under the paint) of the murals (Li, 2010). Crumbling, exfoliation, pitting, cracking etc. aggressively appear on the surface of rock Buddha sculptures (Huang, 1984).

Chemical agents are commonly used to clear and restore decayed murals and sculptures, but with very limited choices because of the cautious attitude toward the usage of chemicals in heritage conservation practice. Currently, polyvinyl alcohol and polyvinyl acetate are two safe and efficient chemicals frequently applied to murals. Epoxy resin was popular in the restoration of rock sculptures and structures, but become unwelcome in recent years as it can be easily discoloured and cause secondary damage to the stone. To enlarge the categories of the materials that can serve cultural heritage conservation and comply with the conservation principles, studies on consolidation materials selection are being carried out in many Chinese universities and research institutes, like Zhejiang University and Dunhuang Academy (Wang X. *et al.,* 2005).

The issues in terms of rock mass instability and deterioration of statues and murals discussed above were the primary problems on which most attention was focused in the early period of cave-temple conservation. They have been largely solved through overcoming key technical challenges. Consequently, the integrity of cave-temples is very well maintained. The accomplishment of relevant conservation work rescued a lot of dilapidated cave-temples and helped the five well-known grottoes, mentioned in section 1.1, to be successfully registered in the UNESCO World Heritage Sites list.

Over the last 30 years, weathering of the rock mass and facades of cave-temples has taken the place of rock mass instability and deterioration of

statues and murals as the major threat to the preservation of cave-temples. The various weathering patterns that are widespread on the rock mass of cave-temples remind us that weathering has been occurring and endangering cave-temples from the start of their history (Duan, 1985, Fu and Li, 1992, Jiang and Feng, 1993, Cui, 2012, Sun, 2019). Less attention has been paid to these phenomena because of the necessary focus on structural integrity and conservation of murals and Buddha sculptures, resulting in vague and imprecise understandings regarding the impact of weathering on the deterioration of cave-temples. The lack of relevant knowledge and understanding, therefore, constrains the design and formulation of scientific conservation strategies. As a result, it is necessary and timely to conduct more in-depth research in this field (Wang and Chen, 2018).

Impacts of human activities derived from tourism and incorrect conservation practice are other unignorable issues affecting the preservation of cave-temples. Cultural heritage conservation aims to preserve values in a sustainable way and pass them on to future generations (Heritage Conservation Defined). Thus, appropriate display is an important function of cultural relics. Public engagement, e.g. visiting the heritage site, is the most common and essential way to share the value of cultural relics. The ability to visit a site cannot be underestimated as a way of improving the public's understanding of local history and culture, but at the same time, it must be noted that the rise in the number of tourists will also bring hidden dangers to the preservation of cave-temples. For instance, the increase in the number of

tourists causes increases in temperature and CO_2 concentrations in caves, accordingly promoting the growth of fungi in Mogao caves (Ma, 2011). Additionally, visitors walking within rock-hewn caves can trigger the resonance of rock mass and initiate the development of cracks and fissures on the fragile parts of murals (Du *et al.,* 2017). These problems which have arisen with the development of the tourism industry should attract more attention from management authorities and academia. In terms of conservation works, decades of experience of conservation practices and researches have revealed that there is insufficient knowledge of the long-term behaviour of the ancient materials that constitute cultural heritage and the new materials that are used in conservation treatment (Cassar *et al.,* 2001). Different changes or degradation may occur on the 'intrinsic' materials and the materials used to treat them under the complex effects of weathering agents, causing potent secondary damage.

1.3. Multi-disciplinary participation in the studies of cave-temples conservation

Multidisciplinary involvement is a remarkable feature of the conservation of cave-temples in China within the past 50 years. Disciplines including materials science, both polymers and inorganic composites, geology, geophysics, engineering geology, computer science, etc. have contributed to solving problems and rescuing cave-temples.

Completed research projects involving materials science include:

1) Application of the grouting material, methyl methacrylate, for rock surface sealing and conservation (Yuan *et al.,* 2007). This project was carried out in No.1 cave and No. 2 cave of the Yungang Grottoes, through the joint participation of the Chinese Academy of Cultural Heritage, formerly known as the Institute of Ancient Architecture Maintenance, and the Institute of Chemistry of the Chinese Academy of Sciences in the early 1960s.

2) Application of polyacrylates and epoxy resins to consolidating and grouting fissures in cave-temples (Li, 1966). This project was cooperatively carried out on the rock in Yungang Grottoes, Longmen Grottoes, and Mogao caves by the same research institutes involved in project 1) and Sichuan Provincial Museum between 1961 and 1966,

3) The preliminary trial of high-modulus potassium silicate materials (PS) on rock to evaluate its efficacy as a consolidant. This trial was carried out on sandstone cube samples in the lab, and simultaneously, on 20 sandstone sculptures in the North Grottoes Temple, Gansu Province, China (Li, 1985, Li and Wang, 2005).

4) Study of hydraulic lime composite materials to be used for cave-temple consolidation, carried out by the Chinese Academy of Cultural Heritage between 2004 to 2014 (Li and Zhao, 2014);

The polymer materials used in the first two studies are particularly popular in conservation and restoration practice in the Chinese cave-temples, because

they are user-friendly, and multi-purpose, so can be used for both anchor grouting and rock consolidation. Moving into the 21st century, conservators have become very cautious in treating historic objects with new materials due to the consensus of the significance of retaining the authenticity and integrity of the historic remains undergoing conservation (ICOMOS-China, 2005). Experience has also indicated that local climatic conditions have a great influence on the effectiveness of those materials，for instance, the efficacy of PS is reduced in humid environments (Zhang *et al.,* 2010).

In terms of geoscience, research has focused since the 1960s on condition survey, investigations of the causes of fissures and their development, and water seepage treatment. The Chinese Academy of Cultural Heritage and the China University of Geosciences (Beijing) have been engaged in this research.

Furthermore, researchers at Dunhuang Academy carried out research on the treatment of the hazards of wind-blown sand at Mogao caves between 1989 and 1999 (Zhang *et al.,* 2000). Techniques of geophysical exploration have also been applied to the study of internal conditions within the rock mass of caves (Zhang and Huang, 2004).

Since 1990s, digital technology has been applied to the restoration of grotto murals, involving the storage and reproduction of information about historic objects. For example, a research group from Zhejiang University,

China successfully developed the ‘Dunhuang Mogao Caves Virtual Tour System’, ‘Dunhuang Mural Auxiliary duplication and Restoration System’, ‘Computer Aided Grottoes Conservation and Restoration System’, and ‘Dunhuang Style Pattern Creation and Display System’ (Pan and Lu, 2003).

1.4. Sustainable conservation and risk management of cultural heritage

Sustainable development is a well-acknowledged goal in today's economic and social context. It was initially raised in the report of the World Commission on Environment and Development 1987, also known as the Brundtland Report, and defined as an approach that '*meets the needs of the present without compromising the ability of future generations to meet their own needs*’ (WCED, 1987, p. 16).

The concept of sustainability has been deployed by the cultural heritage sector and recognized as one of the fundamental principles for cultural heritage conservation, alongside authenticity and integrity (ICOMOS-China, 2005). It indicates the desire for long-term preservation of cultural heritage as well as the intention of minimizing intervention to the original materials and fabric of historic objects amid restoration and conservation (Stubbs, 2004).

To realize this vision of attaining the maximum extent of conservation and protection of cultural heritage with the least intervention on the historic objects themselves, preventive conservation is a feasible 'breakthrough point' when formulating conservation scheme. This notion of cultural heritage conservation

not only ensures that historic objects are preserved as authentically as possible (Wirilander, 2012), but also integrates the protection of that heritage into a comprehensive planning programme of the local region (UNESCO, 1972).

Risk management is a practical and powerful way of supporting conservation practices, especially for immovable cultural heritage like cave-temples whose conditions are largely affected by the surrounding environment.

The Canadian Conservation Institute (CCI) and the International Centre for the Study of the Preservation and Restoration of Cultural Property (ICCROM) jointly published a guide to risk management of cultural heritage

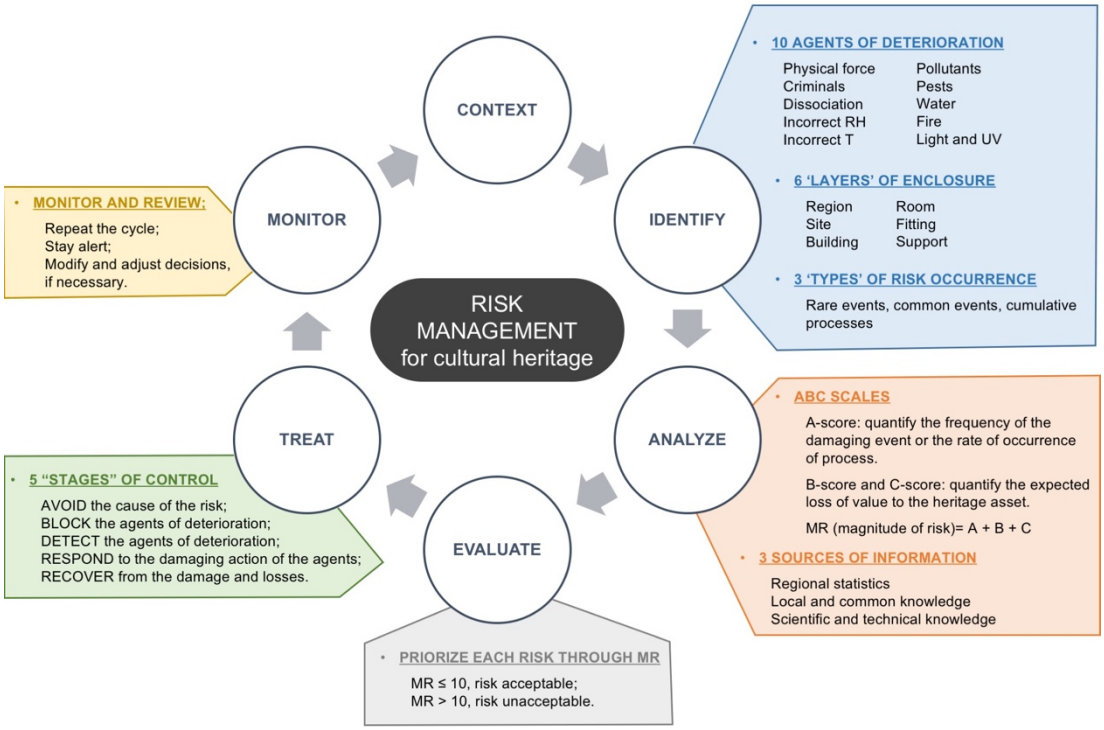

Figure 1.2. The guide to risk management of cultural heritage
Note: information summarized from CCI and ICCROM (2016)

(CCI and ICCROM, 2016) based on the international standard guideline of risk management to all industries and sectors (ISO 31000:2009). This guide to risk management of cultural heritage includes 6 steps, i.e. context, identify, analyse, evaluate, treat and monitor, which constitutes a cycle which is applied repeatedly (see Figure 1.2). Managers and stakeholders of a heritage site can be clearly instructed by the guide to identify deterioration agents and risks in accordance with the given categories. Subsequently, they can give a score to each identified risk followed the 'ABC SCALES' (see Figure 1.2), and then prioritize the risks based upon their scores. The magnitude of the score represents the acceptability of each risk and is the important parameter to make the decision of what kind of treatments can be applied to the site.

This is an efficient means to manage risks threatening the preservation of a cultural heritage site. The most difficult part is the scoring process in the 'ANALYZE' step for each risk because it requires substantial knowledge to quantify the frequency of damaging events or the rate of occurrence of deterioration processes as well as to quantify the potential loss of values of the heritage assets.

Two other assessments, therefore, need to be accomplished prior to conducting the risk management process. One is the so-called 'Heritage Impact Assessment (HIA)' process which estimates the impact of potential development on the Outstanding Universal Value (OUV) of heritage assets (ICOMOS, 2011). The other one is a risk impact assessment which is

significant to understand the influences of risks/deterioration agents on the heritage assets (Atakul *et al.,* 2014.). These assessment processes require a wide variety of knowledge e.g. scientific and technological knowledge from multiple disciplines.

The preservation of cultural heritage is threatened by 3 types of risk events, i.e. rare events/ catastrophic events (such as damaging earthquakes, floods etc.), common events (for instance seepage, handling 'accidents', etc.), and cumulative processes (for example decay of the materials of historic objects, see Figure 1.3). Cave temples, as an example of immovable cultural heritage, are 'embedded' in the surrounding landscapes, and are particularly susceptible to the ambient environment and so can suffer loss of values through rock breakdown due to cumulative rock weathering processes. Scientific research to understand the deterioration mechanism of cave temples can provide reliable knowledge for heritage site stakeholders, and underpin rigorous decision-making process for heritage conservation.

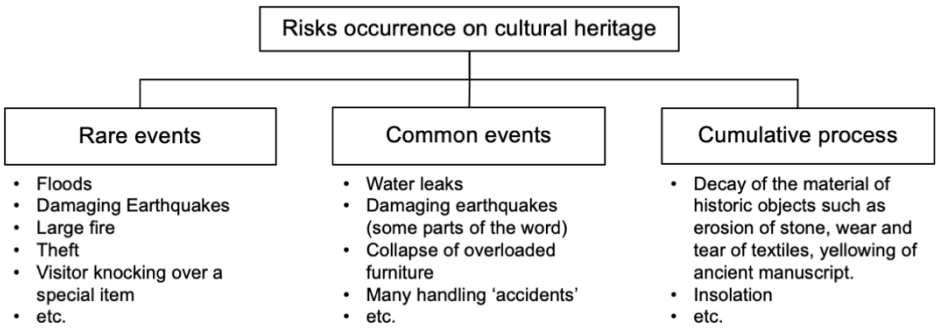

Figure 1.3. Three types risks occurrence on cultural heritage (CCI and ICCROM, 2016)

1.5. Thesis structure and acknowledgement of the SEAHA CDT

The thesis is a hybrid – following a conventional chapter structure but containing 3 scientific papers submitted to peer-reviewed international journals/ conference proceedings.

Chapter 1 introduces the background information regarding history, problems and previous conservation projects of cave-temples in the Longdong area, China. Chapter 2 reviews research on sandstone weathering, geological background to the Longdong area, threats of salt weathering on sandstone cave-temples, and introduces the aims and objectives of the research. Chapter 3 introduces the methodology applied in the three phases in the research.

Chapters 4, chapter 5, and chapter 6 are the paper chapters which jointly explore the main aims of the thesis through respectively addressing the three sub-objectives. Chapter 4 addresses the research question, 'What is the current state of deterioration of the North Grotto Temple, Qingyang, Gansu Province, China?'. Chapter 5 addresses the research question, 'What role do soluble salts play in the deterioration of the North Grotto Temple, Qingyang, Gansu Province, China?' Chapter 6 addresses the research question, 'How do the identified soluble salts affect the deterioration of sandstone under the climate of Longdong area (humid temperate climate)?''

Chapter 7 synthesizes the important findings from chapter 4,5 and 6 and provides a broad discusses of the impact of risks of deterioration and implications of the research for the conservation of cave-temples in the Longdong area.

This research project was carried out as part of the Science and Engineering in Arts, Heritage and Archaeology Centre for Doctoral Training (SEAHA CDT) and received support from the SEAHA CDT Research Training Support Grant (RTSG). SEAHA is an EPSRC funded Centre for Doctoral Training (CDT) which trains doctoral students in cross disciplinary heritage science research. SEAHA CDT students come from diverse disciplinary backgrounds such as physics, chemistry, geography, heritage science. and apply knowledge obtained from their respective discipline to heritage-related studies. They receive support from academic, industrial and heritage supervisors. This research project involved a collaboration with the Dunhuang Research Academy (DRA). DRA is a state-established institute responsible for the conservation, management, and research of the Dunhuang Mogao Grottoes, a World Heritage Site in Gansu province, China.

2. LITERATURE REVIEW

2.1. Sandstone weathering

Sandstone is an important rock type which covers a large proportion of the Earth's surface (Meybeck, 1987). It is found widely across mainland China and forms several sandstone basins, such as the Sichuan basin in southwestern China, and Ordos basin in Northwestern China (Li and Wang, 2002) as well as typical sandstone landscapes, like the Danxia landscape that composes of the late Mesozoic continental red sandstones (Guo *et al.,* 2018)

The principal components of sandstone are quartz, feldspar, and monomineralic or polymineralic rock or lithic fragments and because of this, sandstones can be classified by a ternary composition diagram (see Figure 2.1a).

A great number of Chinese cave-temples and grottoes are hewn from sandstone outcrops, including many World Heritage Sites, such as Yungang Grottoes and Bingling Temple Grottoes both situated in Northern China (see Table 2.1). Studies show that the sandstones in Yungang Grottoes and Bingling Temple Grottoes are quartzo-lithic sandstone (see Figure 2.1b). And the mineralogical composition of the sandstone from North Grottoes Temple situated in NW China (see Table 2.1) demonstrates that it is litho-quartzose sandstone.

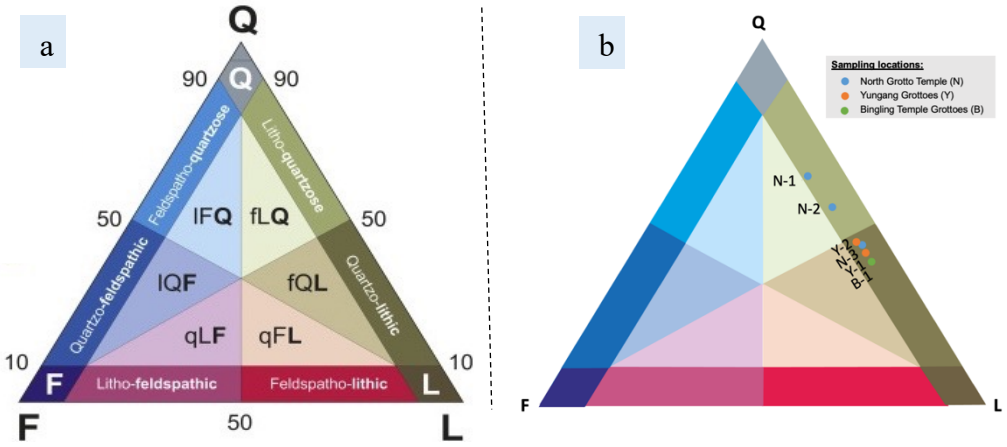

Figure 2.1. a. The QFL triangular diagram for classification of sandstone (Garzanti 2019). Q=quartzose; F=feldspathic; L=lithic; iFQ=litho-feldspatho-quartzose; iQF=litho-quartzo-feldspathic; qLF=quartzo-litho-feldspathic; qFL=quartzo-feldspatho-lithic; fQL=feldspatho-quartzo-lithic; fLQ=feldspatho-litho-quartzose. b. the classification of some Chinese grotto sandstone specimens Note: data plotted in b were from the this DPhil research (North Grotto Temple sandstone) and literatures (Yungang Grottoes sandstone data cited from Salmon et al., 1995, Bingling Temple Grottoes sandstone data cited from Chen et al., 2019) .

Table 2.1 Mineralogical composition (%) of three group of sandstone specimens from Yungang Grottoes, Bingling Temple Grottoes and North Grottoes Temple (XRD data)

Sample No.	Quartz	K-feldspar	Plagioclase	Calcite	Aragonite	Dolomite	Anhydrite	Rutile	Muscovite
Y-1	53	40	0	0	n.a.	2	n.a.	n.a.	n.a.
Y-2	56	13	0	1	n.a.	n.a.	n.a.	n.a.	n.a.
B-1	50	25	0	25	n.a.	n.a.	n.a.	n.a.	n.a.
N-1	79	8	11	2	n.a.	n.a.	n.a.	n.a.	n.a.
N-2	68	16	8	5	n.a.	2	n.a.	n.a.	1
N-3	55	19	9		4	n.a.	10	3	

Note: Y-sandstone from Yungang Grottoes (Salmon et al., 1995), B-sandstone from Bingling Temple Grottoes (Chen et al., 2019), N- sandstone from North Grottoes Temple (from this Dphil research)

The term 'Weathering' generally refers to the breakdown and dissolution processes of rock driven by physical, chemical and biological weathering agents. Weathering of sandstone is an interactive process between weathering agents and sandstone, which significantly influences the appearance of rock and its subsurface condition through modification of the properties of sandstone, such as porosity, strength, phase of cements and

matrix, etc. Figure 2.2 illustrates the complex ways in which a range of weathering agents can modify the surface and subsurface characteristics of sandstone, in this case during the development of cavernous weathering features.

In some cases the net result of these weathering processes is to produce hardening of the surface due to deposition of allochthonous materials and/or growth of biological materials (Viles and Goudie, 2004, Turkington and Paradise, 2005,). More commonly however, weathering agents work together to create damage to sandstone, producing deterioration patterns like granular disintegration, salt efflorescence, cracking, flaking, scaling etc. (ICOMOS-ISCS 2018). Furthermore, in many cases sandstone grains become detached as a consequence of weathering, producing surface retreat.

Research carried out over a long period has shown that water/moisture is a significant influence in the sandstone weathering process (Bryan, 1928, Mustoe, 1983, Turkington and Paradise, 2005). Water can firstly, induce dissolution of acid airborne pollutants, e.g. SO_2 and NO_X, aiding the acid leaching of the sandstone surface and reacting with minerals (Gibeaux *et al.,* 2018). Secondly, water can cause damage by freeze-thaw weathering in cold conditions due to the volumetric expansion of the phase transformation from liquid water to ice (Matsuoka and Murton, 2008). Finally, water can trigger wetting-drying cycles in sandstone as a result of diurnal and other temperature variations which can cause swelling of clay minerals (Gonzalez and Scherer,

2004, Schaffer, 2016) and also drive the occurrence and development of salt weathering (Doehne, 2002).

Salt weathering is a geomorphic process resulting in the physical disintegration and decay of rocks or stones and has been found to be important in many different environments around the world (Yaalon, 1982, Goudie *et al.,* 1997). Various weathering forms are associated with salt weathering, including surface recession, basin erosion, and cavernous weathering features (also called tafoni, or honeycomb and alveolar weathering) (Turkington and Paradise, 2005). During salt weathering damage to rock and stone is largely caused by crystallization and hydration pressures produced by the growth of salt crystals (Steiger, 2005), and that growth is significantly dependent on local environmental conditions (Cooke and Smalley, 1968).

Insolation is another potential factor in sandstone weathering. The sun's energy heats exposed surfaces and can cause breakdown as a result of differential thermal expansion. The importance of this process depends on the range of minerals present in the stone, such as the content of smectite and phyllosilicates, besides, more importantly, the moisture content of the stone (Weiss *et al.,* 2004). This is particularly crucial for stone-built heritage because the different orientation of the faces of a structure cause uneven receipt of solar energy, producing 'hot spots' of weathering. For example, higher weathering rates were discovered on the southeast facing wall of the historic sandstone structure in the Alberuela Castle site, Spain (Sancho *et al.,* 2003).

Furthermore, similar to the function of water/moisture in the stone deterioration, insolation can facilitate other weathering processes, such as salt weathering.

Biological agents are usually recognised as a harmful factor in rock weathering and stone deterioration. The growth of organisms on the rock surface not only affects the appearance of the structure (Warscheid and Braams, 2000) but can also release corrosive acids which dissolve and etch the clay matrix producing subsequent weakening of the binding system (Huang and Keller, 1970, Manley and Evans, 1986). Furthermore, biodeterioration can exert stresses on the minerals constituting the rock because of the shrinking and swelling cycles of the colloidal biogenic slime inside the pores (Warscheid and Braams, 2000). However, researchers also propose a bioprotective role for some lithobionts (rock- dwelling organism), as they can produce umbrella-like protective effects which prevent contact between stone surfaces and weathering agents (Favero-Longo and Viles, 2020).

It is worth noting that sandstone weathering is typically driven by a synergistic association of weathering agents (as exemplified in Figure 2.2). Thus, understanding weathering in natural and building contexts is very complex. Weathering is an inevitable process involving the irreversible breakdown of rock, which, from a geomorphological perspective, plays a key role in shaping landscapes. However, weathering can also pose a fatal threat to the preservation of cave-temples as its occurrence can erase the values embodied in this kind of cultural heritage.

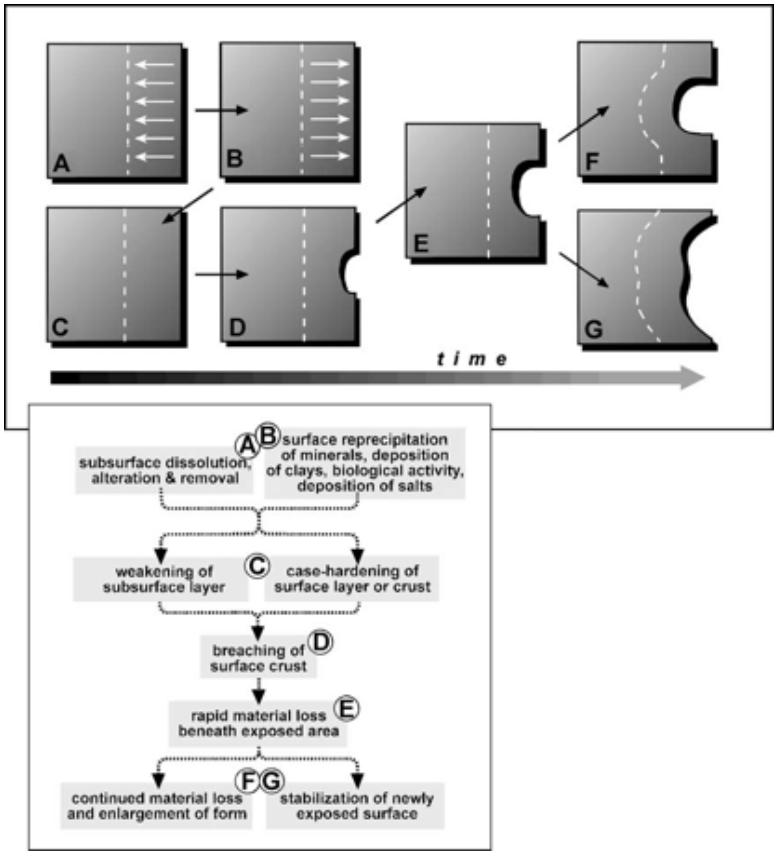

Figure 2.2. The process of cavernous weathering induced by complex weathering agents on modification of sandstone's surface (Turkington and Paradise, 2005)

2.2. Testing methods in built heritages research

To understand the nature of built heritage structures and their current conditions, 'diagnosis' and assessment is necessary and involves multiple techniques. With the development of science and technology in recent years, the test methods that can be applied to cultural heritage research are many and various. According to the degree of invasiveness of these detection technologies to the historic objects during the detection process, they can be roughly divided into two categories: non-destructive tests (NDT), and

destructive tests (DT) (Bosiljkov *et al.,* 2010). Through these detection methods a range of information on built heritage can be collected：1）physical properties of the materials composing the heritage object, e.g. porosity, water absorption coefficient, density, strength etc., 2) discontinuities, e.g. voids, fissures, small cracks etc., 3) stress and dynamic response, e.g. vibration and residual stress (Leucci, 2018).

NDT methods are useful to minimize the impact of the detection process on heritage objects, and can reflect the in situ properties. Such methods have become, therefore, extremely popular with heritage scientists and conservators in recent years. For example, high resolution Ground-Penetrating Radar (GPR) is commonly used in inspect infrastructures and buildings and has been employed by conservators and heritage scientist to map hidden voids and anomalies within built heritage (Lai *et al.,* 2018), and recently utilized to measure and monitor moisture in stone masonry (Orr *et al.,* 2019). However, GPR has its limitations for use in inspecting cave-temples because of the requirement of relatively flat and smooth examining surface for the high-resolution GPR measurement wheel. Many cave-temple surfaces are rough with irregular surface profiles which can be challenging for successful GPR measurements. Electrical Resistivity Tomography (ERT) is another powerful NDT tool for investigating capillary moisture movement (rising damp) in porous building materials through calculating the resistivity distribution between a suite of electrodes installed on the profile of a rock outcrop (Mol and

Viles, 2013, Ceniceros *et al.,* 2019), but similarly facing practical issues like weak contact between rough stone surface and electrodes. Importantly, for many built heritage applications the use of ERT is limited by the potential damage to the surface caused by the electrodes. Rebound hardness testers, such as the Proceq Equotip® hardness tester and the Schmidt Hammer have been widely applied in geomorphology and heritage science to surface hardness and rock strength (Fort *et al.,* 2010, Viles *et al.,* 2011, Wilhelm *et al.,* 2016). These are convenient devices to efficiently assess the surface condition, although the Schmidt Hammer with its high impact energy can cause damage to fragile built heritage surfaces. The Equotip has lower impact energy, and thus is more suitable for built heritage applications, but produces more variable data and thus requires larger datasets to be collected. Aoki and Matsukura (2008) created an approach to estimate unconfined compressive strength of intact rock through Equotip hardness readings, which extends the utility of the equipment for research on stone-built heritage.

DT methods are also very important for heritage conservation and research. For instance, the core drilling method has been used in a wide range of studies on built heritage. Researchers drill a small cylindrical rock core or dust core to detect its salt content and evaluate the extent of salt contamination in the interior of the bricks and stone (Wedekind and Ruedrich, 2006, Rothert *et al.,* 2007). Although DT methods are not widely accepted to be applied on built heritage due to the risk of destroying the original appearance and integrity, such methods can be used on heavily weathered built heritage so that the

researchers can accurately understand the degree of weathering and efficiently formulate rescuing treatment measures. In addition, scraping a certain amount of weathering products from the rock surface for characterization can be justified where it is required to understand the weathering conditions. For determination of the local magnitude of the compression and stress-strain behaviour of masonry, the so-called flat-jack tests can be used on stone built heritage. These can obtain value of compression of the masonry structure in the local situation, but cannot be applied in low rise buildings because of the lack of stress response in the upper storey derived from the low stresses acting on it (Binda *et al.,* 2003.).

Various testing techniques have helped to accumulate a rich amount of data from heritage sites, but, in the meantime, difficulty in data interpretation and comparison between data obtained from different sites and devices also appears, because of the nonuniformity of the rock outcrops in which the cave-temples are usually hewn from and complex interrelationships between climate and rock decay. In addition, almost all testing methods are originally designed and formulated for industrial fields, such as the metal manufacturing industry, with specific measuring standards for the related fields which are irrelevant to the heritage sector. It is, therefore, essential to carry out extra calibration trials under known conditions for the equipment prior operating it on-site, in order to generate useful data.

Therefore, '*No single test is self-sufficient for the solving of a particular problem, so a combination of different NDT and DT should be performed.*' (Bosiljkov *et al.,* 2010, p. 239), so as to gain a comprehensive and deep understanding about the nature of stone-built heritage and provide meaningful information for conservation.

2.3. Geology of Longdong area in China

The Longdong area (See Figure 2.3), China refers to the area (35º15'– 37 º 10'N, 106º20'–108º45'E) to the east of the Long mountains, i.e. the southern section of the Liupanshan mountain chain, in Gansu Province, covering an area of 38,297.6 km^2 and experiencing a temperate climate (Liu *et al.,* 2007).

This region is located in the southwest of the Ordos Basin, the second largest sedimentary basin in China (He *et al.,* 2015). The Ordos basin is a typical Mesozoic continental depression lacustrine basin developed on the

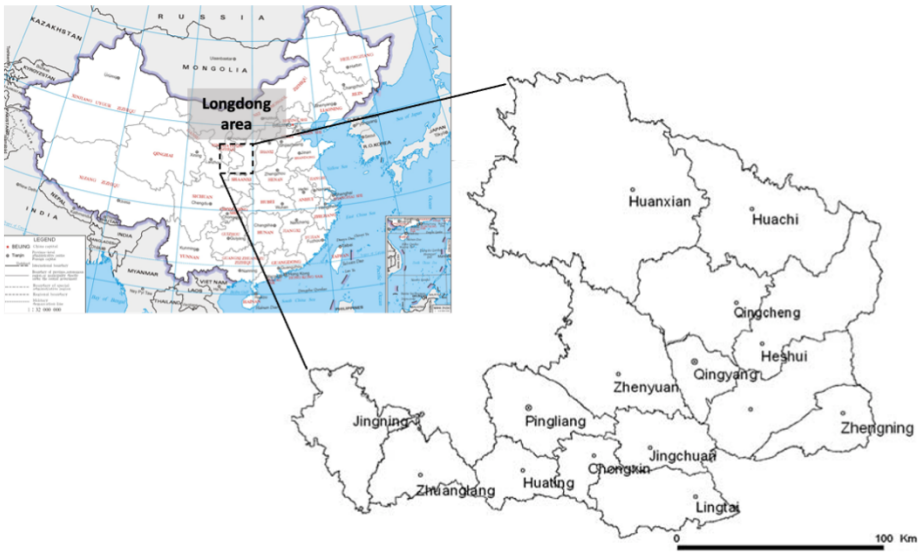

Figure 2.3.The geographic Location of the Longdong area, Gansu, China (Liu et al., 2007)

base of the North China Craton, featuring a wide and gentle lake basin, with evidence of shallow water conditions, multiple provenances, large deposition area and stable structure (Liu and Huang, 2014) and it forms an important hydrocarbon province in central China (Yang, 2005).

The interior of the basin can be divided into six structural units: the Yimeng uplift zone in the north, the Weibei uplift zone in the south, the Jinxi flexural fold zone in the east, the Yishan slope in the midsection, the Xiyuan obduction zone, and the Tianhuan depression in the west (Duan *et al.,* 2008). The Longdong area lies within the Yishan slope of the southwestern Ordos Basin, where the Yanchang Formation, made up of clastic deposits of fluvial and delta facies, is the main hydrocarbon bearing formation consisting of a set of low permeability sandstone reservoirs formed in a shallow water delta (Liu *et al.,* 2014). The typical landscape in this region is loess tableland with thick deposits of loess. Taking the Dongzhi tableland where Qingyang is located as an example, the average thickness of loess deposition exceeds 100 m (Guo *et al.,* 2006).

2.4. The threat of salt weathering on sandstone cave-temples in Longdong area, China

The information regarding geological ages, construction time and stone types of the 78 cave-temples found in the Longdong area is summarized in Table 2.2, according to the records in the literatures (DRA and GCHA, 2011, Zhang and Liu, 2013). All the 78 cave-temples are presumably hewn from

sandstone cliffs and predominantly host sandstone Buddha sculpture due to the existence of the sedimentary sandstone basin, i.e. Ordos basin, in the region; unlike the Mogao Caves situated at the western parts of Gansu province where conglomerate rock prevalently presents and hence host many statues made from clay. Because of the nature of the sandstone in which these cave-temples are hewn, and the environmental and climatic characteristics of the Longdong area, salt weathering is likely to be the main agent of deterioration.

As reviewed in section 2.1, sandstone, as a heterogeneous material, is at risk from salt weathering. Comparative laboratory experiments have showed sandstone to be more affected by salt weathering than tuff, rhyolite, travertine, dolomite and granite (Yu and Oguchi, 2009). Salt weathering is therefore likely to be an important process threatening the preservation and protection of sandstone cave-temples in the Longdong area. Furthermore, water seepage problems are common among cave-temples in the Longdong area and may also exert a strong control on sandstone weathering. For example, wetted rock surfaces are frequently observed in North Grotto Temple and Maijishan Grottoes which are located in the middle and east parts of Longdong area respectively (Ma, 1994, Cui, 2012). This is the reason why treating water seepage has always been a vital part of the conservation of cave-temples. As reviewed in section 2.1 water is an important component of sandstone weathering, acting for example as the carrier for soluble salts to enter the interior of porous materials, such as rock. The continuous penetration of water

will inevitably bring dissolved salt into the rock increasing the risk of deterioration from salt weathering.

Last but not least, the recent trend of aridification in Longdong area provides favorable climatic conditions for the occurrence of salt weathering. Researchers who studied temperature and precipitation data from 1961 to 2004 found that the average annual temperature increased during this period at a rate of 0.5 ºC per decade (Guo *et al.,* 2006), while the average annual precipitation has reduced over the same period by 30 mm per decade (Liu *et al.,* 2014). This increasingly dry and warm climate creates an external environment that is beneficial to the migration and evaporation of water from inside a rock mass towards its surface, as well as the crystallization and deposition of soluble salts. This may accelerate the occurrence of salt weathering in the rock mass, consequently causing deterioration of the rock-hewn cave-temples.

Table 2.2. Historical and geological information of cave-temples in the Longdong area
Note: information from 1. DRA and GCHA 2011, Zhang and Liu 2013; 2. Liu and Huang, 2014.

No.	Name of the cave-temple[1]	Location[1]	Dynasty[1]	Stone types[2]	Geological age[2]
1	North Grottoes Temple	Qingyang, Xifeng district	Northern Wei, Tang, Song, Ming, Qing	Sandstone	Cretaceous
2	Chaojiachuan Grottoes	Qingyang, Xifeng district	Song, Liao, Jin		
3	Xiaohewan Grottoes	Qingyang, Xifeng district	Tang		
4	Shizui Grottoes	Qingyang, Xifeng district	Ming		
5	Laodongmiao Grottoes	Qingyang, Xifeng district	Song,Yuan, Ming,Qing		
6	Wanshansi Grottoes	Qingyang, Qingcheng county	Tang		
7	Shangwan Grottoes	Qingyang, Huachi county	Song, Liao, Jin		
8	Fosibian Grottoes	Qingyang, Huachi county	Song, Liao, Jin		
9	Lianhuasi Grottoes	Qingyang, Heshui county	Tang, Song, Liao, Jin	Sandstone	Cretaceous
10	Baoquansi Grottoes	Qingyang, Heshui county	Northern and Southern	Sandstone	Cretaceous
11	Zhangjiagoumen Grottoes	Qingyang, Heshui county	Northern and Southern	Sandstone	Cretaceous
12	Anjiagoumen Grottoes	Qingyang, Heshui county	Song, Liao, Jin		
13	Yuchitai Grottoes	Qingyang, Heshui county	Northern and Southern		
14	Andingsi Grottoes	Qingyang, Heshui county	Song, Liao, Jin		
15	Shijiaogoukou Grottoes	Qingyang, Heshui county	Song, Liao, Jin		
16	Mashaochang Grottoes	Qingyang, Heshui county	Northern and Southern		
17	Luohandong Grottoes	Qingyang, Heshui county	Ming	Sandstone	Cretaceous
18	Lijiazhuang Grottoes	Qingyang, Heshui county	Song, Liao, Jin		
19	Yuewangdong Grottoes	Qingyang, Heshui county	Ming		
20	Xishan Grottoes	Qingyang, Heshui county	Song, Liao, Jin		
21	Dongshan Grottoes	Qingyang, Heshui county	Song, Liao, Jin		
22	Shanghao Grottoes	Qingyang, Heshui county	Ming		
23	Shiheigou Grottoes	Qingyang, Heshui county	Ming		
24	Dongguan Grottoes	Qingyang, Heshui county	Ming		
25	Yangpo Grottoes	Qingyang, Heshui county	Ming		
26	Dishuiya Grottoes	Qingyang, Heshui county	Ming		
27	Guanyinya Grottoes	Qingyang, Heshui county	Ming		
28	Baoquansigou Grottoes	Qingyang, Heshui county	Northern Wei		
29	Jinjiabian Grottoes	Qingyang, Heshui county	Northern Wei, Yuang		
30	Hongqugoukou Niches	Qingyang, Heshui county	Northern Wei		
31	Wajiaobei Grottoes	Qingyang, Heshui county	Song, Jin		
32	Yushansi Grottoes	Qingyang, Zhenyuan County	Song, Liao, Jin		
33	Luoyangsi Grottoes	Qingyang, Zhenyuan County	Song, Liao, Jin		

Table 2.2. Continued

No.	Name of the cave-temple[1]	Location[1]	Dynasty[1]	Stone types[2]	Geological age[2]
34	Dajv Grottoes	Qingyang, Zhenyuan County	Song, Liao, Jin		
35	Zhuchuan Grottoes	Qingyang, Zhenyuan County	Song, Liao, Jin		
36	Shikongsi Grottoes	Qingyang, Zhenyuan County	Tang - Qing	Sandstone	Cretaceous
37	Yonglesi Grottoes	Qingyang, Zhenyuan County	Northern and Southern, Ming		
38	Shikongsi Grottoes	Qingyang, Zhenyuan County	Song		
39	Shifoxia Grottoes	Pingliang Kongtong District	Northern and Southern		
40	Wangmugong caves	Pingliang, Jingchuan District	Northern Wei - Republic of China	Sandstone	Cretaceous
41	Fenghuanggou Grottoes	Pingliang, Jingchuan District	Northern and Southern, Tang		
42	Jiangjiaping Grottoes	Pingliang, Jingchuan District	Northern and Southern		
43	Nanshiya Grottoes	Pingliang, Jingchuan District	Qing		
44	South Grottoes Temple	Pingliang, Jingchuan District	Northern and Southern, Tang	Sandstone	Cretaceous
45	Luohandong Grottoes	Pingliang, Jingchuan District	Northern and Southern, Qing		
46	Qiangfoya Grottoes	Pingliang, Jingchuan District	Northern and Southern		
47	Zhangbasi Grottoes	Pingliang, Jingchuan District	Northern and Southern		
48	Taishansi Grottoes	Pingliang, Jingchuan District	Northern and Southern		
49	Haojia Grottoes	Pingliang, Jingchuan District	Northern and Southern		
50	Hanjiagou Grottoes	Pingliang, Jingchuan District	Northern and Southern		
51	Qianfosishan Grottoes	Pingliang, Lingtai County	Ming		
52	Xiakou cave-temple	Pingliang, Chongxin County	Tang, Qing		
53	Zhouzhaishigong cave-temple	Pingliang, Chongxin County	-		
54	Shigongsi Grottoes	Pingliang, Huating County	Northern and Southern, Song, Liao, Jin	Sandstone	Cretaceous
55	Chaoyangdong Grottoes	Pingliang, Huating County	Qing		
56	Hongshan Grottoes	Pingliang, Huating County	Tang- Ming		
57	Foyeya Grottoes	Pingliang, Huating County	Ming		
58	Lianhuataiqianfo cave	Pingliang, Huating County	Ming		
59	Hejiaxia Grottoes	Pingliang, Zhuanglang	Tang, Qing		
60	Shijqiao Grottoes	Pingliang, Zhuanglang	Ming		
61	Dianxia Grottoes	Pingliang, Zhuanglang	Ming		
62	Qiaoyangsi Grottoes	Pingliang, Zhuanglang	Ming, Qing		
63	Sanjiaodong Grottoes	Pingliang, Zhuanglang	Ming		
64	Zhulinsi Grottoes	Pingliang, Zhuanglang	Tang, Ming, Qing		

Table 2.2. Continued

No.	Name of the cave-temple[1]	Location[1]	Dynasty[1]	Stone types[2]	Geological age[2]
65	Fogouya Grottoes	Pingliang, Zhuanglang	Northern and Southern		
66	Hongyasi Grottoes	Pingliang, Zhuanglang	Northern and Southern, Ming, Qing		
67	Xisi Grottoes	Pingliang, Zhuanglang	Ming		
68	Luohandong Grottoes	Pingliang, Zhuanglang	Ming		
69	Dasi Grottoes	Pingliang, Zhuanglang	Ming		
70	Dianwan Grottoes	Pingliang, Zhuanglang	Ming		
71	Yunyasi Grottoes	Pingliang, Zhuanglang	Northern Wei , Ming, Qing	Sandstone	Cretaceous
72	Jinwansi Grottoes	Pingliang, Zhuanglang	Northern Wei , Ming, Qing		
73	Gejiadong Grottoes	Pingliang, Zhuanglang	Ming, Qing		
74	Foyawan Grottoes	Pingliang, Zhuanglang	Northern and Southern - Qing		
75	Chenjiadong Grottoes	Pingliang, Zhuanglang	Northern and Southern - Qing		
76	Shijiaohetan Grottoes	Pingliang, Zhuanglang	Song, Liao, Jin		
77	Qianfoya stone carving	Pingliang, Zhuanglang	Ming		
78	Lijialiang niches	Pingliang, Zhuanglang	Ming		

2.5. Aim and objectives

As reviewed in section 1.3, conservation of cave-temples in China has made considerable progress and produced fruitful results after three generations of hard work. However, it must be admitted that understanding of the main agents leading to the weathering of the cave-temples is still poor, especially the impact of salt weathering on the decay of cave-temples (Huang *et al.,* 2018). This seriously impedes the progression of the conceptual framework of immovable heritage conservation from rescue conservation to both rescue and preventive conservation, as well as from conserving the historic objects themselves to sustaining the environment surrounding the objects (Huang, 2018, Wang, 2018). The reason for the dilemma boils down to the lack of sufficient fundamental research in relevant fields (Wang and Chen, 2018).

Accordingly, this research aims to clarify the weathering mechanism of the sandstone cave-temples in the Longdong area through a systematic study, to enrich the understandings and theories of this field, as well as make up for any deficiencies. This research employs a series of approaches including on site non-destructive measurement, in situ soluble salt extraction through cellulose poultice, thermodynamic model, laboratory characterization and laboratory simulation. Among them, the combined application of the material, cellulose poultice, and the thermodynamic model, ECOS-RUNSALT, was used as a tool for semi-quantification of the salt content and mapping the salt

distribution on the sandstone grottoes façade for the first time. In addition, it is also the first-time exploration of using real environmental parameters, i.e. temperature & humidity, from a temperate area to simulate the salt weathering process on two types of British sandstone and one Chinese sandstone. The ultimate goal is to provide scientific advice and evidence in order to improve future conservation of sandstone rock-hewn cave-temples in the Longdong area.

In order to fulfil the main project aim, the research has been carried out through meeting a series of objectives which address the following three research questions:

[1]. What is the current condition of deterioration of the sandstone rock-hewn cave-temples in the Longdong area, Gansu Province, China?

Objective: to use field-based portable and non-invasive equipment to assess the current state of deterioration of North Grotto Temple (NGT), a representative sandstone rock-hewn cave-temple within the Longdong area (chapter 4).

[2]. What role do soluble salts play in the deterioration of the sandstone rock-hewn cave-temples in the Longdong area, Gansu Province, China?

Objective: to use an in situ non-invasive salt extraction method (cellulose poultice) to map soluble salts across the façade and a thermodynamic model

ECOS-RUNSALT (Price, 2000, Bionda, 2005,) to predict the behaviour of salt mixtures in changing environmental conditions (chapter 5).

[3]. How do the identified soluble salts affect the deterioration of sandstone under the climate of Longdong area (humid temperate climate)?

Objective: Design a salt deliquescence-dehumidification simulation experiment to assess salt weathering damage, including material loss, appearance changes, petrophysical properties modification etc. (Benavente *et al.,* 2007, Sousa, 2014), under realistic environmental conditions derived from real humidity and temperature record in the NGT and three different widespread damaging salts identified from the site (chapter 6).

3. METHODOLOGY

Rock-hewn cave-temples are carved into rocky outcrops. As with all natural outcrops, the decay and breakdown of cave-temples is a response to the lengthy processes of reaction or a rock face with weathering agents such as water, salt, wind, organisms, gravity etc. Research into the impact of salt weathering on cave-temples, therefore, not only requires understanding of the rocks themselves, but also demands knowledge of their surrounding environment, in order to obtain more reliable and representative research results. Hence, this research adopts a combined approach including field investigation, laboratory experiment, and computer model prediction.

North Grotto Temple (NGT) is the largest and most content-rich cave-temple with a long history of construction and use which represents the highest historic and aesthetic value of the cave-temple culture in the Longdong area, Gansu Province, China (Song, 2009). It lies above oil-rich sandstone reservoirs and is covered by a thick deposit of loess, which is a typical geological feature in the Longdong area as introduced in section 1.5. Hence, the NGT is characteristic of this region and research on it will be relevant to other sandstone cave-temples. Because of the challenges of working at more than one site, and the representativeness of NGT, it was selected as the study site of the research and will be introduced in section 2.1.

The overall research is divided into three phases:

Phase (a). Discovering the principal weathering agents affecting the preservation of NGT through fieldwork to investigate the types and locations of deterioration patterns forming on the NGT sandstone façade.

Phase (b). Detecting the spatial extent and severity of impact of the principal weathering agents through mapping the distribution of weathering products and characterizing their types.

Phase (c). Simulating and evaluating the impacts of the principal weathering agents depicted in the former two phases through a laboratory experiment on sandstone blocks chosen to represent conditions on different parts of the facade.

3.1. Study site

3.1.1. Introduction to the study site

North Grotto Temple (NGT) is a historic grottoes complex in Longdong area, Gansu Province, North West China (35°36′35″ N and 107°32′00″E, see Figure 3.1). Situated on the west face of Fuzhong Mountain (覆钟山) at the confluence of rivers Pu and Ru, it is located 25 kilometres east of Qingyang (庆阳). Qingyang is a vital 'transport hub' adjacent to two provinces, that are Ningxia province at west and Shaanxi province at east. Because of the important location, Qingyang, historically known as Jingzhou (泾州), was a military hotspot in the western part of the territory of the North Wei Dynasty.

Meanwhile, it was also the access to the Central Plain of China from the mid-eastern and western countries via the Silk Road (Zhang, 1987, Li, 1999).

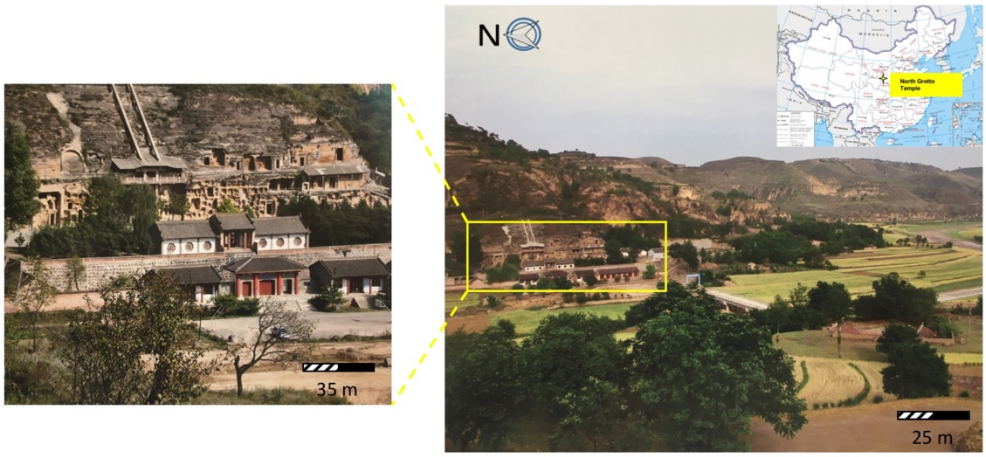

Figure 3.1. Location of the North Grotto Temple, Qingyang, Gansu province, China (NGTCI), 2013)

NGT encompasses 295 caves and niches in which 2126 rock Buddha sculptures were carved (Song, 2009) (see Figure 3.2). Among the notable caves, is 165 cave which is the largest and oldest cave hewn and created in the second year of Yongping (永平二年), Emperor Xuanwu (宣武帝) of the Northern Wei Dynasty (509 CE) on the orders of the Jingzhou Governor (泾州刺史) Xi Kangsheng (奚康生) (Li, 1999). *'After him, grottoes were continually repaired and built at the North Grotto Temple through the dynasties of North Wei, Western Wei, Northern Zhou, Tang and Song, especially during the Tang dynasty, when general peace and prosperity reigned over the whole*

country and Buddhism had an opportunity for further development. There was an universal zeal for the cutting of grottoes and shrines cut during the Tang dynasty alone totaling 196, accounting for nearly two thirds of the total number of grottoes of the place.', according to the archaeological investigation completed by the archaeological team of Gansu province and the North Grotto Temple conservation institute (1985, p. 153).

Regarding the geological conditions of the surrounding environment of NGT, the District sits on Dongzhiyuan (董志塬) which is the thickest loess

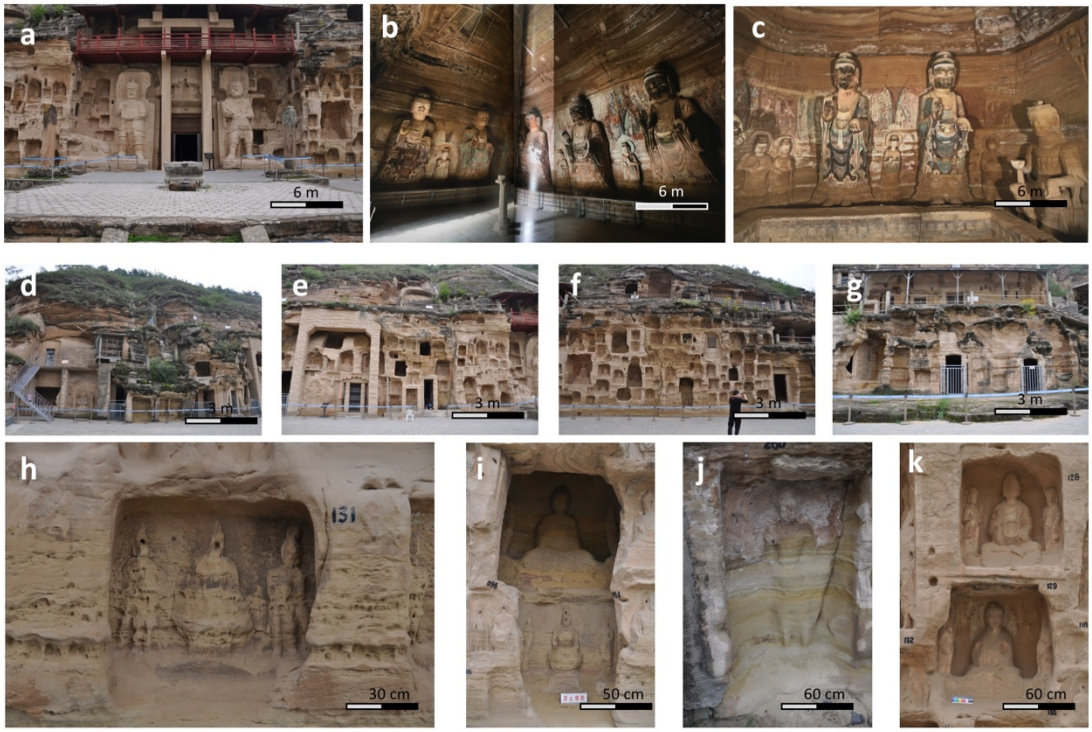

Figure 3.2. Images of caves and niches of the North Grotto Temple (NGT)
a. the main view of Cave 165 which is situated in the middle of the NGT; b. Buddha sculptures at the east wall (3 sculptures) and at the north wall (2 sculptures) in Cave 165 (NGTCI 2013); c. 2 Buddha sculptures at the west wall of Cave 165 (NGTCI 2013); d. the north end NGT façade; e. the north NGT façade; f the south NGT façade; g the south end NGT façade; h. 151 niche; i. 84 niche; j. 200 niche; k. 128 and 129 niches.

deposit in China's loess plateau. Beneath the loess plateau, a sedimentary sandstone basin presents, and rich oil reserves found. According to published sources, the Qingyang oilfield is an important uncompartmentalized and super-low-permeability petroleum reservoir with a proven reserve of more than 100 million tons (CNPC n.d. p.23).

3.1.2. Conservation history of NGT

A review of two important sources of evidence has been performed to explore the conservation history of NGT. They are the field investigation report of North Grotto Temple co-published by the Archaeological Team of Gansu Province and the North Grotto Temple Conservation Institute (1985) and the published work note written by the first director of North Grotto Temple, Zhang Luzhang (NGTCI, 2016). The main conservation practices since 1960s are summarized and listed in Figure 3.3.

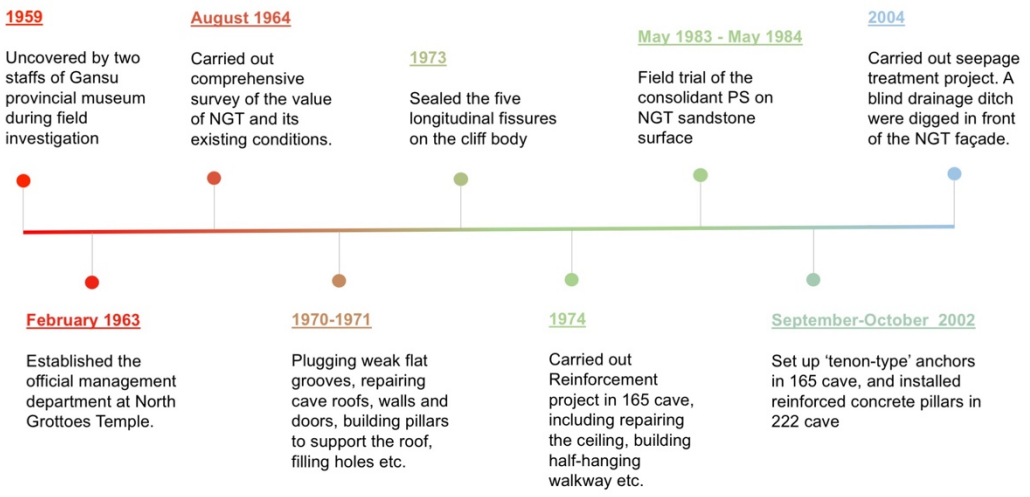

Figure 3.3. Summarized timeline of main conservation practices implemented at NGT after 1960s

North Grotto Temple (NGT) was abandoned due to warfare in the late Qing Dynasty (c. 1900 CE), afterwards being covered by dense weeds. It was uncovered in 1959 by two staff members of the Gansu provincial Museum, Chen Xianru (陈贤儒) and Zhao Zhixiang (赵之祥), during the general investigation of cultural heritage in the Longdong area. On-site investigation, including numbering, photographing and describing, was immediately organized in 1961 and accomplished by Zhao Zhixiang (赵之祥), Wu Bonian (吴柏年) from the Gansu Provincial Museum and Huo Xiliang (霍熙亮) from the Dunhuang Academy. In 1962, deposits of mud and dust were removed and cleaned from the caves, and preliminary excavation work was also carried out at the ruins in front of Cave 165 the largest caves in NGT, by Yue Banghu (岳邦湖), Zhao Zhixiang (赵之祥), Chu Shibin (初世宾) and Wu Bainian (吴柏年).

For a sound and proper protection of the site, a management department for NGT, named Qingyang North Grotto Temple Cultural Relic Depository, was established in February 1963. Zhang Luzhang (张鲁章) was appointed as the first director and took the position in November 1963. After this, systematic conservation and protection of the North Grotto Temple started.

In the early stage of Zhang's tenure, he focused on constructing the official building of NGT Cultural Relics Depository, cleaning mud and weeds in the front yard of NGT, planning green spaces for growing crops, categorizing archaeological objects in the warehouse in NGT, and participating in the first comprehensive survey of NGT led by Yang Lie (杨烈) and Song Sencai (宋森才) who were experts specialized in Chinese ancient architecture from Beijing, China.

The first 5-day (August 16 - 21, 1964) survey of NGT assessed the value of the site and its existing condition. Four things were completed during the survey, i.e. registering detailed information about typical caves and niches, creating a floor plan of NGT, photographing key caves, and determining the timeline of the NGT caves. A report was formulated after the survey which suggested that, in accordance with the features of decay of NGT, physical weathering and salt weathering in the spring and autumn are the main agents causing deterioration and decay of the site, having extremely harmful impacts on the preservation of the sandstone sculptures. In addition, five longitudinal fissures caused by earthquakes were found on the NGT façade, which were identified as huge threats to the stability of the cave-temple. Furthermore, suggestions with respect to conservation were given. Firstly, mitigating the problem of water seepage in caves through laying waterproof materials and sealing fissures and cracks, secondly, stabilizing cave walls and ceilings to prevent rock collapse. Last but not least, monitoring change, especially

recording the expanding magnitude of the five longitudinal fissures in a fixed time.

Between 14 September and 17 September 1964, three iron wire devices were installed in the large fissures and small cracks to monitor the expansion of the longitudinal fissures.

The initial condition of NGT when it was uncovered in 1959 was very poor (see Figure 3.4). The vast majority of caves were dilapidated, and there was massive development of secondary fissures within the rock mass causing serious water seepage, which threatened the preservation of NGT. In order to solve this thorny problem, Director Zhang Luzhang recruited personnel to dig drainage ditches on the top floor of the northern NGT in 1964 and carried out repeated maintenance works, such as dredging and reinforcing, over the following 7 years. Moreover, restoration of the caves was carried out with the main intention of preventing rainwater flowing into the caves, between 1970 and 1971, in which the main work included plugging weak flat grooves, repairing cave roofs, walls and doors, building pillars to support the roof, filling holes etc. (see Figure 3.5 a and 3.5 b). Many different materials were used in

Figure 3.4. Historic images of NGT taken in 1960s-1070s
NOTE: three pictures provided by the North Grotto Temple conservation institute

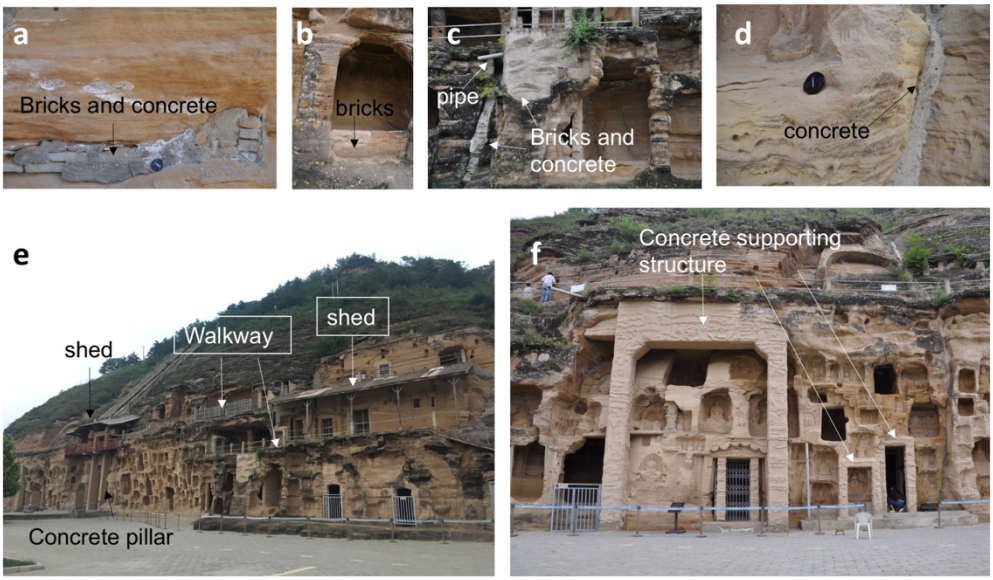

Figure 3.5. Examples of filled-fissures and added new supporting structures at NGT: a. bricks and concrete applied to fill the gap at bottom; b. brick-constructed doorstep; c. repaired part applied with concrete, filling fissures with bricks and concrete; d. filling fissure with concrete; e. sheds, walkway on the first floor and concrete pillar in front of 165 cave; f. concrete supporting structures.

the restoration, including brick, cement, iron sheet, concrete, sand and local earth (see Table 3.1).

During the 1960s and the 1970s, Chinese society was in a great state of flux. People desperately wished to construct industry and infrastructure in every corner of the country, fulfilling the so-called ‘modernization’. The same enthusiasm appeared in the surrounding area of NGT. Projects, such as the construction of power stations, agriculture irrigation systems, highways etc., were conducted in the surrounding mountains of NGT, involving rock blasting. This aroused concerns from the NGT staff, especial Director Zhang. He worried that vibration derived from the blasting would harm the stability of the rock mass of NGT. Unfortunately, damage was caused. Director Zhang took

Table 3.1. Materials applied in restoration and reinforcement of North Grotto Temple and the establishment of scaffolding pole
Note: information cited from the Zhang Luzhang's work note on the 14 Sep 1973 (NGTCI 2016).

ITEMS	AMOUNT	UNITS
Ashlar	120	m^3
White cement	1	Ton
Cement 500	16	Ton
Calcium carbonate powder	4	Ton
Sands	90	m^3
Pebble	18	m^3
Thick timber	14.5	m^3
Wooden poles	3	m^3
Hemp rope	30	kg
Soil	100	kg
Rebar (steel reinforcing rod)	3.8	Ton
Iron nails	30	kg

the initiative and communicated repeatedly with the construction staff, explaining the potential damage that the blasting may bring to the site, and reporting to the superior administration department. It was impossible to totally stop the construction, although all parties were aware of the potential hazards.

In 1973, maintenance works continued. Five longitudinal cracks on the cliff body were sealed by applying cement, mortar, asphalt, oil felt, etc. (see Figure 3.5 c and 3.5 d). Between 25 October and 30 December 1974, reinforcements were carried out on the rock mass of NGT with the aim of reducing the risk of rock collapse. The work included constructing reinforced concrete beams on the ceiling of 165 cave, building a half-hanging walkway on the first floor in front of the window of 165 cave, and fixing cantilever beams

on the top of the NGT (see Figure 3.5 e). At this point, the fundamental 'repair' of NGT came to an end.

After 1980, heritage conservation at NGT entered its scientific stage. An increasing number of experts and scholars from different fields joined the 'scientific conservation' of NGT. Between May 1983 and May 1984, Li Zuixiong carried out a trial to consolidate the sandstone through spraying PS (high-modulus potassium silicate consolidation material) on the sandstone surface of 10 caves and niches (Li, 1985). In 2002 and 2003, the roof of Cave 165 collapsed again, and there were fears about further large-scale collapses. The rock mass reinforcement and seepage treatment project was approved by the State Administration of Cultural Heritage and designed and implemented by Northwest Research Institute Co., Ltd of C.R.E.C. The rock mass reinforcement project was implemented between September and October 2002. In order to increase the stability of the rock mass as well as prevent the rock mass detaching along the structural fissures, 4 reinforced concrete pillars were installed on the south side of Cave 222, several 8-meter steel rails were horizontally set up under the ceiling in 165 cave, and the two rock strata above and underneath a horizontal weathering fissure were connected and reinforced by "tenon-type" anchors follower with sealing and grouting the empty places between anchors and fissures with high-strength cement mortar, chemical materials and small pieces of stone (Song, 2009). The seepage treatment project was carried out in 2004. The main tasks were to dig a north-to-south blind drainage ditch underneath the ground at depth of 4 to 4.5 meters

at the location which is 6-meters away from the NGT facade, and to form a complete underground drainage system with drainage boreholes and catchment wells. The drainage system now works effectively. The displacement is 6 tons per day, and the groundwater level in front of the cave has dropped from the original depth of 2.2 to 2.6 m to today's depth of 4.0 to 4.5 m (Li, 2006).

3.1.3. Weathering of NGT

Granular disintegration, flaking and collapsing are the most frequently recorded weathering patterns found by previous researchers at NGT (see Figure 3.6). For example, these patterns have been found to occur intensively in Cave 165 which is the largest and oldest cave as recorded by Zhang

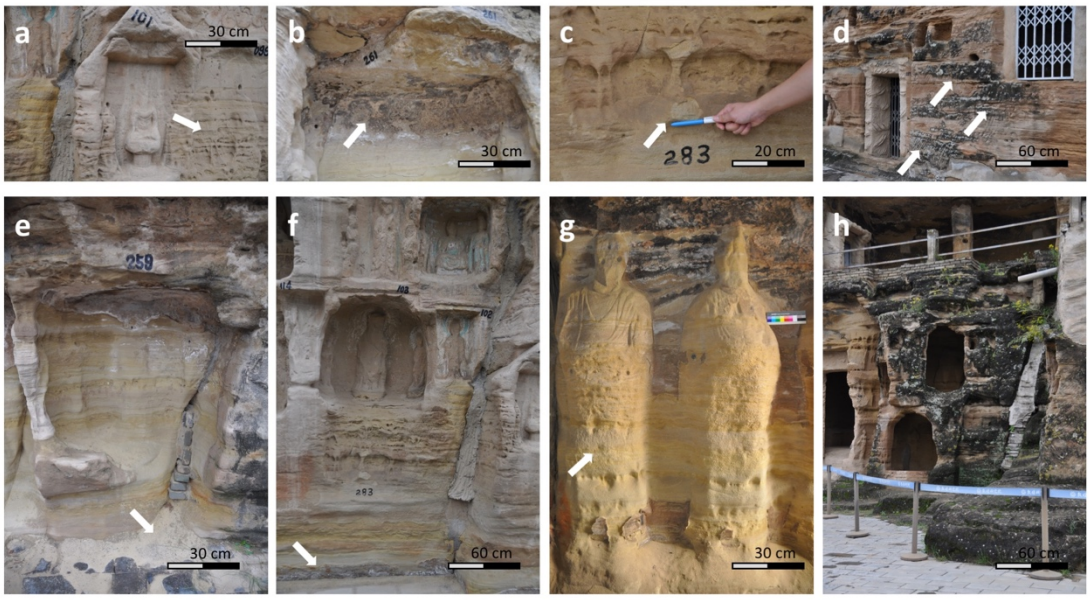

Figure 3.6. Typical deterioration patterns existing in NGT: a. alveolar on the NGT façade; b. crusting on the ceiling of 261 niche; c. flaking; d. biological colonization; e. granular disintegration causing sand accumulation at the bottom; f. salt crusting at bottom of the façade; g. surface erosion; h. biological colonization on the façade.

Luzhang (ICGNGT, 2016) who found that granular disintegration occurred continuously on the ceiling of Cave 165 and was more severe in spring when rising temperatures cause thawing of ice and snow. In addition, he noted that blasting activities in the nearby mountains can cause great vibrations in the cave-temple, which in turn enhance the detachment of sand grains from rock faces.

The amount of sand detaching from the ceiling of Cave 165 were measured once every three months in 2010, 2013, 2014,2015 and 2016 by Cui Huiping (崔惠萍), a staff member of the NGT Conservation Office, in order to monitor the severity of ceiling rock breakdown (see Table 3.2). This relatively more comprehensive 5-year records similarly display that sand detachment induced by granular disintegration on the ceiling of Cave 165 occurred intensively in the first half (January-June) of these five monitoring years, but presenting decreasing tendency when comparing with the record in 2001 (See Table 3.2).

Table 3.2. Weight (kg) record of detaching sands collected from 165 cave
Note: Data from Wang 2002[1]，provided by Cui Huiping[2].

	Year					
Months	2001[1]	2010[2]	2013[2]	2014[2]	2015[2]	2016[2]
Jan-Mar	46.2	53.05	74.8	51.7	38.35	41.8
Apri-Jun	127.5	69.1	65.33	45.6	54	88.8
Jul-Sep	n.a.	25.35	19.8	18.3	29.15	25.5
Oct-Dec	n.a.	41.1	38.5	14.6	13.2	12.9
Annual sum	n.a.	188.6	198.43	130.2	134.7	169

It can be seen that the phenomenon of falling sand from the ceiling of Cave 165 takes place constantly with the time. In order to quantify the weight loss (WL) of the sandstone unit right above Cave 165, the estimated mass of the sandstone unit and the estimated total mass of the detaching sand grains within approximate 1510 years (from initial construction to 2019) were calculated in accordance with the average yearly sum of sand detaching (see Table 3.2), the density of the sandstone, the size of Cave 165 (length, width and height), and the thickness of the sandstone unit right over Cave 165. The calculation process shows below:

$$m_a = \sum_{k=1}^{5} m_k \,/5 \tag{1}$$

$$m_{1510} = (1) \bullet 1510 \tag{2}$$

$$S = l \bullet \mathrm{w} \tag{3}$$

$$m_t = \rho_a \bullet \mathrm{h} \bullet (3) \tag{4}$$

$$WL = {}^{[(4)-(2)]}\Big/_{(4)} \bullet 100\% \tag{5}$$

m_a : average annual mass of falling sand according to the 5-year monitoring records (see Table 1), m_a = 163 kg,

S : area of Cave 165,

l : length of Cave 165 (21.7 meters) (see Figure 3.7 a),

w : width of Cave 165 (15.7 meters) (see Figure 3.7 a),

h : the thickness of the sandstone unit right over Cave 165 (3 meters) (see Figure 3.7 b),

ρ_a : average density of 2 sandstone samples obtained from different height on NGT façade (2.02 g/cm^3) (Song, 2009).

WL : the weight loss of the sandstone unit right above Cave 165.

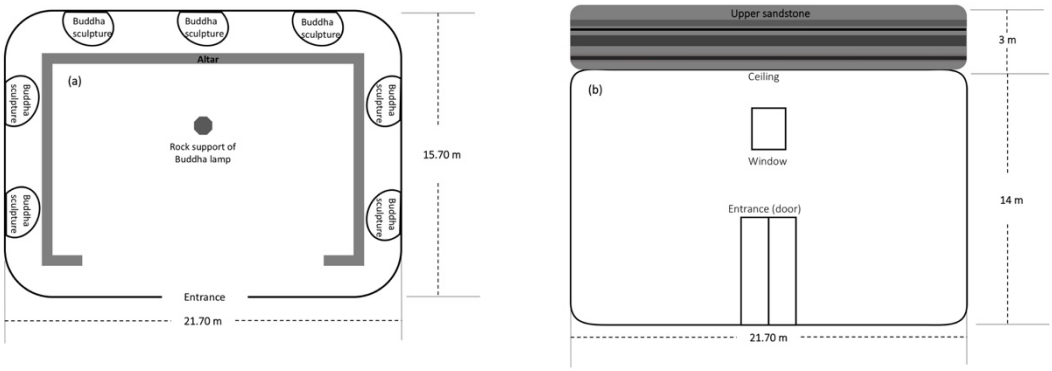

Figure 3.7. (a) the floor plan of 165 Cave, and (b) the Main view of 165 Cave
Note: the size information from ATG and NGTCI (1985)

Based upon the calculation, the total mass of the sedimentary sandstone unit right over cave 165 as well as the mass of falling sands within 1511years (504 CE – 2020 CE) are estimated to be over 2,400 tonnes and 250 tonnes respectively. Accordingly, there is an approximate 10% estimated weight loss in the sandstone unit during the past 15 centuries.

However, c. 10% weight loss may be an overestimate. Compared with the data in the first half of 2001, the amount of disintegration of sand grains and rock pieces after 2010 in the same months (January to June) has dropped significantly (see Table 3.2). This infers a potential shrinking of the amount of falling sand. The rock mass reinforcement project implemented in 2002 introduced in section 3.1.2 may be the reason causing the reduction of the measured amount of falling sands. But a continuous evaluation and monitoring will be necessarily required to accurately evaluate the effectiveness of the project.

Some detailed observations from cave 165 illustrate the episodic nature of rock detachment in some cases. Three recorded events show large amounts of rock and sand debris falling from the ceiling of the cave (72 kg on 3/8/1995 at 12 noon, 16 kg on 15/6/1996 at 11 pm and 6.5 kg on 26/5/2001 at 10 pm. (Song, 2009).

It is worth noting that rock weathering progressively weakens the strength of the rock itself and reduces the cementation between rock grains. Thus, the remaining rocks that have not yet collapsed may also be in a more fragile and vulnerable state. Small-scale granular disintegration may evolve into the rapid development of secondary fissures and cracks, or even sudden large-scale collapse.

3.2. Research methods and techniques

In order to produce a comprehensive understanding of the deterioration of NGT building on the work already carried out at the site (section 3.1.2), the research followed five main steps, i.e. field investigation/survey, laboratory characterization, predictive modelling, laboratory simulation, and rock properties' evaluation. Figure 3.8 illustrates the flow of work within and between these phases.

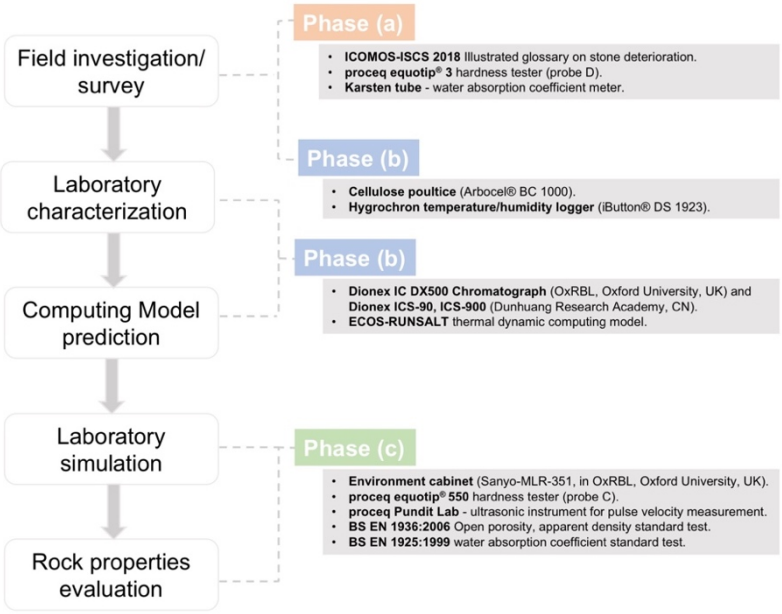

Figure 3.8. Research flowchart and involved techniques, equipment and testing standards in each phase.

3.2.1. Phase (a)

Phase (a) included the field survey of the state of deterioration in NGT which was designed and carried out between 25 August 2017 and 1 September 2017. During the field survey, information on the layout of two basic components of NGT i.e. caves and niches was collected, and deterioration patterns appearing on the sandstone façade were investigated and recorded based on the ICOMOS glossary of deterioration patterns which is designed for use on stone-built heritage (ICOMOS-ISCS, 2018) (see Figure 3.9).

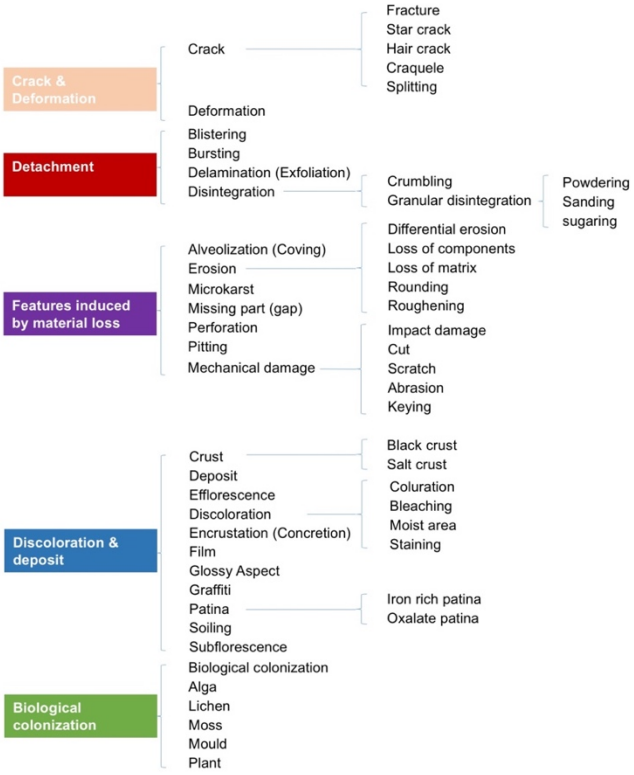

Figure 3.9. Summary of the glossary of deterioration patterns found from stone-built heritages (ICOMOS-ISCS 2018)

Furthermore, two pieces of portable non-destructive equipment, the Karsten tube and Proceq Equotip® 3 hardness tester (with probe D) (see Figure 3.10), were applied at several locations on NGT sandstone façade in order to assess its existing condition. Such field-portable, NDT methods are becoming commonly used in heritage science as they allow rapid, low cost data collection without damaging valuable heritage objects or sites (Cutler *et al.,* 2013, Fort *et al.,* 2013, Mol and Gomez-Heras, 2018,)

The Karsten tube is a convenient and efficient tool to exam the water absorption coefficient (WAC) of rock and porous building materials, and is widely used to evaluate changing water absorption after surface treatments

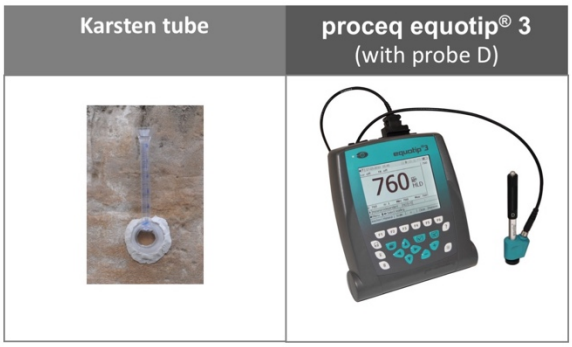

Figure 3.10. Karsten tube and Proceq Equotip 3 (with Probe D)

(Svahn, 2006). Water penetration/wetting rate varies between stone types due to their characteristic interior capillary structure and pore size distribution, which are both influenced by diagenesis and weathering. Karsten tube results (expressed as the volume of water absorbed by rock surface within a specified time period), therefore, are useful to understand the nature and extent of deterioration (RILEM, 1987).

It is especially suitable for using in the field because it is portable, non-destructive and easy to operate. The only disadvantage is that Karsten tube can easily fall off the highly weathered powdering/sanding rock surface. This is because the loosen grains on the weathered rock surface influence the efficacy of the adherence capacity of the plastiline that used to fix Karsten tube on the rock surface (Vandevoorde *et al.,* 2012). In addition, the WAC measured by the karsten tube is the area from between surface and sub-surface of the rock, and the WAC value is not only influenced by the pores in this area, but also affected by the internal conditions of the rock, such as crack development, initial water content etc. Therefore, it is necessary to carefully

design the locations of measurement points, the amount of measurements, and to collect substantial information surrounding the measurement point, in order to interpret the measured data effectively.

Surface hardness of the different sandstone strata on the NGT façade was detected using the Proceq Equotip® 3 hardness tester with the D probe that can yield 0.0115 Nm impact energy (Proceq SA, 2017). This impact energy is only a fraction of that of the Schmidt Hammer (0.735 Nm ~ 2.207 Nm) that is a popular hardness tester applied in geomorphological studies (Viles *et al.,* 2011), hence the Equotip® hardness tester would cause relatively low impact on the appearance of the measurable objects. Because of its non-destructive basis, it has been widely applied to stone-built heritage as a proxy measure of the level of deterioration (Verwaal and Mulder, 1993, Wilhelm *et al.,* 2016, Desarnaud *et al.,* 2019, Zhang *et al.,* 2019), although this rebound hardness tester was initially designed for the metal industry. Hardness is measured by the Proceq Equotip® 3 in the form of HL (Leeb units) values, which are based on the ratio of the rebound velocity to the impact velocity multiplied by 1000 based on the principle of energy measurement (Proceq SA, 2007).

Several test protocols are introduced in the operate booklet but only regarding to the determination of the hardness value of metallic materials (Proceq SA, 2019). Aoki and Matsukura (2007) formulated two data collection methods to determine the hardness value from rock surface. One is named Single Impact Method (SIM) which means randomly hitting at different points

on one rock surface and collect 10 readings and calculate their average value. Another one is called Repeated Impact Method (RIM) which means repeatedly hitting the same points on one rock surface, collecting 35 readings and average the top 3 readings. Value of SIM represents the surface hardness of the rock surface and the value of RIM stands for the intact hardness of the entire rock samples because of the compacting effects derived from the process of repeated hitting.

In accordance with data gained from this stage, I obtained a preliminary understanding of the variation of physical properties of the sandstone related to different deterioration patterns and the spatial deterioration state across the site. This helped me to narrow down my study to focus on salt weathering and to formulate the salt sampling strategy for the phase (B).

3.2.2. Phase (b)

Phase (b) was designed to collect in situ climate data and more detailed information on the salt problems at the site in order to predict the severity of salt damage. In situ salt extraction (carried out between 19 June 2018 and 10 August 2018 at NGT), laboratory characterization and computer modelling prediction are the three main components of this phase.

Cellulose poultice (Arbocel® BC 1000, fibre length 700 μm) was selected to extract soluble salt directly from the sandstone façade of the NGT because this long fibre can enhance cohesion of the wetted poultice with rock surface

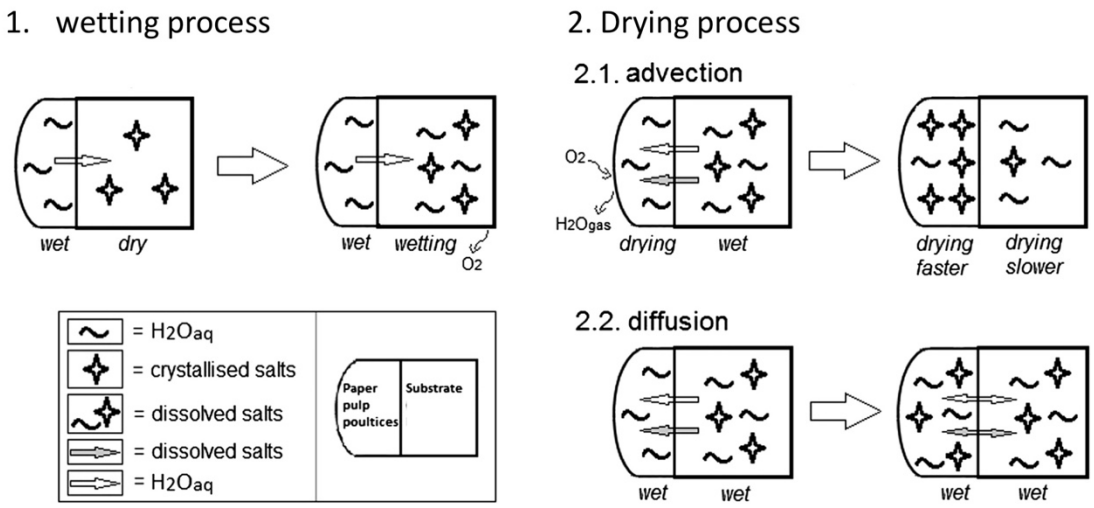

Figure 3.11. Interaction in porous material and poultice (Egartner and Sass, 2016)

than short fibre poultice, like Arbocel® BC 40 with fibre length 200 µm (Lubelli and van Hees, 2010). This porous fibre material can be wetted by immersing in water. When applying an amount of wetted poultice to another porous material such as rock, hydraulic contact is created between the two materials and water is supplied to the latter porous material through continual capillary flow between wetting area to drying area (Egartner and Sass, 2016). When a poultice is applied to a rock surface, soluble salts within the rock will dissolve and move towards the rock surface, because drying occurs from the poultice through evaporation, thereby soluble salts in rock being extracted into the dried-out poultice (see Figure 3.11). This measure is widely used for desalination in stone heritage conservation (Vergès-Belmin *et al.,* 2011). Recent research has demonstrated that such cellulose poultices can also provide semi-quantitative information on salt distribution on stone built heritage (Egartner and Sass, 2016). The non-destructive, non-invasive nature of

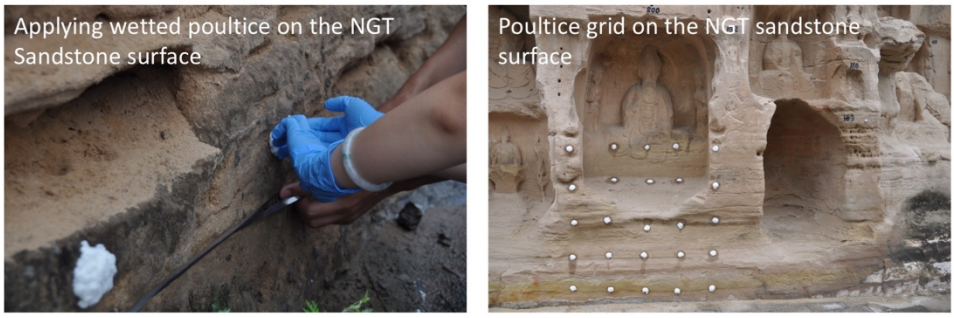

Figure 3.12. Cellulose poultice in practice in NGT

cellulose poulticing makes it ideal for use on valuable heritage sites where destructive sampling is unlikely to be permitted.

When applying in the study site, NGT, the size of each round wetted poultice point is around 6 cm diameter. 25 poultice points were evenly applied on a 1.2m length and 1.2 m width grid (see Figure 3.12).

To evaluate the salt content extracted from the sandstone surface, Ion chromatography analysis was carried out using a Dionex IC DX500 Chromatograph in the Oxford Rock Resilience and Landscape Lab (OxRBL), University of Oxford, UK and Dionex ICS-90, ICS-900 in Dunhuang Research Academy, China to identify the ionic concentration of Na^+, K^+, $Mg^{2+}, Ca^{2+}, F^-, Cl^-, NO_3^-$ and SO_4^{2+} which are common ions comprising soluble salts and widely detected from stone-built heritages (Goudie *et al.,* 1997, Arizzi *et al.,* 2012, Pandey *et al.,* 2017). Concentration results of both the cations and anions were expressed in ppm and used to feed into the computer modelling predictions. IC samples were prepared as follows:

① Immerse poultice in 80 ml deionized water,

② Sonicate samples for 1 hour at room temperature and pour out supernatant solutions into sealed test tube,

③ Agitate samples on flask-shaker at 250 strokes/min for 1 hour,

④ Filter samples through Whatman filter (0.2 μm pore) and inject solution into two ion chromatographic analyzers (one for cations and one for anions).

5 hygrochron temperature/humidity logger (iButton® DS 1923) with an accuracy of ±0.5°C were fixed on the façade of NGT to monitor T and RH at hourly intervals between 4 July 2018 and 13 July 2018. This climate data were collected for operating the model, ECOS-RUNSALT.

In order to further understand the likely weathering impacts of the soluble salts extracted by the poultice, ECOS-RUNSALT was applied. This is a chemical equilibrium model involving the thermodynamic treatment of the equilibria in phases changes of salt mixture within a fluctuate ambient temperature (T) and humidity (RH) (Price, 2000, Bionda, 2005). It can be used to predict the crystallization pathways for salt mixtures, and also the environmental conditions for salt phase transitions so as to decide the safe climatic conditions, i.e. temperature and relative humidities, under which salt damage could be mitigated (Steiger and Heritage, 2012). It is a user-friendly model with a simple interface (see Figure 3.13). Input data include ionic composition ($Na^+, K^+, Mg^{2+}, Ca^{2+}, Cl^-, NO_3^-$ and SO_4^{2+}) detected from an

aqueous extract of the salt-contaminated stone and environmental conditions, namely T and RH (Price 2007).'

The model provides two modes for data processing. The first one is calculating with changing relative humidity (RH) between 15% and 98% and constant temperature (T) between -30°C and 50°C. The second one is calculating with changing T (-30°C ~ 50°C) and constant RH (15% ~ 98%). The second mode was used to assess potential salt behaviour based on the local temperature (T) and relative humidity (RH). Because of this wide range of acceptable T and RH in ECOS-RUNSALT, it is a very useful tool to evaluate the potential damage derived from salt attack under 'real' climatic conditions (Heinrichs and Azzam, 2015, Godts *et al.,* 2017, Menéndez, 2017).

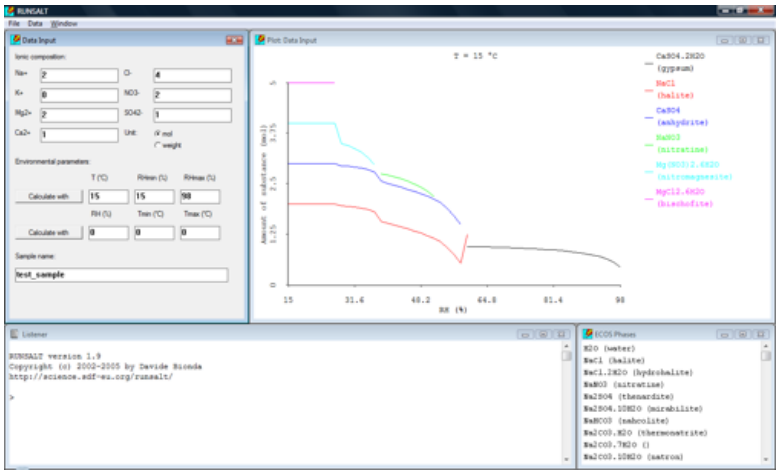

Figure 3.13. Interface of the ECOS-RUNSALT model

3.2.3. Phase (c)

The goal of Phase (c) was to simulate the salt weathering process occurring on the NGT sandstone façade, and accordingly to evaluate its impact on the sandstone properties.

Laboratory salt ageing tests are a common and effective way of studying the how salt weathering influences rock properties and produces deterioration (Goudie, 1986, Smith *et al.,* 2005, Ludovico-Marques and Chastre, 2016.). There are several Test Standards regarding salt weathering simulation in lab, however researchers seem reluctant to use these Standards because of the limitations (Lubelli *et al.,* 2018). For example, the standard EN 12370 (1999) employs very extreme ageing conditions, i.e. immersing rock samples in highly concentrated sodium sulphate solution followed by drying at 105 Celsius, and, the RILEM standard (1980) requires a total immersion of rock sample in soluable salt solution. These existing Test Standards can usually yield notable rock breakdown phenomenon, which benefits to the observation and quantification of the salt-induced damage but fail to reproduce the weathering process occurring in the field since the real environment is not as extreme as the given ageing conditions. In addition, the inconsistent detailed settings in each standard, e.g. total immersion and partial immersion of the samples, make experimental results between tests mutually incomparable.

Hence, a laboratory salt ageing test embedded with reliable climatic parameters and salt mixtures was designed and carried out using three sandstones with different porosities based on the findings obtained from Phase (b), in which 30 rock samples were partially immersed in the soluble salt solution and placed in environmental cabinet (Sanyo-MLR-351, OxRBL,

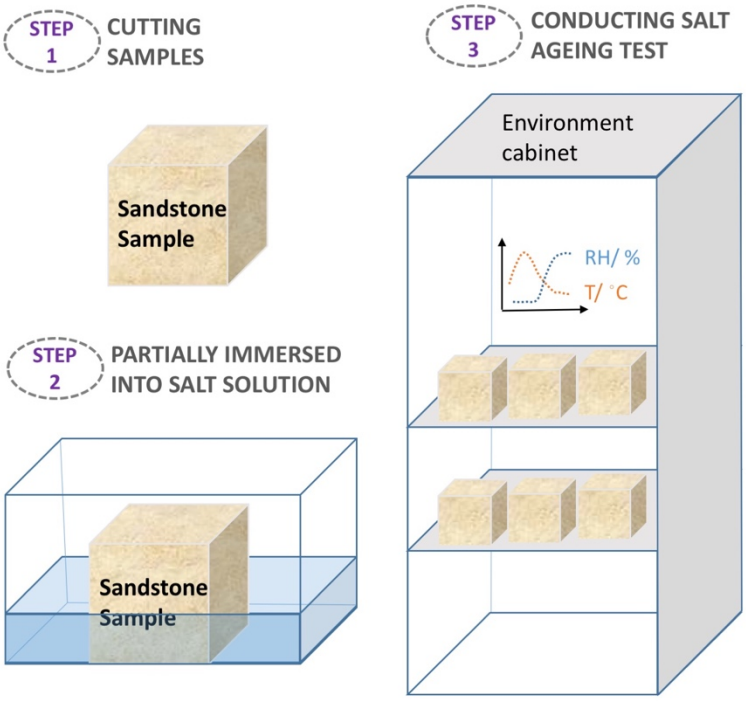

Figure 3.14. Three main steps in laboratory salt ageing tests

Oxford) for 90 ageing cycle (see Figure 3.14). The protocol of the laboratory salt ageing test is shown in Appendix I.

The ageing condition was derived from the on-site temperature (T) and humidity (RH) record in 2017 provided by the NGT Conservation Office, large annual ranges of T and RH were found, in which T and RH respectively range within -9.5 °C ~ 38.5 °C, and 9.5 % ~ 92.6 %. The annual mean T was 12.7°C and the annual mean RH was 60.1%. Precipitation was concentrated in a short period of time, i.e. between the end of August 2017 and the beginning of September 2017. Based on the climate record, an ageing cycle with two-phase temperature-humidity settings was developed. Temperature and relative humidity data between 7:15 pm, 5 Sep 2017 and 5:45 pm 6 Sep 2017 were

selected as the reference because of the long-lasting hours at high humidity (>80%) giving sufficient time for deliquescence of salts. The first ageing phase is the deliquescence phase which are derived from the average T and RH between 7:15 pm 5 Sep 2017 and 10:45 am, 6 Sep 2017 over the same period. The second phase is dehumidification phase where are derived from the average T and RH between 10:45 am, 6 Sep 2017 and 5:45 pm, 6 Sep 2017.

Salt efflorescence and rock breakdown, e.g. crumbling, sanding, etc., can be observed during salt ageing tests. In many cases, these salt-induced damages are quantified simply by weight loss calculations although other metrics of rock breakdown and deterioration are also used such as changes in visual appearance (Viles and Goudie, 2007, Labus and Bochen, 2012).

In order to assess the damage induced by the salt ageing test, rock properties were measured from the control groups and salt-contaminated groups of all three types of sandstones. Measured properties including surface hardness, internal coherence, Water absorption coefficient through capillarity, open porosity and apparent density (see Figure 3.15).

Figure 3.15. Detection sequence of petrophysical properties

Petrophysical properties define the physical properties of rock which which control pore size distributions and fluid movements within a rock (Archie, 1950). Research has shown that the efficacy of salt weathering is correlated with the petrophysical properties of the rock, especially rock strength, porosity, pore size distribution, permeability, and water transport coefficient. In turn, the salt weathering process modifies the petrophysical rock properties and further enhances the rock breakdown (Benavente *et al.,* 2007). The changes in petrophysical rock properties, i.e. hardness, internal coherence, water absorption coefficient by capillarity (WAC), open porosity and apparent density, therefore, over a salt weathering simulation can be used as proxy indicators of deterioration of rock.

Portable and non-invasive is the preferable standard for measurement equipment selection of this research phase, in order to avoid damaging the rock samples and interfering the results while measuring.

The proceq equotip® 550 hardness tester (see Figure 3.16) is an upgraded version of proceq equotip® 3 used in phase (a) and applied to detect the hardness of the sandstone samples. And the probe C (0.003 Nm) that has lower impact energy than the probe D thereby causing harmless effects to the rock samples, was selected to applied in the detection due to the light weight of the examining samples (Proceq SA, 2017). It need to note that the rebound reading collected based on the probe C and and probe D is not comparable due to the different measured pre-impact and post-rebound speed induced by

different impact energy (initial energy) of the probe (Brencich and Campeggio, 2019).

Proceq PunditLab (see Figure 3.16) is an ultrasonic instrument for pulse velocity (p-wave) measurement, which can be used to indicate the interior structure of the rock, e.g. voids and cracks (Cabello Briones, 2013, Çelik, 2019). Measurements were conducted with the direct arrangement of the two transducers to ensure the maximum signal transmission under 54 KHz (Proceq, 2014). One measurement was obtained from each sandstone sample.

Open porosity, apparent density and water absorption coefficient through capillarity (WAC) were tested following the standard test method BS EN 1936:2006 and BS EN 1925:1999 respectively. The experimental step in thes two standards are summarized in Appendix II and Appendix III.

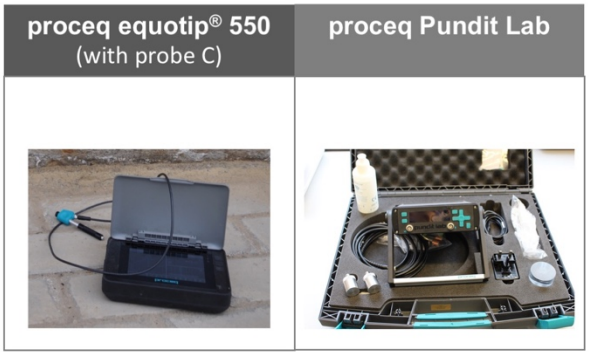

Figure 3.16. Images of proceq equotip® 550 with probe C and proceq Pundit Lab

4. EVALUATING THE CONDITION OF SANDSTONE ROCK-HEWN CAVE-TEMPLE FAÇADE USING IN SITU NON-INVASIVE TECHNIQUES

The chapter is based on the published journal paper: Wang, Y., Pei, Q., Yang, S., Guo, Q., Viles, H., 2020. Evaluating the Condition of Sandstone Rock-Hewn Cave-Temple Façade Using in Situ Non-invasive Techniques. Rock Mechanics and Rock Engineering 53(6):2915-2920. Https://doi.org/10.1007/s00603-020-02063-w Only reformatted to fit in the thesis, but otherwise identical to the published version.

Yinghong Wang[1*], Qiangqiang Pei[2], Shanlong Yang[2], Qinglin Guo[2], Heather Viles[1]

1. Oxford Resilient Buildings and Landscapes Lab (OXRBL), School of Geography and the Environment, University of Oxford, Oxford, OX1 3QY, UK.
2. Dunhuang Research Academy, Gansu Province, China.

ABSTRACT: Cave-temples are an important rock-hewn type of global cultural heritage. They not only provide evidence for studying the evolution of Buddhism in China but also reflect marvellous ancient techniques in the construction of rock-hewn structure. On the eastern section of the ancient Silk Road in China, a cave-temple site, called North Grotto Temple (NGT), has existed for 1500 years. This temple site, comprising 308 carved caves and niches which contain over 2170 statues, is a typical representation of Buddhist art in the Longdong area of China. This paper investigates the nature and

causes of the spatial pattern of deterioration of the sandstone in NGT. A condition survey coupled with information on the petrographic and physicochemical characteristics of the sandstone (based on thin section, XRD, Equotip, Karsten tube and ion chromatography data) provide a methodology for *in-situ* condition evaluation of NGT. The sandstone is found to be weakly cemented and clay-rich. The condition survey clearly demonstrate that NGT has deteriorated sharply, especially towards the southern end. High moisture content in the sandstone interior within this area is the likely cause. Surface hardness of the NGT sandstone at ground level is found to be lower than that of the sandstone higher up, which implies more severe weathering towards the ground level. Soluble salt analysis and the condition survey illustrate the importance of salt subflorescence and salt weathering related to interior and exterior water movement in NGT. Overall, the spatial pattern of deterioration of the sandstone façade at NGT is shown to be very complex and caused by multiple factors, including petrographic properties, moisture, vegetation growth, and salt. Additionally, this study shows that the combination of portable, non-invasive, field-based measurements with targeted laboratory analyses of small samples provides good information on the condition and deterioration of a large-scale immovable stone heritage which contributes to sustainable conservation strategy.

Keywords: sandstone, rock-hewn, cave-temple, deterioration patterns, Karsten tube, sorptivity, Equotip hardness tester, surface hardness.

4.1. Introduction

Rock-hewn cave-temples are a form of Buddhist temple architecture. They are important elements of world cultural heritage. Cave-temple art entered China and thrived after the introduction of Buddhism in A.D. 65 (Chan, 1957). The majority of Chinese cave-temples are found along the Silk Road; with, for example, approximately 170 sites containing cave-temples in Gansu province in the north-west of the country.

The conservation of rock-hewn cave-temples is a matter of historical, artistic and cultural importance. Since 1949 a range of conservation practices have been implemented on many rock-hewn cave-temples in China which have largely solved large-scale structural instability problems. However, small scale weathering processes affecting the rock surfaces at these sites have not been well-studied, although they can negatively affect the appearance of the site, damage valuable carvings and produce further large-scale instabilities. The lack of scientific research on the deterioration of rock-hewn cave-temples, especially in terms of investigating and evaluating the condition of the rock mass, is currently a serious problem affecting the formulation of further conservation strategies (Wang and Chen, 2018). The difficulties lie in the lack of effective *in situ* testing measures and evaluation criteria. Therefore, this paper aims to carry out a preliminary study to assess the condition of the façade of rock-hewn cave-temples using *in situ* non-invasive portable methods commonly used on stone-built heritage.

4.2. The site

The North Grotto Temple (NGT), representative of rock-hewn sandstone cave-temples of the Longdong area (eastern Gansu Province), China, is located in Qingyang city, Gansu Province (35º36′35″ N and 107º32′00″E) at an altitude of between 1064 m and 1083 m above sea level. It was initially constructed in A.D. 509 during the North Wei Dynasty and enlarged periodically until A.D. 1722. The NGT comprises two main components – larger caves and smaller niches. Hundreds of niches are carved into the west-facing sandstone façade (see Figure 4.1-1) and are the focus of this study with *in situ* measurements carried out on and around five niches within the façade.

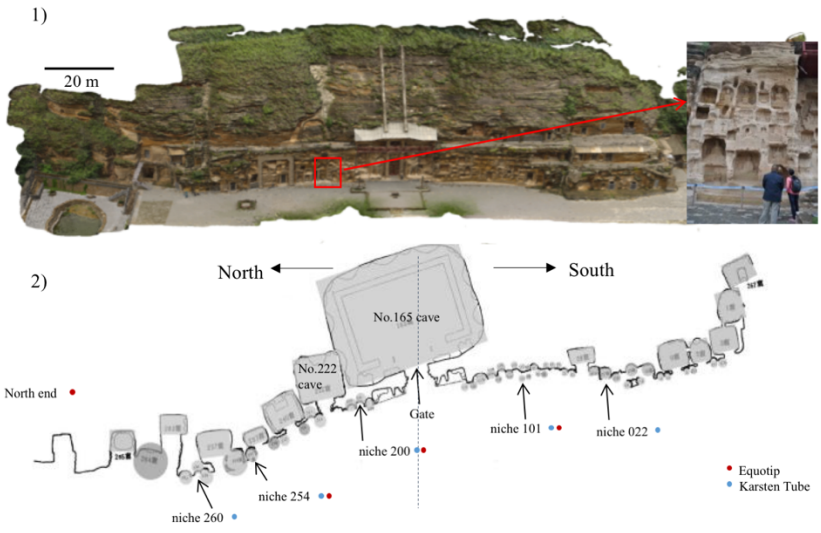

Figure 4.1. (1) 3D model of the North Grotto Temple, (2) Plan view of the site and measurement locations

Geographically, the site is located in a loess-covered landscape. The NGT was hewn from the westward-facing scarp slope of Fuzhong mountain, which has two geological units: cretaceous sandstone at the bottom and Quaternary loess cover above (Li, 2006). Horizontal bedding planes can be observed on the surface of the sandstone. Today, the area experiences a continental semi-arid climate (in 2017 the NGT Preservation Institute recorded an annual average temperature of 12.7 °C and an annual average relative humidity of 60.11%). According to official records, five areas of the façade were consolidated with high-modulus potassium silicate consolidants 30 years ago. These areas were avoided in this study to prevent any interference caused by the consolidation.

4.3. Methodology

Field studies on the NGT sandstone façade were undertaken between 25th August 2017 and 2nd September, 2017 (average temperature and relative humidity over this period: 18.3°C, 81.8%). Six measurement locations were selected from NGT façade (see Figure 4.1 and 4.2). After the survey of deterioration patterns on each measurement location (ICOMOS-ISCS, 2008), two pieces of portable non-destructive equipment were utilised.

Firstly, following the BS EN standard 16302:2013, the Karsten tube was applied to determine the amount and rate at which water is absorbed through the sandstone surface of five niches (see Figure 4.1-2 and Figure 4.2-1 ~ 4.2-5) for the evaluation of the water absorption capacities. Karsten tube can

effectively reflect the current state of rock, it is, therefore, widely used on the assessment of porous building materials (Svahn, 2006). However, after long-term practices, researchers found that the accuracy of the test results can be affected by experimental errors (i.e. reduction of effective contact area between water and rock surface due to sealant deformation) and changes in the shape of wetted zone inside rocks (Hendrickx, 2013). In order to eliminate these affects, Hendrickx (2013) improved the calculation method of water absorption coefficient by combining the analytical solution of soil permeability in soil science with geometric analysis of wetted volume and provided formulas for calculation. Based on the formulas, sorptivity (S, the capacity of a porous medium to absorb or desorb liquid by capillarity [Philip, 1957]) and capillary saturated moisture content (θ_{cap}, the volume of water that the rock needs to became saturated through capillarity [Hendrickx, 2013]) were obtained. They can be used to characterize the water absorption capacity of rocks.

Sorptivity (S) and capillary saturated moisture content (θ_{cap}) are calculated as formulas:

$$x(t) = R_{wet}(t) - R_e \qquad (1)$$

$$V_{wet}(t) = \frac{2}{3}\pi\left(x(t)^3 + R_e x(t)\right) + \pi R_e^2 x(t) \quad (2)$$

$$\theta_{cap} = \frac{V_{abs}(t)}{V_{wet}(t)} \quad (3)$$

$$V_{abs}(t) = \pi R_e^2 S\sqrt{t} + \frac{\pi R_e \gamma S^2}{\theta_{cap}} t \quad (4)$$

$x(t)$: penetration distance of wet front at time t.

$R_{wet}(t)$: radius of wetting area at time t.

$V_{wet}(t)$: wetted volume of stone at time t.

R_e: radius of effective contact zone.

θcap：capillary saturated moisture content.

V_{abs}: absorbed water volume, i.e decrease in volume of water observed in Karsten tube.

γ: constant, 0.75.

S：sorptivity, capacity to absorb water by capillarity.

Secondly, hardness of each sandstone bed (up to 1.5m above the ground) at four sites (three niches and the natural rock face to the north of the NGT façade) was measured using a Proceq Equotip 3 hardness tester (with D probe) (see Figure 4.1-2 and Figure 4.2). This non-invasive hardness tester can be used to estimate rock strength (Verwaal and Mulder, 1993) and has been used to infer the deterioration of stone heritage (Mol and Viles, 2010, Viles *et al.,* 2011, Wilhelm *et al.,* 2016, Desarnaud *et al.,* 2019) due to its high sensitivity to the weathered layer on the stone surface, small impact energy and small impact area (Aoki and Matsukura, 2007).

The Single Impact Method (SIM), where one rebound reading is taken at a range of measurement points, was used here because SIM values have

been found to reflect the strength of the rock surface, rather than the intact rock strength, and help to understand the deterioration occurring on it (Aoki and Matsukura, 2007). Eight SIM measurements were randomly taken from each sandstone bed and an average calculated (see Table 4.1). Due to biological colonization and powdering surface, rebound readings could not be obtained from niche 022 and 260.

4.4. Results and discussion

4.4.1. The capacity of the NGT sandstone to absorb water by capillarity

As shown in Figure 4.3, the water absorption rate generally shows a gradual upward trend from niche 022 at the southern end to niche 260 at the northern end and the same trend is presented from sorptivity and $\boldsymbol{\theta}_{CAP}$ (see Table 4.1). This variation demonstrates a heterogeneous feature of NGT sandstone from south to north and probably implies greater mean pore radius in the northern NGT sandstone due to the positive correlation between water absorption coefficient and mean pore radius of rock (Benavente, 2011).

Comparing with the value of sorptivity and $\boldsymbol{\theta}_{CAP}$ (see Table 4.1) and the deterioration patterns (see Figure 4.2), the magnitudes of sorptivity and $\boldsymbol{\theta}_{CAP}$ are consistent with the degree of deterioration observed. Greatest sorptivity and $\boldsymbol{\theta}_{CAP}$ was obtained from the sandstone surface of niche 260 which is seriously deteriorated and contains a series of different deterioration patterns,

including powdering, sanding, crust, efflorescence and flaking (see Figure 4.2-5). Niche, 200 has only minor deterioration features (several small pits and fine scratches) (see Figure 4.2-3) and has relatively small sorptivity and $\boldsymbol{\theta}_{CAP}$. Niche 254 has intermediate levels of deterioration (see Figure 4.2-4) matched by intermediate values for sorptivity and $\boldsymbol{\theta}_{CAP}$. Niche 022 colonizing by vegetation (see Figure 4.2-1) has the smallest sorptivity and $\boldsymbol{\theta}_{CAP}$. In summary, deterioration probably plays a significant role in the modification of pores to NGT façade so that can further promote the water transportation on the rock surface, except for bio-deterioration on niche 022.

Furthermore, it worth to noting that the south-to-north upward trend of water absorption rate does not present in the results obtained from niche 101 and, 200. Table 4.1 shows that the sorptivity of niche 101 is greater than that of niche 200, although $\boldsymbol{\theta}_{CAP}$ of niche 101 is smaller (see Table 4.1). This means that niche 101 has strong water absorption capacity but require less amount of water to reach saturation through capillarity. It can be seen in Figure 4.2-2 that water absorption forms a horizontal spindle shape wetted zone around the

Table 4.1. Sorptivty (S), capillary saturated moisture content (θ_{cap}), surface hardness and deterioration patterns around each Karsten tube measurement point

Orientation in NGT	Measurement location in NGT (Niche No.)	S ($kg/m^2\sqrt{s}$)	θ_{cap} (ml/ml)	Surface hardness (HL)	Deterioration patterns at the sandstone bed where Karsten tube was applied
SOUTH	022	0.078	0.065	-	Biological colonization
↑	101	0.295	0.074	g. 355	Horizontal hair crack, pitting
↕	200	0.277	0.087	f. 325	Pitting, scratch
↓	254	0.589	0.226	d. 346	Soiling，pitting, powdering, scratch
NORTH	260	1.001	0.288	-	powdering, sanding, crust，efflorescence，flaking

* The surface hardness is the average surface hardness of the bed where the Karsten tube was applied. The letter in front of the surface hardness value represents the layer of the bed on the specific location.
* Effective readings of surface hardness were not obtained from the Niche 022 and 260 due to biological colonization on the sandstone surface and powdering surface respectively.

Karsten tube on the sandstone surface at niche 101. This indicates that the water would penetrate horizontally towards the left and right. The existence of the wide vertical fissure filled with mortar on the left hand side of niche 101 (see Figure 4.2-2) are probably responsible for this phenomenon. No matter what causes of the fissure are, secondary cracks extending towards the vertical fissure are very likely to form in the interior of the sandstone here, because the formation of large fissures can promote the redistribution of stresses within the rock, influencing the development of secondary cracks (Huang and Huang, 2010) and the direction of water penetration in the stone (Wang *et al.,* 2005).

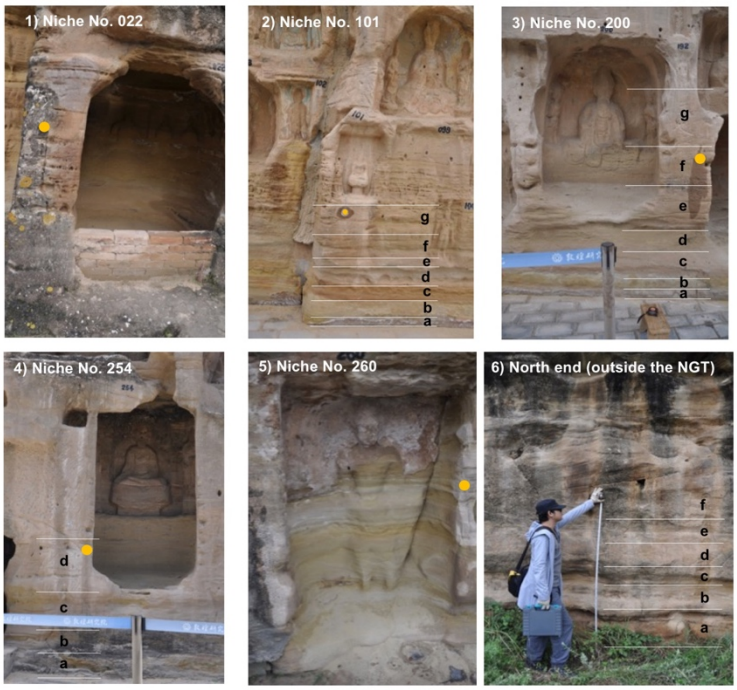

Figure 4.2. Images of six measurement sites on the façade of NGT and the adjacent natural rock outcrop.

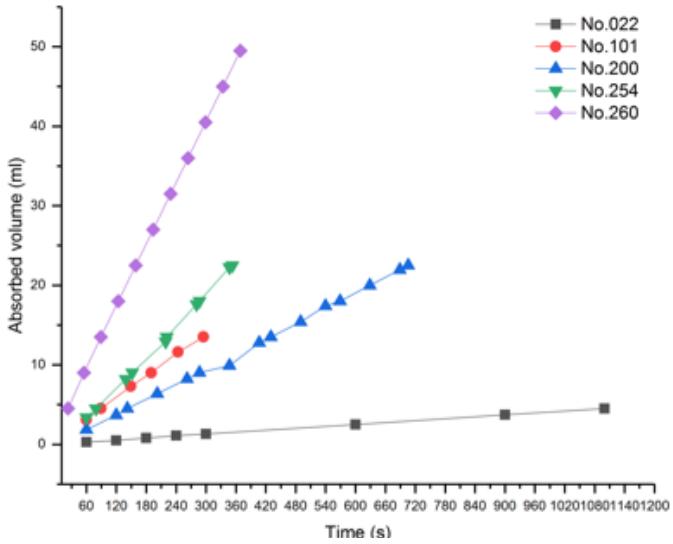

Figure 4.3. Karsten tube test results (absorbed water volume in ml plotted against time in s) from five niches on the façade of NGT.

4.4.2. Surface hardness and deterioration of NGT façade

The surface hardness varies across the four measuring locations from the north to south and from ground level upwards (0 m-1.95 m above the ground). The data from niche 101, 200 and 254 show much greater standard deviation than that from the natural sandstone rock face to the north of the NGT facade, indicating higher variability in surface hardness on the carved façade, i.e. niche101, 200 and 254 (see Table 4.2). From the amount and types of deterioration patterns observed, more severe deterioration is also found on the carved façade, such as cracking, powdering, sanding, flaking etc. (see Figure 4.2-2 ~ 4.2-4). This implies that the significant variation of surface hardness across the beds on the carved façade is very likely to be caused by more intense deterioration. And the deterioration is probably subject to the existence

Table 4.2. Surface hardness values obtained from four measurment locations on the facade of NGT and the adjacent natural rock outcrop

Niche 101			Niche 200			Niche 254			North end (outside NGT)		
Bed No.	Thickness (cm)	Mean hardness (HL)	Bed No.	Thickness (cm)	Mean hardness (HL)	Bed No.	Thickness (cm)	Mean hardness (HL)	Bed No.	Thickness (cm)	Mean hardness (HL)
g	40	355	g	45	407						
f	30	327	f	35	325				f	15	321
e	15	280	e	45	319				e	15	354
d	15	308	d	20	342	d	45	346	d	20	333
c	20	267	c	30	349	c	45	165	c	30	362
b	15	240	b	10	308	b	30	207	b	40	309
a	10	232	a	10	330	a	30	232	a	50	332
average		285	average		340	average		238	average		335
standard deviation		40	standard deviation		30	standard deviation		67	standard deviation		18

of more environmental intervention, such as stronger insolation effects due to the west-facing direction of the carved façade, which can accelerate deterioration (Weiss *et al.,* 2004).

Comparing the surface hardness results in Table 4.2 with the deterioration patterns in Figure 4.2, it is clear that, at each site, those sandstone beds with little visible deterioration have higher surface hardness values. Most of the harder beds are located higher up the measured profiles, such as the top layer at niche101, 200 and 254.

Lower surface hardness values are found on sandstone beds with powdering, efflorescence, black crust and flaking such as layer b at niche 101, layer a at niche 200 and layers a and b at niche 254. When efflorescence and crust are both present on a sandstone bed, the surface hardness is greater than that of beds where only efflorescence forms, but still lower than the average surface hardness of all beds at the measurement location, such as layers a and b at niche 200. In addition, it is worth noting that where alveolar weathering is found, surface hardness values are slightly greater than the

average surface hardness of all beds at that measurement location, such as layer d at niche 101.

4.5. Conclusion

Deterioration of sandstone on the façade of NGT causes variation in sorptivity and hardness. The capacity of the sandstone to absorb water by capillarity is positively correlated with the degree of deterioration when there are no internal cracks or biological colonization. Surface hardness is more variable on the rock-hewn façade than on the natural outcrop, and harder surfaces are generally found towards the top of the measured profiles (which also display less deterioration), with the softer surfaces found towards the base, with higher degrees of deterioration.

The research has demonstrated the value of *in situ*, non-invasive measurement methods, alongside observations of visible deterioration, in diagnosing the severity of deterioration on the façade of sandstone rock-hewn cave temples. Both the Equotip and the Karsten tube provide information about the near-surface characteristics of the façade, without the need for invasive sample collection. Further research is needed to produce larger datasets which can provide more detailed guidance for future conservation efforts.

5. EVALUATION OF THE IMPACT OF SALTS ON THE DETERIORATION OF A SANDSTONE ROCK-HEWN CAVE-TEMPLE IN NW CHINA THROUGH THE COMBINATION OF IN SITU SALT EXTRACTION AND SALT BEHAVIOUR MODELLING

This chapter is based on the published peer-reviewed international conference paper: Wang, Y., Yang, S., Yu, Z., Guo, Q., Viles, H., 2020. Evaluation of the impact of salts on the deterioration of a sandstone rock-hewn cave-temple in NW China through the combination of in situ salt extraction and salt behaviour modelling，Proceedings of the 14th International Congress on the Deterioration and Conservation of Stone, Göttingen, Germany. pp.355-360.

Modifications compared with the published version are that additional supplementary information, which could not be included because of space limitations in the conference proceedings, has been included in the methodology and discussion sections to provide more depth and breadth of coverage.

Yinghong Wang[1], Shanlong Yang[2], Zongren Yu[2], Qinglin Guo[2], Heather Viles[1]

1. Oxford Resilient Buildings and Landscapes Lab (OXRBL), School of Geography and the Environment, University of Oxford, Oxford, OX1 3QY, UK.
2. Dunhuang Research Academy, Gansu Province, China.

Abstract: Salt weathering is an important natural process which contributes to shaping landscapes. However, when it affects rock-hewn heritage, culturally-

valuable elements can be damaged relatively easily and it is important to understand where, why and how salt weathering operates in order to develop suitable conservation strategies. Rock-hewn cave-temples can be significantly affected by salt weathering due to their long-term exposure to, and close association with, the environment. This study reports on the identification of salts on the façade of North Grotto Temple (NGT) in NW China, and the prediction of their impacts under current environmental conditions at the site. A non-destructive method (cellulose poultices) was used to sample salts from the façade, and ion chromatography used to characterise the salt species. Microclimatic data (temperature and relative humidity) was collected on site and used to drive the ECOS-RUNSALT model and predict the behaviour of the identified salt mixtures. Using the poultices, 238 samples were collected from the façade of NGT all with notable amounts of salt, with especially high concentrations on the upper storey. Based on 10 days of monitoring of temperature and relative humidity in July 2018, 12 types of salt were predicted by ECOS-RUNSALT to occur on the façade of NGT, including aphthitalite ($Na_2SO_4 \cdot 3K_2SO_4$), bloedite ($Na_2SO_4 \cdot MgSO_4 \cdot 4H_2O$), picromerite ($K_2SO_4 \cdot MgSO_4 \cdot 6H_2O$), darapskite ($NaNO_3 \cdot Na_2SO_3 \cdot H_2O$), mirabilite ($Na_2SO_4 \cdot 10H_2O$), hexahydrite ($MgSO_4 \cdot 6H_2O$), starkeyite ($MgSO_4 \cdot 4H_2O$), nitromagnesite ($Mg(NO_3)_2 \cdot 6H_2O$), halite ($NaCl$), niter ($KNO_3$), and sylvite ($KCl$). Several of these are known to cause salt weathering in susceptible materials. Whilst the average temperature in NGT is moderate in the summer months, relative humidity shows large diurnal variations, producing

environmental conditions beneficial to the cycle of crystallization-dissolution /deliquescence-recrystallization of salts. Therefore, salt weathering is likely to be a major cause of deterioration at NGT.

KEYWORD: rock-hewn cave-temples, salt weathering, cellulose poultices, ECOS-RUNSALT, salt type prediction, diurnal variation of relative humidity

5.1. Background

Salt weathering has been proven by numerous studies to have an important effect on the deterioration of both rock and stone–built heritage (Goudie and Viles, 1997, Doehne, 2002). The mechanisms involved have also been widely discussed (Charola, 2000, Smith *et al.,* 2008). In summary, salt weathering affects stone-built heritage as follows: Firstly, water (mainly from groundwater and rain) penetrates into the stone through its pore network, simultaneously bringing dissolved ions into the pores. Then, along with the variation of ambient temperature and humidity, evaporation of the water occurs constantly at the boundary of liquid and gas, forming an evaporation front in the stone as well as resulting in concentration raise of the aqueous solution in the pores. When supersaturation is reached, soluble salts crystallize out, meanwhile exerting crystallization pressure against pore walls, and precipitate near the evaporation front. These salt crystals will undergo further alteration processes, such as hydration, deliquescence, dissolution, recrystallization,

because of continuous changes in the ambient temperature and humidity as well as the constant capillary movement happening inside the stone (Charola, 2000), thereby weakening the tensile strength of the stone, and ultimately leading to stone deterioration (Scherer, 2004). This weathering process can cause serious irreversible damage to stone, especially in areas such as the northwestern part of China which experience a continental arid/semi-arid climate (Bian *et al.,* 2013) favorable to salt crystallization. Furthermore, the widespread occurrence of salinized soil in this region provides a steady stream of salt sources for the outcrop above the ground (Guo *et al.,* 2008).

Studies have shown that many sandstone landscapes in NW China are affected by salt weathering and form many typical weathering patterns such as basal erosion and tafoni (Lu *et al.,* 2017). Such weathering is, therefore, very likely to pose a threat to the stone-built heritage in this region as well, especially rock-hewn cave-temples which were directly hewn from rock cliffs and mountains. Studies focusing on the presence and impacts of salts on Chinese rock-hewn cave-temples have shown clear impacts on the preservation of this kind of stone-built heritage. For instance, salt contamination has been found in the murals in Mogao caves registered as UNESCO World Heritage site in 1987 (Qu *et al.,* 1995). Furthermore, peeling and flaking were found on the surface of a Buddha sculpture in Yungang Grottoes enlisted as UNESCO World Heritage site in 2001 (Huang and Yuan, 2004). The emergence of these deterioration patterns is threatening the long-term preservation of rock-hewn cave-temples. It is, therefore, necessary to

clarify the distribution patterns of salts and explain their sources. For this purpose, a combined non-destructive field-based and modelling approach to detect and map the distribution of soluble salts across rock-hewn cave-temples and predict the risks of salt weathering is important and has been used here.

5.2. The site

Our research was carried out at a rock-hewn cave-temple, named North Grotto Temple (NGT), in Gansu province, NW China. NGT is the largest sandstone Buddhist cave-temple in the Longdong area of the Loess plateau (Song, 1998). Monitoring data for 2017 provided by the NGT Preservation Office shows an annual average air temperature of 12.7 °C and an annual average relative humidity of 60.1%.

NGT is 25 kilometres away from Xifeng District, Qingyang City, Gansu province, China (35º36′35″ N and 107º32′00″E). The site is located at the foot of Fuzhong mountain and situated on the east bank of the intersection of Pu and Ru rivers. The altitude of the site is between 1064 m and 1083 m above sea level.

NGT was initially hewn under the command of a provincial governor (also a general), named Xi Kangsheng, in North Wei Dynasty (A.D. 509). Hereafter, the site was continually carved and enlarged over the following millennium until A.D. 1722. In total, there are over 2170 statues within 308 caves and niches. Most niches were hewn from the sandstone façade which is around 20 meters

tall and faces west. NGT has been registered as a Major Historical and Cultural Site protected at the National Level, which is the highest protection level in the 'Immovable Cultural Relics' hierarchy approved by the state administration of Chinese cultural heritage.

A deterioration pattern survey carried out at NGT in 2018 as part of this research project found that its current condition was in general not very good. The majority of niches of different sizes carved on the sandstone façade had deteriorated to variable extents. Some areas of the sandstone façade, mainly at the top and towards both ends, were colonized with a layer of green or dark green vegetation. Deterioration patterns induced by salt weathering were

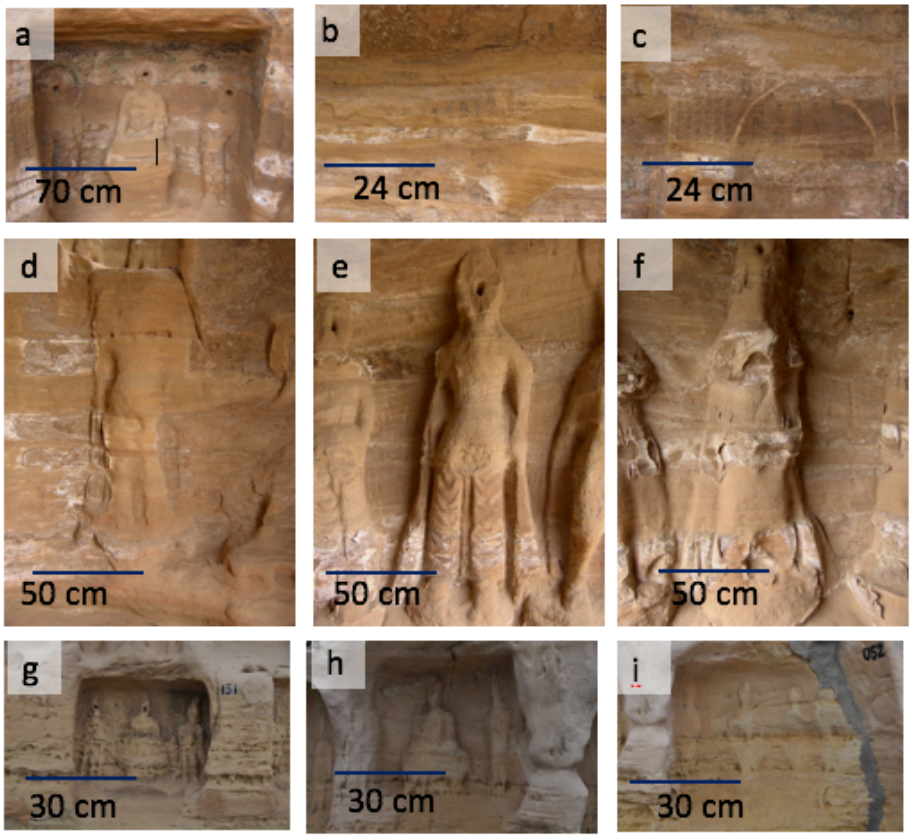

Figure 5.1. Deterioration patterns induced by salt weathering found on the sandstone surface of NGT

widely observed, such as efflorescence (see Figure 5.1 a-5.1 f), crusting (see Figure 5.1 d and 5.1 f), blistering and flaking (see Figure 5.1f) and alveolarization (see Figure 5.1 g ~ 5.1 i). These patterns indicate that salt weathering has had an effect in NGT and continues to pose a threat to it.

5.3. Aims

The aim of this paper is to map the distribution of salts on the sandstone façade of NGT, to understand the impacts that salts are having on deterioration and predict the salts' behaviour under changing ambient temperature and humidity.

Objectives:

1) To map the spatial distribution of soluble salts on the sandstone façade of NGT using a non-destructive method (cellulose poultice).

2) To use ECOS-RUNSALT to diagnose the salt mixtures present and predict their behaviour.

3) To estimate the depth profiles of salt deposits in the near-surface layers of the NGT sandstone.

5.4. Methodology

Phase variation of salts is a direct response to the changes of their surrounding environment. Hence, the impact of salt weathering on stone-built heritage can be evaluated through measuring the salt content of rocks and

understanding the phase variation patterns which may form under the atmospheric temperature and humidity conditions at the site (Bala'awi and Mustafa, 2017, Godts *et al.,* 2017, Menéndez, 2017). Based on this research idea, a combination of *in situ* detection, i.e. salt extraction, laboratory analysis, i.e. ion chromatography, and salt behaviour modelling were used in this paper.

5.4.1. In-situ soluble salt extraction method

Cellulose poultices are widely used for desalination in stone heritage conservation because they possess high operability in the field, low possibility of introducing contaminants and high water absorption capacity (Vergès-Belmin *et al.,* 2011), although there are some arguments about their salt removal efficiency in some materials (Pel *et al.,* 2010). Recent research demonstrates that cellulose poultices can provide semi-quantitative information on salt distribution on stone built heritage (Egartner and Sass, 2016). This method of using cellulose poultices to map salts offers a new, non-destructive way to evaluate salt impact to stone built heritage. It would be especially beneficial for the study of large-scale rock-hewn cave-temples because it can relatively rapidly provide information on salt distribution across large areas without the need for destructive sampling.

We used Arbocel® BC 1000 cellulose poultices, whose fiber length is 700 μm and pore size distribution is 10-30 μm (Lubelli and van Hees, 2010), to extract soluble salts from 10 surface areas of the NGT sandstone facade. These 10 NGT sandstone surfaces were selected from different storeys (see

Figure 5.2): two on the third storey, (north 3 and niche no. 035), two on the second storey, (niche no. 029 and niche no.032), and six on the first (ground) storey, (niche no. 257, no.027, no.271, no. 292, no.247 and no.200). There were 25 extraction points on each surface. The 25 extraction points were evenly distributed in 5 rows and 5 columns forming a square with side length of 1.2 m. The salts were extracted as follows:

① Soak cellulose poultice in deionized water with a pulp-to-water ratio 1:10,

② Weigh 25 g of cellulose poultice and apply onto each extraction point for 60 minutes,

③ Remove cellulose poultices from extraction point and put them into individual, sealed sample containers,

In total, 238 poultices were collected from the 10 NGT sandstone surfaces as 12 poultices were accidently dropped during the extraction. Samples were analysed with ion chromatography (IC) (Dionex™ ICS-90 and Dionex™ ICS-900) in the National Research Centre for Conservation of Ancient Wall Paintings in Dunhuang Research Academy, China. IC samples were prepared as follows:

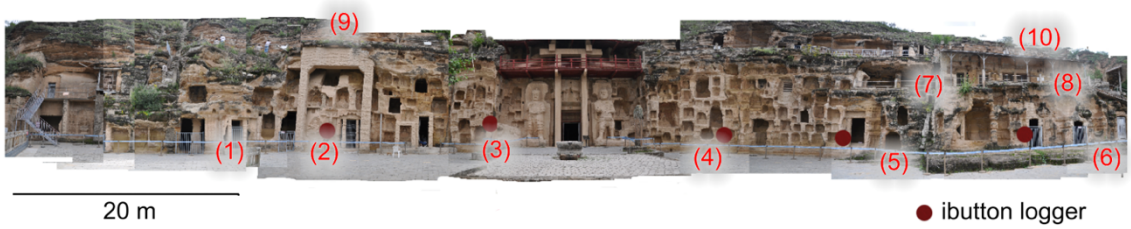

Figure 5.2. Salt extraction locations and ibutton loggers on NGT façade. [(1) niche 257, (2) niche 247, (3) niche 200, (4) niche 292, (5) niche 027, (6) niche 271, (7) niche 029, (8) niche 032, (9) north 3, (10) niche 035.]

① Immerse poultice in 80 ml deionized water,

② Sonicate samples for 1 hour at room temperature and pour out supernatant solutions into sealed test tube,

③ Agitate samples on flask-shaker at 250 strokes/min for 1 hour,

④ Filter samples through Whatman filter (0.2 μm pore) and inject solution into two ion chromatographic analyzers (one for cations and one for anions).

5.4.2. Environmental temperature and relative humidity data collection

Temperature (T) and relative humidity (RH) were monitored between 4 July 2018 and 13 July 2018 using 5 hygrochron temperature/humidity loggers (iButton® DS 1923) set to record at hourly intervals. These loggers were installed directly onto the façade of NGT at 10 m intervals and at a height of 1.60 m above the ground, located at niche 264, 014/015, 203, 232 and 052 (see Figure 5.2).

T and RH monitoring data for the whole of summer 2017 were provided by the NGT Preservation Office (2018 data were not available).

5.4.3. Evaluation of salt content in surface and near-surface layers of NGT sandstone

Powder samples were drilled from three fragments of NGT sandstone at depths of 0-1 cm, 1-2 cm and 2-3 cm. The three sandstone fragments were

collected from niche 015, niche 266 and niche 267 (see Figure 5.2). The sandstone fragments were carefully wrapped by the Japanese paper and stored in plastic sample bags. Ion chromatography analysis (Dionex IC DX500) was carried out on these specimens in the Oxford Resilient Buildings and Landscapes Lab (OxRBL) in the University of Oxford. IC samples were prepared as follows:

① Grind the samples to uniform particle size and weigh out 1.0 g samples

② Immerse the sample in 100 ml deionized water,

③ Sonicate samples for 1 hour at room temperature, and then agitate samples on flask-shaker at 250 strokes/min for another 1 hour,

④ Filter samples through Whatman No.5 paper into 100 ml volumetric flasks, make to volume with deionized water,

⑤ Filter samples again through Whatman filter (0.2 μm pore) and inject the filtered solution into ion chromatographic analyzers.

5.4.4. Salt behaviour model — ECOS-RUNSALT

ECOS-RUNSALT is a thermodynamic model which predicts the behaviour of salt mixtures under given T and RH conditions. This model can be used to estimate susceptible T and RH ranges for salt crystallization (Price, 2000 Bionda, 2005,). To operate the model, two sets of data are required. One is ionic data which can be the amount of substance (mol) or weight (g) of 7 ions,

i.e. $Na^+, K^+, Mg^{2+}, Ca^{2+}, Cl^-, NO_3^-,$ and SO_4^{2+}. The other is RH & T data which can be either a RH (%) range (up to from 15% to 98%) together with a constant T (°C) between -30°C and 50°C or a T range (between -30°C and 50°C) together with a constant RH between 15% and 98%.

In this paper, the ionic data measured from the *in situ* soluble salt extraction were used. Prior to operating the model, selection and correction were conducted on the ionic data, in order to address charge imbalance issues which can be caused by missing ions that are present in the samples but not analysed, or experimental errors in the determination of the ion concentrations (Steiger and Heritage, 2012). Following the recommended treatment of input data for ECOS-RUNSALT (Steiger and Heritage, 2012), 19 groups of ionic data measured from the sandstone surface, i.e. North 3, Niche No. 029, Niche No.257, Niche No.247, Niche No.292, and Niche No.271, were selected as being of high enough quality to produce decent ionic balances.

Two groups of T & RH data were applied in the model to represent different facets of the 10-day monitoring data. One group of T & RH data was chosen to represent a mild variation mode with a constant T of 22°C which is the average temperature of 4 days i.e. 4, 7, 9, 11 July and a RH range between 67.5% and 85%, and another group of data chosen to represent a more dramatic variation mode with a constant T of 24°C which is the average temperature of 3 days i.e. 5, 6, 12 July and a RH range between 85% and 30%.

5.5. Results and Discussion

5.5.1. Salt distribution across the 10 samples NGT sandstone surfaces

Based on the salt content results of 238 poultices given by IC analysis, salt distribution across the façade of NGT cave-temple is displayed in Figure 5.3. In general, the sandstone surfaces on higher storeys have higher salt contents. The highest salt content is found from the sandstone surface at the top of the southern end (see Figure 5.3-10 and Figure 5.4).

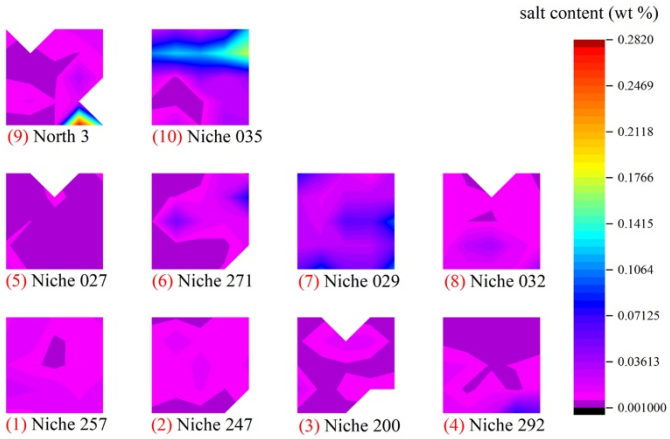

Figure 5.3. Distribution of salt content at the 10 surface.

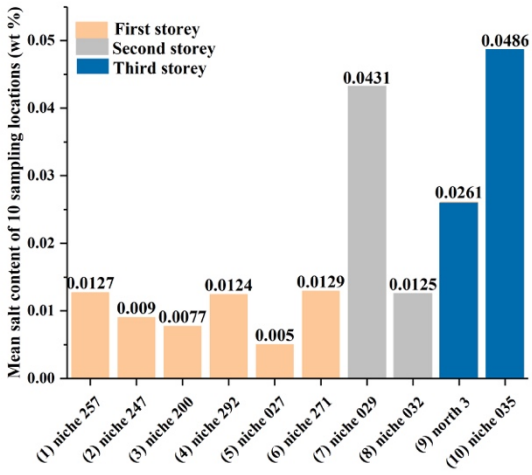

Figure 5.4. Mean salt content (wt %) on 10 surfaces (salt content [wt%] = (mass of salt/ mass of poultice) x 100%)

On each sandstone surface, the higher salinity areas tend to be present in a horizontal belt-shape distribution, as shown in Figure 5.3-7) and Figure 5.3-10). It is well-known that salt crystallization happens when the concentration of salt solution exceeds its solubility. This increase of concentration in a particular aqueous solution can be reached through decline of solvent, i.e. water by evaporation. Stone, whether it is in a natural environment or built heritage settings, will be subject to wetting-drying cycles, and the drying process can promote water evaporation occurring in the stone and gradually increase concentration of the aqueous solution in the stone pores, consequently resulting in salt crystallization (Shahidzadeh-Bonn *et al.,* 2008). Therefore, that the specific layer of the sandstone has higher salt content probably indicates a higher rate of water evaporation here. Evaporation rates of rock are influenced by environment condition, primarily RH, and/or pore network such as open porosity. For the 25 extraction points on each sandstone surface in this experiment, their external environmental conditions should not differ too much, because the spacing between each point is only 30 cm, and they are all located on the same vertical surface facing the same direction. Hence, local variability in open porosity and/or surface area are more likely to be the key factors causing variability in water evaporation rate in these layers. On the other hand, salt crystallization can promote further increases of open porosity and surface area (Orkoula and Koutsoukos, 2001). As a result, a deterioration loop is formed as follows: large open porosity and/or surface area leads to high evaporation rate, high evaporation rate further

causes more salt crystallization in the pores, and then the process of salt crystallization conversely enlarges open porosity and/or surface area of the sandstone. This modification of pore networks is responsible for significant decreases in mechanical properties of the sandstone (Tugrul, 2004), thereby increasing the damage potential to the NGT.

At the same time, the sandstone in other layers is experiencing different rates and stages of salt crystallization. Differential weathering accordingly occurs on the sandstone surface and forms different deterioration patterns on each sandstone layers, such as the belt-shape white efflorescence accompanying with blistering and flaking appearing on every interlayer of the sandstone surface (see Figure 5.1-f). The existence of blistering and flaking is an indicator of subefflorescence occurring here. This is discussed in the following section 5.2.

5.5.2. Salt deposition depth profiles

An incremental gradient of salt content is found from the deeper parts of the NGT sandstone (1-2 and 2-3 cm) to the near subsurface (0-1 cm) from the

Table 5.1. Salt content depth profiles (drilling powder from sandstone samples)

Niche No. (depth/cm)	salt content (wt %)	Niche No. (depth/cm)	salt content (wt %)	Niche No. (depth/cm)	salt content (wt %)
015 (0-1)	5.44E-02	266 (0-1)	3.78E-01	267 (0-1)	4.86E-01
015 (1-2)	3.41E-02	266 (1-2)	2.20E-01	267 (1-2)	4.61E-01
015 (2-3)	3.18E-02	266 (2-3)	1.87E-01		

ion chromatography analysis on the powder samples (see Table 5.1). No efflorescence was observed from the three fragments of NGT sandstone from which the powder samples were drilled. Therefore, it is inferred that the salts are accumulating in the near-surface zone and that there is a high possibility of occurrence of subflorescence, which is considered to be more destructive than efflorescence (La Iglesia *et al.,* 1997).

Furthermore, it should be mentioned that the salt contents in these powder samples is not directly comparable to the salt content of the NGT façade obtained through the *in situ* salt extraction, because of different way of salt extraction process. Knowledge of the extraction depth of the poultice would be required to convert the salt content data into comparable formats. Further research could be carried out to test the extraction depth of the poultice on the NGT sandstone.

5.5.3. Short-term salt behaviour predictions in different temperature and humidity ranges

Predicted salt types which can crystallize out under the two groups of T & RH inputted to ECOS_RUNSALT are listed in Table 5.2. This table shows that a smaller range of salt types forms under a mild T & RH mode (T=22°C, RH= 85% - 67.5%) than under the dramatic variation mode (T=24°C, RH= 85% - 30%). In total, 12 different salt types were predicted by the model. They are four double salts, i.e. aphthitalite ($Na_2SO_4 \cdot 3K_2SO_4$), bloedite ($Na_2SO_4 \cdot MgSO_4 \cdot 4H_2O$), picromerite ($K_2SO_4 \cdot MgSO_4 \cdot 6H_2O$), darapskite

($NaNO_3 \cdot Na_2SO_3 \cdot H_2O$), 4 hydrated salts, i.e. mirabilite ($Na_2SO_4 \cdot 10H_2O$), hexhydrite ($MgSO_4 \cdot 6H_2O$), starkeyite ($MgSO_4 \cdot 4H_2O$), nitromagnesite ($Mg(NO_3)_2$, and 3 single salts, i.e. halite ($NaCl$), niter (KNO_3), sylvite (KCl).

It is worth noting that the ambient humidity is above 67.5% under the mild variation mode. Previous study indicates that the deliquescence relative humidity (DRH) of salt mixtures is found primarily between 66% and 76% (Rörig-Dalgaard, 2014). Hence, it can be concluded that deliquescence of salts, especially mixed salts, is very likely to occur in the mild variation mode. Salt crystal deliquescence would lead to an increase of the concentration and the supersaturation ratio of the aqueous solution in the pores, resulting in more complex salt phase and deterioration patterns (Rodriguez-Navarro and Doehne, 1999). Due to the constant fluctuation of T and RH, crystallization and deliquescence of salts would repeatedly occur. This repeated cycling will cause greater damage to the sandstone (Steiger *et al.,* 2011). On the other hand, the four double salts have incongruent solubility, hence the secondary solid phase of single salt is very likely to form when the double salts dissolve because supersaturation with respect to either one of the two single salt constituents of the double compound can be reached (Lindström *et al.,* 2016). In addition, aphthitalite and picromerite are commonly found as a subefflorescence (Lopez-Acevedo et al, 1997).

The dramatic variation mode of T & RH was found in two continuous days, i.e. 5 July and 6 July (see Figure 5.5). This continuous dramatic variation mode

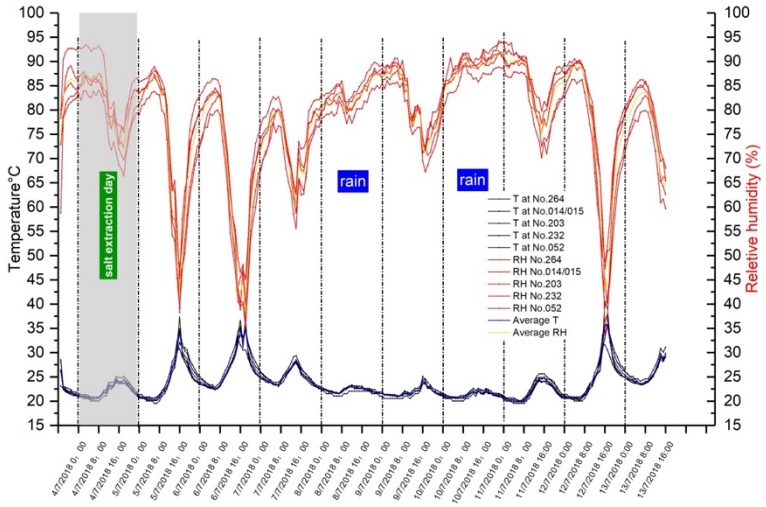

Figure 5.5. In situ T&RH monitoring data for 10 days between 4 July and 13 July 2018.

may make the evaporation front gradually move toward the interior of the sandstone because the evaporation speed of water is faster than the speed of water moving from the more internal part of the rock to the evaporation front by capillarity (Hall *et al.,* 1984). As a result, more salts may precipitate in the interior of the stone making the risk of salt weathering more severe.

In summary, salt phases vary with the ambient environmental conditions. Periodic changes in T & RH and stable water replenishment obtained by capillarity make the crystallization-deliquescence/dissolution-recrystallization cycle occur. During this process, crystallization pressure and/or hydration pressure would be continuously applied to the stone, hereby weakening the tensile strength of the stone. Over time, it will have obvious destructive effects on the stone, such as crack growth and granular disintegration.

Table 5.2. Predicted salt types by ECOS-RUNSALT under two climate mode

Sample No	T (℃)	RH (%)	Salt type						
N3 3-0			mirabilite	aphthitalite	bloedite	thenardite	halite		
029 3-2					bloedite				
029 4-1			none						
257 1-3			mirabilite	aphthitalite	bloedite	thenardite	halite		
257 2-3			mirabilite	aphthitalite	bloedite	thenardite	halite		
257 3-3			mirabilite	aphthitalite	bloedite	thenardite	halite		
257 4-1			mirabilite	aphthitalite	bloedite	thenardite	halite		
257 4-2			mirabilite	aphthitalite	bloedite	thenardite	halite		
257 4-3	**22 ℃**	**85%-67.5%**	mirabilite	aphthitalite	bloedite	thenardite	halite		
257 4-4					bloedite				
247 0-0				aphthitalite	bloedite				
247 1-0					bloedite				
247 3-3				aphthitalite	bloedite			picromerite	
292 0-3				aphthitalite	bloedite			picromerite	
292 0-4				aphthitalite	bloedite				
271 2-3			mirabilite	aphthitalite	bloedite	thenardite	halite		
271 3-2			mirabilite	aphthitalite	bloedite	thenardite	halite		
271 3-4					bloedite			picromerite	hexahydrite
271 4-3				aphthitalite	bloedite	thenardite	darapskite		

Table 5.2. continued

Sample No	T (℃)	RH (%)	Salt type											
N3 3-0			mirabilite	aphthitalite	bloedite	thenardite	halite		darapskite	niter				
029 3-2					bloedite		halite			niter	nitratine	nitromagnesite	starkeyite	
029 4-1							halite			niter	nitratine	nitromagnesite	starkeyite	
257 1-3			mirabilite	aphthitalite	bloedite	thenardite	halite		darapskite	niter				
257 2-3			mirabilite	aphthitalite	bloedite	thenardite	halite		darapskite	niter				
257 3-3				aphthitalite	bloedite	thenardite	halite		darapskite	niter				
257 4-1			mirabilite	aphthitalite	bloedite	thenardite	halite		darapskite	niter				
257 4-2				aphthitalite	bloedite	thenardite	halite		darapskite	niter				
257 4-3	24 ℃	85%-30%	mirabilite	aphthitalite	bloedite	thenardite	halite		darapskite	niter				
257 4-4					bloedite		halite			niter			starkeyite	
247 0-0				aphthitalite	bloedite		halite	picrometrite		niter			starkeyite	sylvite
247 1-0					bloedite		halite			niter	nitratine		starkeyite	
247 3-3				aphthitalite	bloedite		halite	picrometrite		niter			starkeyite	sylvite
292 0-3				aphthitalite	bloedite		halite	picrometrite		niter			starkeyite	sylvite
292 0-4				aphthitalite	bloedite		halite	picrometrite		niter			starkeyite	sylvite
271 2-3				aphthitalite	bloedite	thenardite	halite		darapskite	niter				
271 3-2				aphthitalite	bloedite	thenardite	halite		darapskite	niter				
271 3-4				aphthitalite	bloedite	thenardite	halite	picrometrite		niter			starkeyite	
271 4-3				aphthitalite	bloedite	thenardite	halite		darapskite	niter				

5.5.4. Impact of salt weathering in summer

In order to expand on the analysis of a short period in summer 2018, a fuller data set was obtained from NGT Preservation Office (only available for 2017). Based on statistical analysis of the T and RH monitoring data from summer of 2017 at NGT, Figure 5.6 depicts the proportion of different diurnal ranges of RH (DVR) in summer (92 days in total), showing the RH range and average T under the DVR. A DVR of 30%-40% is the most common (41% of the total days in summer 2017), while a DVR of 50-60% is the rarest (4% of the total days in summer 2017).

It can be seen that the mild T & RH mode (T = 22 ° C, RH = 85%-67.5%) and the dramatic variation mode (T = 24 ° C, RH = 85%-30 %) derived from the 10 days monitoring in July 2018 and presented in section 5.3 above fall in

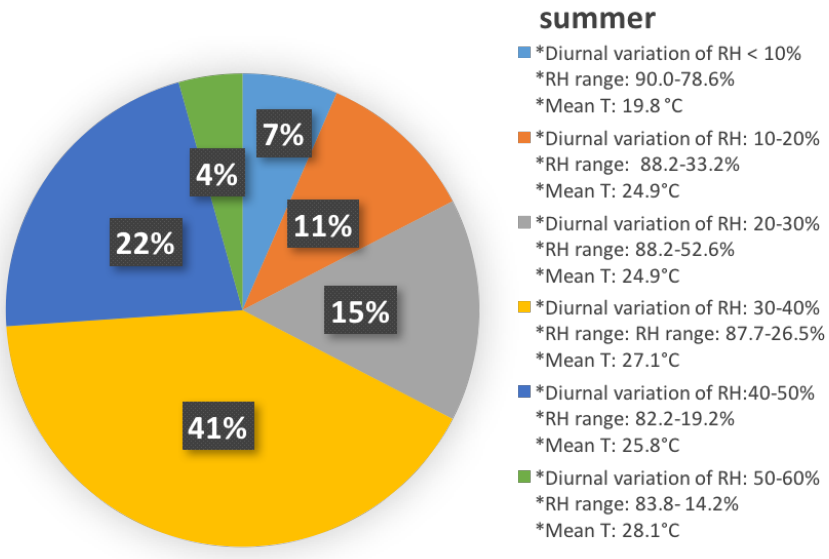

Figure 5.6. Pie chart of the percentage of diurnal variation of relative humidity (DVR) in 2017 summer at the North Grotto Temple

the DVR of 10-20% and 50-60% respectively. The days which RH varied within these two ranges accounted for 11% and 4% of the total summer days in 2017 respectively. In most days in summer 2017 (78%), DVR fell in the middle of the above two ranges, i.e. 20% -50%. The prediction results of the ECOS-RUNSALT model show (see Table 5.2) that the higher the average T and the greater the RH fluctuation, the more salt types can form. It can, therefore, be inferred that, for most of the summer 2017, the degree of salt crystallization may be stronger than that in the mild T & RH mode, and weaker than the degree of crystallization in the dramatic variation mode as used in section 5.3.

In addition, as shown in Figure 5.6, the RH fluctuates greatly during most of summer 2017, which provides favorable ambient conditions for repeated crystallization-dissolution/deliquescent-recrystallization cycling of soluble salts. Furthermore, insolation is another non-negligible factor in summer. Direct sunlight can heat the sandstone and make T and RH rise in the pores, thereby affecting the evaporation rate and the speed of crystallization of soluble salts inside the pores.

5.6. Conclusion

The *in situ* soluble salt extraction method with cellulose poultices and the thermodynamic model ECOS-RUNSALT is an effective combined approach to evaluate the distribution of soluble salts and predict the likely salt types occurring on rock-hewn cave-temples. The 'susceptible' region of salt weathering can be inferred based on the comparison of measured salt

contents across the site. The soluble salt extraction using cellulose poultices showed a strong correlation between the distribution of soluble salts and the appearance of efflorescence. Several simple and complex types of soluble salts are predicted to form in the sandstone facade of the NGT rock-hewn cave-temple, and their phases may repeatedly change with the change of temperature and humidity. Due to the large diurnal variation of relative humidity, summer provides the environmental conditions beneficial for these soluble salts to undergo many cycles of crystallization - dissolution / deliquescence – recrystallization.

6. LABORATORY SIMULATION OF SALT WEATHERING UNDER MODERATE AGEING CONDITIONS: IMPLICATIONS FOR THE DETERIORATION OF SANDSTONE HERITAGE IN TEMPERATE CLIMATES

This chapter is based on the published paper: Wang, Y., Viles, H, Desarnaud, J., Yang, S. Guo, Q.. Laboratory simulation of salt weathering under moderate ageing conditions: implications for the deterioration of sandstone heritage in temperate climates, Earth Surface Process and Landforms. 2021;1-2. https://doi.org/10/1002/esp.5086. Only reformatted to fit in the thesis, but otherwise identical to the published version.

Yinghong Wang[1], Heather Viles[1], Julie Desarnaud[2], Shanlong Yang[3], Qinglin Guo[3],

1. Oxford Resilient Buildings and Landscapes Lab (OxRBL), University of Oxford, Oxford, UK.
2. Belgian Building Research Institute (BBRI), Brussel, Belgium.
3. Dunhuang Research Academy, Dunhuang, Gansu, China

ABSTRACT: Salt weathering is a significant process affecting the deterioration and conservation of stone-built heritage in many locations and environments. While much research has focused on the impact of salt weathering under arid or coastal conditions with characteristic climatic conditions and salt types, many sites found to be experiencing salt-induced deterioration, such as sandstone rock-hewn cave temples in Gansu Province, China and sandstone buildings in northern UK, experience high humidities and

moderate temperature ranges and different salt types. In order to evaluate the impact of salt weathering on sandstone-built heritage under such mild humid environmental conditions, a lab simulation experiment was designed. The experiment was carried out on three types of sandstone (used in northern UK and Gansu Province, China) and utilised a realistic diurnal humidity and temperature cycle (85%RH/16°C + 60%RH/22°C), and three widespread damaging salts, i.e. Na_2SO_4, $MgSO_4$ and the mixture of Na_2SO_4-$MgSO_4$. The nature and extent of deterioration was monitored by photography, weight loss and the changes in petrophysical properties measured using hardness, ultrasonic pulse velocity (P-wave velocity), water absorption coefficient by capillarity, open porosity and apparent density. All three sandstones were found to be susceptible to $MgSO_4$ and the mixture of Na_2SO_4-$MgSO_4$, but weakly affected by Na_2SO_4 under mild humid environmental conditions.

KEYWORDS: sandstone, built heritage, salt weathering, lab simulation, Na_2SO_4, $MgSO_4$, mixture of Na_2SO_4-$MgSO_4$, petrophysical properties, weight loss

6.1. Introduction

Salt is not only an important agent of weathering causing geomorphological change in the natural environment, but is also a major cause of deterioration to stone built heritage around the world, e.g. the Harappan city of Mohenjo-Daro in Pakistan, the Pharaonic temples and the Sphinx in Egypt, the Nabatean site of Petra in Jordan, and the Yungang Grottoes in China (Goudie, 1977, Goudie and Viles,1997, Fitzner *et al.,* 2003, Heinrichs, 2008, Jiang *et al.,* 2015). A series of deterioration patterns, such as efflorescence, salt crust, fracture, sanding, alveolization, etc., can be produced on rock by salt weathering (He *et al.,* 1997, Huang, 1997), thereby diminishing the artistic and historical values of stone-built heritage, and causing a major challenge for their long-term conservation.

Sources of salts and fluctuating ambient temperature and humidity are necessary conditions for the occurrence of evaporation, salt crystallization/hydration and volumetric change of crystalline salts (Cooke, 1979). Therefore, dry and hot desert and coastal regions are traditionally recognized to be the most significant areas affected by salt weathering (Cooke and Smalley, 1968). Much effort has gone into evaluating the impact of salt weathering on rock disintegration under hot desert conditions (e.g. Goudie *et al.,* 1970, Cooke, 1979, Sperling and Cooke, 1985, Smith *et al.,* 2005, Warke, 2007). Further, a range of other researchers have focused on assessing the influence of seawater on rock and stone heritage (e.g. Cardell *et al.,* 2003, Tingstad, A. 2008, Morillas *et al.,* 2020). Recent research has demonstrated

that salt weathering is also influential to the deterioration of stone-built heritage situated in areas where the climate is more humid and cooler than warm deserts (e.g. Watt and Colston, 2000, Corvo *et al.,* 2010, Rabat *et al.,* 2020). Many researchers have used laboratory experiments to simulate salt weathering, and most experiment to date have used relatively simple conditions, with extreme temperature cycles, low relative humidities and single salts. These experiments successfully prove the potential destructive effects of salt weathering under certain conditions, but it is unclear how transferrable they are to other climatic contexts. There is a clear need for laboratory experiments to evaluate the potency of salts under cool, humid conditions.

Salt weathering can occur due to deliquescence-recrystallization/rehydration of salt crystals under conditions of oscillating humidity due to the hygroscopic property of the majority of soluble salts (commonly found in the nature and built environment), e.g. halite (NaCl), sylvite (KCl), thenardite (Na_2SO_4), potassium sulfate (K_2SO_4), nitratine ($NaNO_3$), nitre (KNO_3), sodium carbonate (Na_2CO_3), potassium carbonate (K_2CO_3) and bloedite (Na_2SO_4•$MgSO_4$•$4H_2O$) etc. (Doehne, 2002, Lubelli *et al.,* 2004, Gonçalves *et al.,* 2006, Godts *et al.,* 2017). Hence, salt-related damage can be caused by the interaction of salts with atmospheric humidity where there are no other source of moisture (Franzen and Mirwald, 2009, Sato and Hattanji, 2018), although the high humidity would reduce the evaporation rate and consequently affect the supersaturation ratio and crystallization patterns and precipitation location of salt crystals (Rodriguez-Navarro and Doehne, 1999). However, how relative humidity

fluctuations affect salt solutions within porous media is still unclear. Despite much progress in research on salt weathering of sandstone, the impact of moderate environmental conditions, especially the role of humidity fluctuations, on the processes of salt weathering is still an open question (Doehne, 2002).

Furthermore, salt types and their properties also play significant roles in the salt crystallization process and ultimate deterioration patterns forming on the stone (Doehne, 2002). Single salts, such as sodium sulfate, magnesium sulfate and sodium chloride, have been widely applied in salt weathering experiments to assess the resistance of stones to salt and to study salt weathering mechanisms (e.g. Goudie *et al,* 1970, Gomez-Heras and Fort, 2007, López-Arce *et al.,* 2009, Sato and Hattanji, 2018, Çelik and Aygün, 2019). However, criticisms have been raised about the ability of such single salt experiments to represent the 'real world' because salt mixtures are more commonly found in both natural and built environment s(Flatt *et al*., 2017, Lubelli *et al.,* 2018). Mixtures of salts have been found to form more complex phase changes during lab simulations, resulting in higher damage potential under certain environmental conditions (Lindström *et al.,* 2015, Lindström *et al.,* 2016, Shen *et al.,* 2020). Therefore, for a comprehensive understanding of the impact of salt weathering on stone heritage, experiments should use salt mixtures found in natural and built environments .

As part of an ongoing UK-China collaborative research project on the deterioration and conservation of sandstone heritage under humid climatic

conditions, this paper focuses on the role of salt weathering on representative sandstones from northern UK and the southern part of Gansu Province, NW China. Areas of northern UK, such as Glasgow, Edinburgh, Belfast and Sheffield, as well as the south area of the Loess plateau in Gansu Province, China are two areas owning a great amount of sandstone-built heritage, including historic buildings and cave-temples (Hyslop *et al.,* 2006, DRA and GCHA 2011, Zhang and Liu, 2013). Both areas experience humid temperate climates (Peel *et al.,* 2007, Zheng *et al.,* 2010). The preservation of such heritage is severely affected by sandstone deterioration which shows a close relationship with the occurrence of salt weathering on those sandstone blocks and sandstone outcrops based upon the observed salt-induced patterns, e.g. salt efflorescence, alveola, sanding etc. (McCabe *et al.,* 2013, Meng *et al.,* 2011, Guo and Jiang, 2015, Jiang *et al.,* 2015, Wang *et al.,* 2020). As part of this larger project, this paper aims to simulate the salt weathering process on sandstones collected from both areas under a humid ageing conditions derived from real climatic data with salts known to be found at a range of heritage sites.

6.2. Methodology

In order to simulate salt weathering on sandstones under humid temperate climatic conditions in the laboratory, an experimental workflow has been designed (see Figure 6.1). The experiment included six main steps: preparation of experimental materials, salt impregnation, exposed face control, simulation ageing test, removal of salt efflorescence and detached rock grains,

and measurement of petrophysical properties. Sandstones were cut and grouped at the beginning of the experiment and partially immersed in saline solution for 4 hours until they reached stable weight. The sandstone samples were then tightly wrapped with aluminium foil with one vertical face open to mimic the exposure of the vertical façade of stone structures, followed by 90 cycles of the salt ageing test, salt efflorescence identification and measurement of petrophysical properties (measurements were carried out following the sequence listed in Figure 6.1). Samples of salt efflorescences generated in the experiment were subjected to PANalytical Empyrean Series 2 powder diffractometer (operating at 40 kV and 40 mA with a Co Ka source) for crystal identification in the Powder X-ray Diffraction Laboratory, Department of Earth Science, University of Oxford.

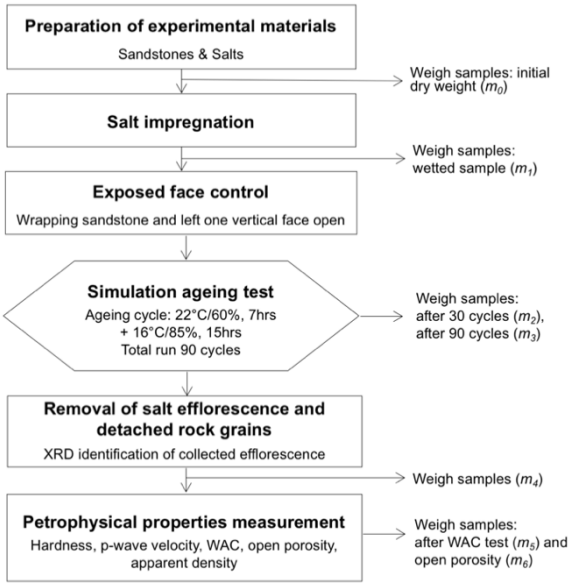

Figure 6.1. Experimental workflow used in the salt weathering lab simulation (Note: P-wave: ultrasonic pulse velocity; WAC: water absorption coefficient through capillarity; m_0: dry weight of sandstone samples; m_x: weight of sandstone samples within the experiment, x=1~6.)

6.2.1. Experimental materials

6.2.1.1. Sandstone samples

This study utilized three types of sandstones. The first one is freshly quarried Cretaceous sandstone (NS) near the cave-temple site of North Grotto Temple (NGT) in Qingyang, NW China. The site is situated on the west face of Fuzhong Mountain at the confluence of rivers Pu and Ru, with 20-30 m thick loess sediments above the sandstone outcrop unit. Horizontal bedding planes were observed in this sandstone unit. NS is a dull yellowish fine-grained sandstone composed of 60-78% quartz, 8-10% k-feldspar, 15-18% plagioclase, 3-5% rock fragments and 1-2% calcite, and cemented by clay minerals, i.e. muscovite, smectite, illite and kaolinite (Song, 2006). On the basis of previous evidence (Li, 2006), two different porosities, i.e. 19.6% and 27.5%, were detected from the surficial sandstones sampled from different heights of the sandstone outcrop unit, i.e. below and above 809 m altitude. However, only 3.2% ~ 4.2 % open porosity was measured from the freshly quarried specimens using the standard method (BS EN 1936:2006). This difference in measurement results may be due to a different determination method since the applied testing method for porosity was not indicated by Li (2006). Nevertheless, this could also be an indicator of the essential nonuniformity of NGT sandstone at different depths and/or a highly extent of deterioration occurring on the surficial sandstone of NGT.

Locharbriggs sandstone (LS) is a dull reddish to pink medium-grained Permian sandstone with 20%-23% porosity, which often has noticeable bedding planes,

freshly quarried from Dumfries, southern Scotland (Pandey *et al.,* 2014). The Dumfries Basin is a synclinal half-graben structure bounded to the west by an NNW-trending fault (Akhurst and Monro SK, 1996). LS is composed of 79% quartz, 13% feldspar, 1% rock fragments, and is cemented by predominant clay-sized hematite, and a small portion of pyrite, feldspar overgrowth and quartz overgrowth (Baraka-Lokmane *et al.,* 2009). This sandstone is widely used in construction and maintenance of historic stone buildings in Glasgow, such as St Agnes church, Balshagray house, Springburn public hall etc. (Hyslop *et al.,* 2006)

Stoke Hall sandstone (SS) is a buff coloured fine to medium Carboniferous sandstone with 11% porosity, from Hope valley, Derbyshire, England (Pandey *et al.,* 2014). Hope valley is a broad valley underlain by limestones, shales and millstone grit (Fearnsides *et al.,* 1932). SS is made up of 72% quartz, 7.3% plagioclase, 11.5% k-feldspar, 4.4% kaolin and 2.9% dioctahedral 2:1 clay (Breen *et al.,* 2008). It has subtle bedding planes. SS is acknowledged as a durable stone and used in several historic stone built structures such as Howden and Derwent reservoirs and Sheffield Town Hall in Britain (ESF 2018).

For the salt weathering experiment, SS and LS were cut into cubes with a side length of 2.5 cm, with 16 samples produced from each stone type. Because of the limited size and quantity of NS that can be obtained from the field and the size requirement for standard tests, NS was cut into 8 cuboids with 3 cm height, 3 cm length, and 1.5 cm width. Each type of sandstone was divided into four

groups, i.e. a control group and three salt contaminated groups. Each group contained 4 samples (SS and LS) or 2 samples (NS). All sandstone samples were washed with deionized water and dried at 60°C in the oven after cutting and placed with bedding planes parallel to the ground during the simulation.

6.2.1.2. Salt types

Three types of salt solution were chosen for this study: sodium sulfate (Na_2SO_4, 0.96 *mol/kg*), magnesium sulfate ($MgSO_4$, 2.90 *mol/kg*) and a mixture of sodium sulfate & magnesium sulfate (1.50/2.49 *mol/kg*). Sodium sulfate and magnesium sulfate were chosen because they are widely present in many locations and environments (Goudie and Viles, 1997) and have destructive effects in stone-built heritage (Přikryl *et al.,* 2003, Warke *et al.,* 2006, Ruiz-Agudo *et al.,* 2007, Li *et al.,* 2008. López-Arce *et al*., 2009, Balboni *et al*., 2011, Guo and Jiang, 2015).

Complex mixed saline solutions are rarely used in salt weathering lab simulation, but they commonly exist in the natural environment and will cause salt weathering in greater complexity (Flatt *et al*., 2017). Bloedite ($Na_2SO_4 \cdot MgSO_4 \cdot 4H_2O$), has been identified in efflorescences on many stone buildings (e.g. Kuchitsu *et al*., 2000, Matsukura *et al*., 2004, Erić *et al*., 2015, Wang *et al*., 2020), and has been found to have very high damage potential in experiments due to its feature of incongruent dissolution (Lindström *et al*.,

2016). Hence, the mixture of sodium sulfate & magnesium sulfate was chosen in our study to mimic its damage process and compare with the other two salts.

6.2.2. Experimental conditions

The ageing conditions selected for the experiment (Figure 6.2) were based on the climatic record provided by the NGT Conservation Office at NGT where temperature and humidity were recorded on the surface of NGT sandstone façade at fifteen-minute intervals using a temperature and humidity sensor over a period of 12 months. Temperature and relative humidity data collected between 5 Sep 2017 and 6 Sep 2017 were selected from the record, as they are representative of the climatic condition during the autumn in the identified area which is the most humid season in the region. The cycle was smoothed to produce a practicable cycle in the environment cabinet, with 15 hours at 85% RH, 16°C for 15 hours (phase 1), followed by 1 hour 40 mins to heat to phase 2, which consisted of 7 hours at 60% R, 22°C, followed by 20 minutes to cool

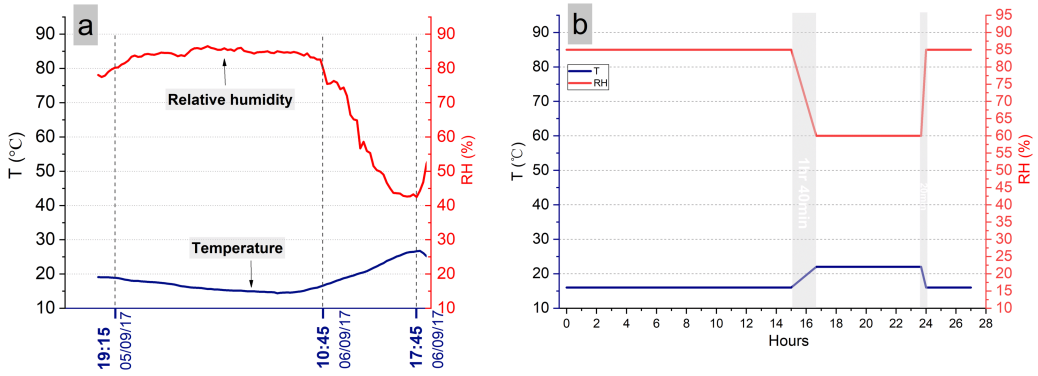

Figure 6.2. a) Temperature and RH data collected at North Grotto Temple, 5-6th September 2017 on which the cycle was based, b) 24 hour T and RH cycle as programmed into the environmental cabinet.

down, ready for the next phase 1 to start. The ageing test was conducted in an environmental cabinet (Sanyo-MLR-351, OxRBL, Oxford) and ran for 90 cycles in total.

6.2.3. Weight change monitoring

To quantify the deterioration induced by the salt ageing test, the variation of specimens' weight was monitored during the experiment. The changing weights were measured and recorded at the beginning of the entire experiment (the initial dry weight, m_0) and immediately after each experimental step (after the operation of salt impregnation (m_1), after 30 ageing cycles (m_2), after 90 cycles (m_3), after the physical clearance of salt efflorescence & rock debris through gently brushing (m_4), after the water absorption coefficient test (WAC) (m_5) and after the open porosity test (m_6)) (see Figure 6.1).

Weight loss (DWL) of individual specimen was calculated after each weight measurement. In order to present the successive weight loss of specimens in which the lost material includes both salt crystals and rock particles, the dry weight of the impregnated salt (m_s) was included in the initial dry weight of specimens for the calculation. DWL was calculated by the following formula:

$$DWL_x = [(m^* - m_x)/m^*] \cdot 100,\ x=1,2,3,4,5,6,$$

$$m^* = m_0 + m_s,$$

$$m_s = (m_1 - m0) \cdot C \cdot M_s$$

DWL: Weight loss of specimen, (%),

m_0, Initial dry weight of specimen, (g),

m_s: The dry weight of the impregnated salt, i.e. salt uptake, (g),

m: Gross weight of specimen, (g),*

m_x: Changing weight of specimen during the experiment, x=1,2,3,4,5,6, (g),

C: Salt concentration, (mol/kg),

M_s: Molar mass of salt (kg/mol).

6.2.4. Measurement of petrophysical properties

In order to evaluate the impact of salt weathering on the sandstone samples, the following measurements were taken on control samples and salt contaminated samples after the salt ageing test: surface hardness, pulse velocity (P-wave), water absorption coefficient by capillarity (WAC), open porosity and apparent density. The measurements were made in that order as the WAC, open porosity and apparent density measurements required immersion in water, which is likely to affect the distribution of salts within the samples.

Surface hardness measurements were taken with a Proceq Equotip 550 Leeb with C probe (OxRBL, Oxford), used as a proxy for strength (Wilhelm *et al.,* 2016, Desarnaud *et al.,* 2019). Two sets of surface hardness values were obtained and calculated based on the two measurement methods introduced by Aoki and Matsukura (2007). The first set of hardness value includes 10

rebound readings obtained through randomly hitting different points across the exposed vertical surface, and calculating the mean of the 10 rebound reading to represent the surface hardness of the specimen (SIM). The second set of hardness value includes 20 rebound readings obtained through repeatedly hitting the same point, and selecting the top 3 out of the 20 readings and calculating the average of the selected top 3 readings to represent the intact hardness of the specimen (RIM).

Ultrasonic pulse velocity (p-wave/ longitudinal wave velocity) measurements were taken using a Proceq Pundit® Lab+ (OxRBL, Oxford) to indicate interior structural changes induced by salt weathering such as void ratio changes and/or cracks growth, porosity variation etc. (Weiss *et al.,* 2002, Warke, 2007, Kahraman and Yeken, 2008). Measurements were conducted with the direct arrangement of two p-wave transducers (a transmitter and a receiver) on two opposite vertical faces on the two sides of the open face to ensure maximum signal transmission under 54 KHz with a transmit time of 25.4 μs (Proceq, 2014). One measurement was obtained from each sandstone sample.

Water absorption coefficient through capillarity, open porosity and apparent density were measured with the water flux perpendicular to the bedding planes following the standardizing test protocols BS EN 1925:1999 and BS EN 1936:2006.

After obtaining all values of petrophysical properties, a Mann-Whitney U-test, which is a nonparametric test widely used in rock weathering studies (e.g. Gómez-Pujol *et al.,* 2006, Dragovich and Egan, 2011, Cabello-Briones and Viles, 2017), was applied to test for significant differences between control and ageing groups.

6.3. Results

6.3.1. Changes in appearance

The exposed vertical faces of the sandstone samples in each salt contamination groups show consistent changes and deterioration patterns, so one sample was selected from each group to present in Figure 6.3. As shown in Figure 6.3, the three soluble salts have varying effects on the appearance of the vertical exposed surface of the sandstone samples, with LS exhibiting

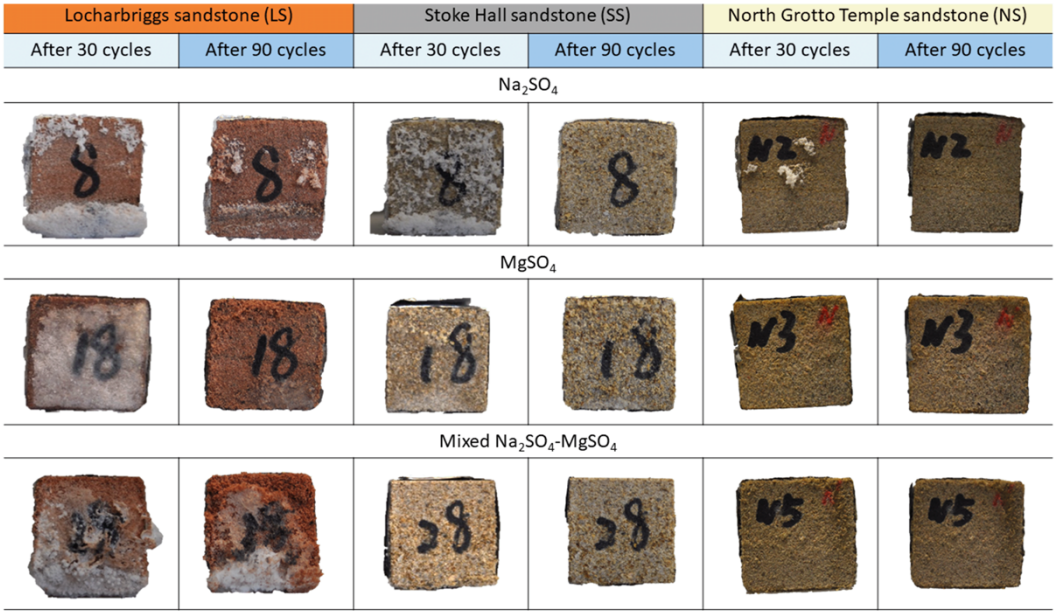

Figure 6.3. Surface changes of the three types of sandstone

the most evident changes, meanwhile, NS and SS show relatively slighter visual changes on their exposed vertical surface, except for a higher amount of salt efflorescence precipitating on the surface of the Na_2SO_4 contaminated groups.

For the LS contaminated by Na_2SO_4 solution, efflorescence, identified as 77% thernardite, 14% gypsum and 9% quartz through XRD (see Table 6.1), was observed on the sandstone vertical surface after 30 ageing cycles and primarily precipitated at the bottom and the top corners, covering 37.5% of the surface. The efflorescence was loosely bound to the surface and could easily be removed by touching. The vertical LS surface was re-exposed after 90 ageing cycles as the majority of efflorescence naturally dropped off the surface during the experiment, and the coverage of the precipitation of sodium sulfate on the surface decreased to 18.8%. Only slight granular disintegration, of a

Table 6. 1. Minerological identifications of efflorescences from sandstone samples subjected to experimental ageing (XRD data)

Stone type	Salt type	Bulk Mineralogy									
		Quartz (%)	Feldspars (%)	Thernardite (%)	Epsomite (%)	Gypsum (%)	Aragonite (%)	Hexahydrite (%)	Muscovite /Biotite (%)	Kaolinite (%)	Chlorite (%)
LS	Na_2SO_4	9		77		14					
LS	$MgSO_4$	8		6	83		3				
LS	mixed	8		6	68			18			
SS	Na_2SO_4	16	tr	75					9	tr	tr

Note: LS- Locharbriggs sandstone, SS- Stoke Hall sandstone, tr- trace

mixture of white salt crystals and brownish-red sandstone grains, could be observed on the upper and bottom edges of the sample surface.

A glossy hard milky-white crust formed after 30 ageing cycles on the LS sample contaminated by $MgSO_4$ solution, which was tightly bonded to the surface and covered 87.5% of the surface. The crust was composed of 83% epsomite, 6% thernardite, 3% aragonite and 8% quartz (identified by XRD, see Table 6.1). After 90 ageing cycles, the crust disappeared, and evident granular disintegration was visible near the edges of the vertical surface.

Cauliflower-like efflorescence showed on the vertical surfaces of the LS samples which were contaminated with mixed Na_2SO_4-$MgSO_4$ solution and was maintained to the end of the salt ageing test. The efflorescence mainly consisted of 68% epsomite, 18% hexahydrite, 6% thernardite and 8% quartz (identified by XRD, see Table 6.1). In the late stage of the ageing test, flaking and peeling occurred, producing a newly soft vertical surface comprising loosely-attached rock grains.

For SS, efflorescence, mainly consisting of thernardite (identified by XRD, see Table 6.1), initially appeared after 30 cycles only on the vertical surfaces of samples contaminated with Na_2SO_4 solution covering most area of the surface, and the exfoliating. Neither crusting nor efflorescence were observed on the surfaces of the SS samples contaminated by the $MgSO_4$ solution and the mixed solution during and after the ageing test. But, granular disintegration

was clearly observed on these specimens, with the $MgSO_4$-contaminated group showing the most loose grains on the upper edge of the vertical surface.

Only small amounts of efflorescence formed on the vertical surface of NS samples contaminated by Na_2SO_4 solution after 30 cycles and then exfoliated leaving near pristine surfaces. No other visible deterioration patterns, except slight sanding, could be identified on the vertical surface of the rest of NS samples which were contaminated by $MgSO_4$ solution and mixed Na_2SO_4-$MgSO_4$ solution respectively. Overall, negligible changes formed on the vertical surface of the NS samples.

6.3.2. Weight changes during the experiment

Weight changes for each sandstone in each saline solution treatments are depicted in Figure 6.4. As shown in the figure, all three types of sandstone samples initially gained additional weight ($DWL_1 < 0$) due to salt impregnation, with LS absorbing a greater amount of salt than others (see Table 6.2). Afterwards, weight loss took place but varying loss rates were observed on sandstone specimens in different saline solution treatment groups, with the weight of LS dropping more rapidly than NS and SS.

During the ageing test, the weight loss rate was much faster in the first 30 ageing cycles (DWL_2) and slowed down in the following 60 cycles (DWL_3). The drying process of specimens happened in the early stage of ageing test, i.e. the first 30 ageing cycles, in which water evaporation and initial crystallization

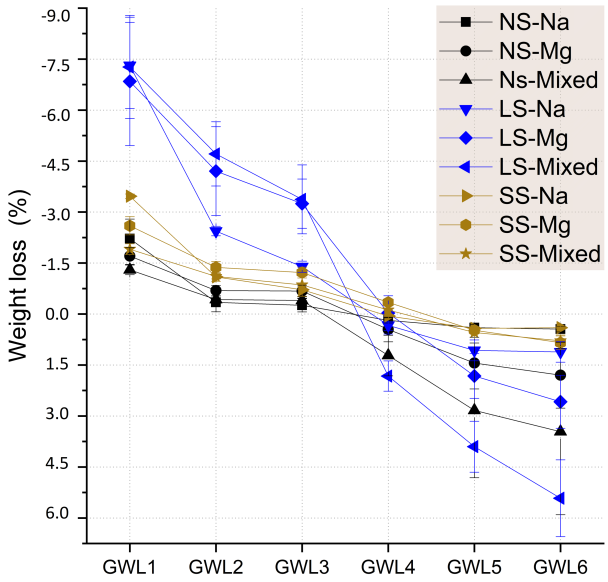

Figure 6.4. Continuous weight loss (DWL%) experienced by the three types of sandstone in each saline solution treatment group during the experiment (DWL_1- after salt impregnation, DWL_2-after 30 ageing cycles, DWL_3-after 90 ageing cycles, DWL_4-after removal of efflorescence and debris, DWL_5-after water absorption coefficient test, DWL_6-after open porosity test.)
(Note: 1. Graphed values for Locharbriggs sandstone (LS) and Stoke Hall sandstone (SS) are average of 4 specimens of each treatment. Values for North Grotto Temple sandstone (NS) are average of 2 specimens of each treatment. 2. -Na: specimen contaminated by sodium sulfate, -Mg: specimen contaminated by magnesium sulfate, -Mixed: specimen contaminated by mixture of sodium sulfate & magnesium sulfate.)

of salt occurred. Hence the reduced weight at this stage was more likely caused by loss of moisture evaporated from the specimen. With the RH and T oscillation, the following 60 cycles facilitated the process of salt deliquescence-dissolution-recrystallization/hydration. It is worth noting that weight loss was negligible in NS and SS compared with LS in the following 60 cycles which implies a smaller degree of deterioration on NS and SS. Weight loss of all samples continued after the removal of the efflorescence and debris ($DWL_4 > 0$) and progressively increased after the standard WAC test (DWL_5) and open porosity & apparent density test (DWL_6). The sudden exacerbation of weight loss is probably due to the application of liquid water during the two

standardizing tests, which may wash out the salt crystals and loosen grains inside and outside the sandstones and/or induced further deterioration through osmotic swelling of the sandstone matrix and/or hydration of salt crystals through wetting process (Steiger *et al.,* 2011), consequently resulting in greater weight loss.

Table 6.2. Gravimetric salt content (%) of the three types of sandstone after each saline solution treatment

Salt types	Concentration (mol/kg)[1]	salt uptake (wt%)[2]		
		NS	LS	SS
Na_2SO_4	0.96	0.42	0.9	0.47
$MgSO_4$	2.90	0.42	2.18	0.92
Mix- [3]	1.50/2.49	0.46	3.37	0.99

1. *Under the temperature of 20 °C.*
2. *Absorbed salt content as percentage of the initial dry weight of sandstone samples. (values are average of 2 NS samples of each treatment and average of 4 LS and SS samples of each treatment)*
3. *Mix-: Mixture of Na_2SO_4 & $MgSO_4$*

6.3.3. Petrophysical properties

Petrophysical properties of the sandstone samples are listed in Table 6.3. Mann-Whitney U-test results (see Table 6.4) illustrate statistically significant declines in both hardness (SIM) and intact hardness (RIM) after the ageing test for LS and NS samples contaminated with $MgSO_4$ and the mixture of Na_2SO_4-$MgSO_4$ and the SS samples contaminated with $MgSO_4$. The mixture of Na_2SO_4-$MgSO_4$ yielded a significant drop in the intact hardness of SS but

no significant difference in surface hardness. Sodium sulfate caused no significant difference in hardness on all three types of sandstones.

The p-wave velocities (V_P) of LS and SS contaminated with Na_2SO_4 significantly increased after the salt ageing test. Similar increases were found in the SS contaminated with the mixture of Na_2SO_4 & $MgSO_4$. This could be as result of crystalline salts forming and precipitating inside the pores, simultaneously causing a reduction in open porosity as shown in Table 6.3 (Angeli *et al.,* 2007). NS contaminated with the mixture of Na_2SO_4 & $MgSO_4$ showed a significant decrease in V_P. This may be due to the interior microstructural changes of the specimens, such as crack growth (Akin and Özsan, 2011, Sun and Zhang, 2019).

No significant differences were found in the WAC, apparent density and open porosity of LS and NS after the ageing test (Table 6.3). The connected pores of all SS samples treated by three salt types were clogged by salt crystals after the ageing test, resulting in a significant decline in the value of open porosity (Table 6.3). Furthermore, $MgSO_4$ and the mixture of Na_2SO_4 & $MgSO_4$ created a significant increase in apparent density and decrease in WAC to SS.

Table 6.3. Petrophysical properties of three sandstone types of each saline solution treatment and control group specimens

Stone type	Salt type	SIM (HL)		RIM (HL)		V_P (m/s)		WAC ($g/m^2 \cdot s^{0.5}$)		Apparent density (kg/m^3)		open porosity (%)	
		MEAN	(SD)	MEAN	(SD)	MEAN	(SD)	MEAN	(SD)	MEAN	(SD)	MEAN	(SD)
NS	Control	538.43	(35)	698.39	(12)	3758	(515)	4.30	(0.9)	2551	(10)	3.76	(0.3)
	Na_2SO_4	558.40	(7)	711.00	(11)	4412	(0)	1.90	(0.1)	2554	(5)	3.41	(0.1)
	$MgSO_4$	361.65	(8)	500.67	(74)	3161	(100)	5.42	(2.0)	2533	(9)	3.73	(0.0)
	Mixture	314.35	(50)	421.33	(150)	2760	(301)	4.01	(0.3)	2530	(10)	3.71	(0.2)
LS	Control	421.93	(32)	680.00	(10)	2509	(159)	10.15	(13.4)	2062	(79)	20.61	(2.8)
	Na_2SO_4	438.85	(16)	660.08	(43)	2869	(235)	36.76	(23.7)	2115	(85)	16.81	(3.0)
	$MgSO_4$	316.13	(33)	577.00	(30)	2810	(218)	96.95	(90.2)	2091	(65)	16.80	(1.9)
	Mixture	274.73	(19)	509.67	(62)	2751	(94)	48.11	(27.6)	2092	(62)	15.84	(2.4)
SS	Control	552.80	(13)	690.42	(41)	3139	(154)	41.08	(2.1)	2339	(6)	10.28	(0.1)
	Na_2SO_4	521.80	(26)	681.08	(44)	3598	(44)	13.74	(2.2)	2360	(29)	9.33	(0.5)
	$MgSO_4$	480.53	(18)	664.17	(18)	3364	(168)	12.50	(0.4)	2358	(3)	7.86	(0.8)
	Mixture	492.33	(59)	683.08	(27)	3739	(171)	11.22	(1.1)	2357	(3)	8.02	(0.5)

1. *NS: North Grotto Temple sandstone, LS: Locharbriggs sandstone, SS: Stoke hall sandstone.*
2. *SIM: surface hardness of the sandstone, RIM: Intact hardness of the sandstone.*
3. *Mixture-: Mixture of Na_2SO_4 & $MgSO_4$*
4. *MEAN: average of 2 NS samples of each treatment and average of 4 LS and SS samples of each treatment.*
   SD: Standard deviation.
5. *V_P : ultrasonic pulse velocity (p-wave velocity).*

Table 6.4. Mann-Whitney U-test results comparing the petrophysical properties of control and salt-contaminated groups of three sandstones.

	LS-Na	**LS-Mg**	**LS-Mix**	**SS-Na**	**SS-Mg**	**SS-Mix**	**NS-Na**	**NS-Mg**	**NS-Mix**
SIM	4	0	0	2.5	0	4	4	0	0
RIM	7	0	0	7	0	0	4	0	0
V_p	1	2	2	0	3	0	2	1.5	0.5
WAC	2	1	2	4	0	0	0	5	3
A-density	5	3	3	4	0	0	5	2	1
O-porosity	2	3	4	0	0	0	2	5	5

1. *U_stat: Mann-Whitney U; U_critical : critical values of the Mann-Whitney U (check from the Mann-Whitney table based on the amount specimens of each saline solution treatmen); A-density: apparent density; O-porosity: open porosity;*
2. *U_stat is calculated between control group and salt-contaminated group;*
3. *For SS and LS, U_critical=1, For NS, U_critical=2.*

6.3.4. The relationship between petrophysical properties and rock breakdown

Correlation coefficients (R) between final weight loss (DWL_6) and rock properties are shown in Table 6.5. A strong negative correlation is calculated between DWL_6 and both parameters of hardness, in which the surface hardness exhibits a stronger negative correlation with DWL_6. It evidently records destructive effects of salt weathering on the strength of the sandstones.

There is a strong positive correlation between DWL_6 and salt uptake (SP) (R=0.84), meanwhile, SP has a moderate correlation with open porosity (R=0.65). This implies that sandstone with a higher porosity is likely to have a

greater capacity to absorb salt, which may in turn cause a greater degree of deterioration.

Table *6.5*. Pearson correlation coefficients (R) between weight loss (DWL) of sandstones and petrophysical properties

	DWL_6	**SIM**	**RIM**	**V_P**	**A-density**	**Open porosity**	**WAC**	**SP**
DWL_6	—							
SIM	-0.87	—						
RIM	-0.78	0.76	—					
V_P	-0.68	0.82	0.63	—				
A-density	-0.46	0.49	0.10	0.65	—			
Open porosity	0.40	-0.45	-0.05	-0.64	-0.97	—		
WAC	0.35	-0.45	-0.18	-0.46	-0.62	0.58	—	
SP	0.84	-0.74	-0.42	-0.59	-0.73	0.65	0.52	—

NOTE: A-density: Apparent density, SP: Salt uptake, of sandstone, WAC: water absorption coefficient, V_P *:* ultrasonic pulse velocity (p-wave velocity).

6.4. Discussion

From the lab simulation, different salts show contrasting effectiveness in terms of rock breakdown. According to the final weight loss values (DWL_6), NS and LS are both susceptible to $MgSO_4$ and the mixed Na_2SO_4-$MgSO_4$, while SS is susceptible to $MgSO_4$. This is consistent with the visual appearance changes observed on the vertical exposed surfaces of the three sandstones.

Despite sodium sulfate having a reputation of being very damaging, greater degrees of deterioration were recorded on the specimens contaminated by magnesium sulfate and the mixture of sodium sulfate & magnesium sulfate than those contaminated with sodium sulfate under the high humidity

conditions in the experiment. The low amount of damage induced by Na_2SO_4 may be partly due to the high humidity (greater than 60% RH) in which the precipitation of sodium sulphate will more likely either occur at the sandstone surface or concentrated in a very narrow subsurface layer of subsurface because of the slow rate of evaporation and low supersaturation ratio (Rodriguez-Navarro and Doehne, 1999). Further, lower uptake of sodium sulfate is another significant factor based on the strong positive correlation between DWL and SP. Salt uptake from a saturated solution greatly depends on the solubility of the salt (Goudie, 1993). Sodium sulfate has the lowest solubility of the three types of salts used here, thus, the salt uptake is least for sodium sulfate. Furthermore, an assumption is that the conversion from thenardite to mirabilite, i.e. hydration of thernardite, did not occur or only happened to a limited extent under the ageing conditions in the experiment, but the process of precipitation and dehydration of mirabilite as well as the process of thernardite dissolution and mirabilite reprecipitation may take place on the stone surface and subsurface, resulting in less damage (Rodriguez-Navarro *et al.,* 2000, Tsui *et al.,* 2003, Steiger and Asmussen, 2008). However, this needs further study since we have no solid evidence showing the phase changes during the experiment, though only thernardite was identified from the collected efflorescences.

Hydration of $MgSO_4$ is thought to have occurred during the experiment because of identified epsomite ($MgSO_4 \cdot 7H_2O$) from the specimens contaminated with $MgSO_4$, generating pressures on the confined pores during

the process of phase changes induced by fluctuation of humidity and temperature, consequently causing rock deterioration (Steiger *et al.,* 2008). Both thernardite and epsomite precipitated from the specimens contaminated with the mixture of Na_2SO_4 & $MgSO_4$ forming more complex precipitation patterns and higher degrees of deterioration. But, it is unclear whether these two types of single salts crystalize out due to incongruent dissolution of bloedite (Lindström *et al.,* 2016).

In addition, as demonstrated in section 3.1, there was no visible efflorescence or crust showing on the vertical exposed surfaces of the NS and SS samples which were contaminated with $MgSO_4$ and the mixture of Na_2SO_4-$MgSO_4$ respectively, but sanding and slight weight loss were observed to have occurred during the experiment. This implies that subflorescence of salts occurred on NS and SS, causing internal disintegration. Apart from the ambient environmental conditions, the properties of saline solution, e.g. surface tension, vapour pressure and viscosity, should influence the location of crystal precipitation (Ruiz *et al.,* 2007). This needs to be taken into account in future research.

6.5. Conclusion

The lab simulation demonstrates that firstly, deterioration of sandstone can be caused by salt weathering under an ageing cycle with relatively high humidity and a modest temperature range using single and mixed salts likely to be found

at sandstone heritage sites in the south area of the Loess plateau in China and northern UK.

Secondly, different types of salts produce differing degrees of breakdown. The sandstones in the experiment were particularly susceptible to magnesium sulfate and the mixture of sodium sulfate & magnesium sulfate under the concentrations and environmental conditions simulated.

Furthermore, sodium sulfate produced very limited impact on the disintegration of the sandstones used in this experiment, which is associated with less salt uptake, surface-prone precipitation and phase conversion under the given environment conditions. And, the deterioration of sandstones in the experiment correlates with salt uptake and porosity. Locharbriggs stone, with the highest porosity, shows the greatest degree of deterioration. Further experiments should be done using other concentrations and combinations of salts, and more information collected on the influence of lithological factors in order to confirm and extend the findings presented here.

Finally, for sandstone built heritage in temperate climates, particularly with high humidity and modest temperature regimes, salt weathering is a cumulative risk factor affecting their preservation. The response of sandstone built heritage to salt weathering will vary depending on the humidity and temperature regimes, rock properties, and saline solution type. Therefore, lab simulations under realistic conditions are necessary to help with risk assessment and formulation

of preventive conservation strategies, such as environmental control for immovable sandstone-built heritage.

7. DISCUSSION

7.1. Synthesis of findings from chapters 4, 5 and 6.

The approaches used in my doctoral research, namely field investigation, computer model predictions, and laboratory analysis and simulation, have been deployed in three phases and have demonstrated:

Phase (a). Through field investigation the prevalent deterioration patterns appearing on the NGT sandstone façade have been identified and a preliminary assessment made of the rock properties on the façade through two pieces of portable non-destructive equipment (Equotip rebound hardness tester and Karsten tube),

Phase (b). Through field investigation, laboratory analyses and computer model prediction the distribution and nature of the mixed soluble salts on the NGT sandstone façade have been identified through the use of in situ poultice extraction, ion chromatography, and salt hazard prediction using the thermodynamic model, ECOS-RUNSALT,

Phase (c). Through laboratory simulation the diverse salt-induced deterioration processes affecting the NGT sandstones and their impacts on the petrophysical properties of the sandstones have been evaluated highlighting the universal impact of salt weathering on the façade of NGT.

The three phases of research are complementary and progressive (see Figure 7.1). The determination results obtained by the NDT methods in phase (a) revealed the effects of differential weathering on NGT sandstone façade, manifesting in the different properties of rocks in the various sedimentary layers, such as differences in hardness and water absorption coefficient, as well as differences in types of deterioration patterns. This complex weathering condition is closely related to the heterogeneous characteristics of the sandstone at NGT and is likely to be found at other large grotto sites carved in sandstone outcrops. The rock properties of different sandstone strata affect the response of the sandstone to weathering agents, and consequently influence the modification of rock properties and the appearance of deterioration patterns. Additionally, for a large sandstone outcrop, the weathering agents acting on the different parts of the sandstone unit may differ according to height above ground level, for example the water/moisture driven by capillarity (Baker *et al.,* 2007). Thus, the weathering processes happening

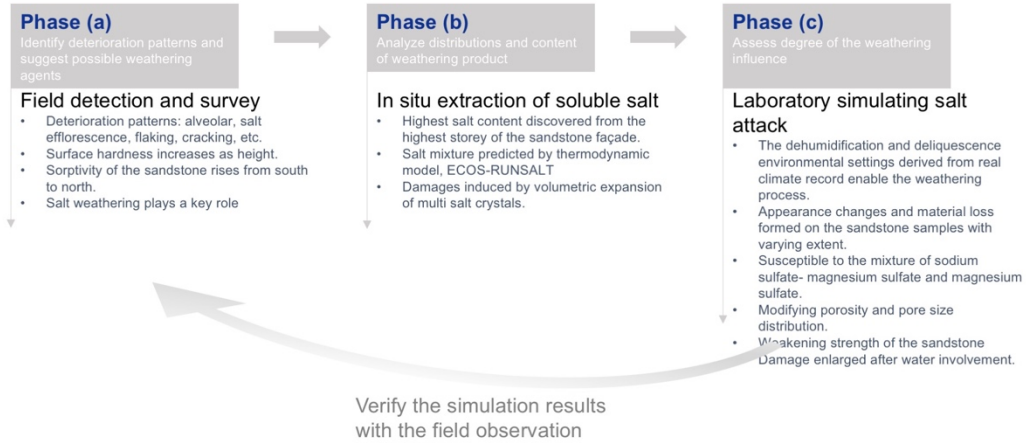

Figure 7.1. Summarized findings from the three research phases and the interrelationship within them

on the rock mass of sandstone cave-temples can become very complicated. Under the combined action of these two factors, i.e. heterogeneity of sandstone and complexity of weathering agents, the deterioration patterns appearing on the rock mass in large sites such as the Cave Temple have become very intricate.

The field survey in phase (a) also revealed that the deterioration phenomenon of alveolar weathering, is widely distributed across the lower sandstone layer (between 1 m and 1.5 m above the ground), while salt efflorescence is found intensively across the lower parts of the sandstone façade (< 0.5m above the ground), and granular disintegration is found widely across the large and small caves and niches in NGT. These deterioration patterns described above conjointly point to the impact of one weathering agent, that is soluble salt.

There are diverse sources of soluble salts which can enter rock pores. Groundwater is one of the main sources and is predominantly driven by capillary force (Dullien and Batra, 1970). The other main sources are irrigation water and rainwater which infiltrates into the caprock through the soil covering above and penetrates deeper into the rock mass through fissures (Li, 2006). Driving rain and condensation water from the atmosphere are other important sources bringing cations and anions into the rock of cave-temples (Guo and Jiang, 2015). After entering the porous rock, repeated processes of crystallization, dissolution, recrystallization and hydration take place under the

fluctuation of environmental temperature and humidity, simultaneously yielding crystallization and hydration pressures on pore walls, which can eventually overcome the forces of cohesion between minerals and producing deterioration.

Sandstone strata situated at different heights on the outcrop can be differentially affected by salt weathering because of difference in access to soluble salt will vary, thereby causing uneven salt distribution and 'boundaries' between areas where salts penetrate and areas where salts do not penetrate. For example, the height of rising damp derived from groundwater usually does not exceed 2 m in stone-built buildings, which is the 'equilibrium line' determined by the depth of the water table, tortuosity of pores and rate of water evaporation at the rock surface (Franzoni, 2014). The permeability of rock also influences the depth that water can infiltrate from the upper strata. In consequence, salt should become distributed across the façade in areas close to frequent entry points depending on the local porosity and permeability.

Through the in situ soluble salt extraction, identification and computer modelling prediction in phase (b) of the research, it can be seen that on the NGT façade higher salt contents are found in the upper layers with a smaller amount of salts in the lower layers. This implies that the main source of soluble salt in the NGT façade is probably irrigation water and rainwater, which infiltrates the loess soil covering above, afterwards partially penetrating into the rock mass through pores and seeping into caves through fissures. The

much lower salt contents detected from the bottom of NGT may have resulted from the construction of drainage channels in front of the façade which act to lower the water table. According to the predictions from the thermodynamic model, the types of soluble salts that appear on the NGT sandstone façade are complex and diverse, including sodium sulfate and magnesium sulfate, which are commonly applied as contaminating salts in laboratory salt durability tests for rock (Sperling and Cooke, 1985, Goudie, 1986). The model also predicted double salts composed of two cations and two anions, such as bloedite ($Na_2SO_4 \cdot MgSO_4 \cdot 4H_2O$) and aphthitalite ($Na_2SO_4 \cdot 3K_2SO_4$). These salt mixtures will lead to a more complicated salt weathering process than single salts (Flatt *et al.,* 2017).

In phase (c), the laboratory simulation test designed based on the findings of phase (b) demonstrated the destructive effect of the soluble salts in the crystallization-deliquescence process under relatively humid environmental conditions representative of those found at NGT. This destructive process significantly indicates a significantly high likelihood of a salt attack occurring on the cave-temples in the Longdong area due to the nature of the sandstone, e.g. nonuniformity, type of cement etc., and the wide range of humidity oscillations in the ambient environment. The sandstone in this area is still capable to access moisture from the earth's atmosphere because of the hygroscopic property, thereby causing repeated dissolution-reprecipitation / recrystallization /hydration of crystalline salt even though the volume of rainfall is limited in this area (Franzen and Mirwald, 2009, Godts *et al.,* 2017, Sato and

Hattanji, 2018). Moreover, the lab simulation results showed that both $MgSO_4$ and the mixed salt Na_2SO_4-$MgSO_4$ had stronger damaging effects on the sandstones than Na_2SO_4 that is commonly acknowledged as the most damaging soluble salt to porous materials and widely applied in standardizing test protocols, e.g. BS EN 12370 and RILEM MS-A.1., for assessment of resistance of the materials to salt. This indicates that salt susceptibility of the sandstone would differ as changes of environmental conditions. It, therefore, points out the significance of the local environmental conditions in determining the extent of deterioration induced by salt weathering.

Furthermore, in the lab experiment salt weathering has three main consequences: it affected the appearance of the sandstone blocks, and caused the material loss and the modificantion of rock properties (such as lowering of surface hardness. These influences were particularly evident in the sandstone samples with high porosity (Locharbriggs sandstone, 20%~23%). In addition, salt uptake was also an important variable affecting the degree of sandstone deterioration based on the strong correlation (R = 0.84) between salt uptake and damage degree (as measured by weight loss). Accordingly, the results of the experiment indicate that salt weathering under humid conditions could also cause damage to sandstone heritage in temperate maritime climates, such as in the northern UK.

7.2. Risks to North Grotto Temple (NGT)

Based upon the field investigation, computer modelling and lab simulation, the preservation of NGT has clearly been shown to be threatened by sandstone deterioration, with different degrees of deterioration found in different parts of the facade. According to the findings in Chapter 6, greater weight loss was found on the sandstone samples with relatively high porosity (Locharbriggs sandstone), which implies that the sandstones in the upper layers at NGT are more susceptible to salt weathering because these sandstones also have higher porosities. This variation of porosity at different heights on the façade of rock-hewn cave-temples is associated with sediment compaction during sandstone diagenesis, which commonly results in decreasing porosity as burial depth increases (Magara, 1980, Lander and Walderhaug, 1999, Bjørlykke, 2014). There are, therefore, likely to be higher risks of damage caused by salt weathering in the upper layers of NGT.

Observation of deterioration patterns during the lab simulation found that granular disintegration and salt efflorescence are the two dominant patterns. This echoes the field observations of massive detachment of sand grains from the ceiling of 165 cave introduced in section 3.1.3. Furthermore, previous evidence (Wang, 2002) pointed out that the peaks in the amount of sand detaching from the cave roof are related to the occurrence of weather events such as heavy rain storms. This might be related to the impact of water derived from rainfall accelerating the deterioration of salt-contaminated sandstone, as suggested by the laboratory experiment in phase c, in which weight loss was accelerated by the re-introduction of liquid water. It is therefore worth noting

that blocking the contact between the NGT sandstone, especially the upper layers, and water, such as rainfall, is likely to be a necessary step to reduce the risk of salt weathering.

In addition, conservation practices, especially the utilization of a wide range of conservation materials such as concrete, mortar, and chemical materials in NGT's previous consolidation program, have great potential to influence the rock properties, moisture flow within pores and salt content inside the bedrock, and consequently affect the ongoing preservation of NGT. A thorough evaluation of the impacts of past conservation strategies should be carried out in future. Furthermore, for a comprehensive risk assessment for NGT, catastrophic risks, like earthquake, flooding, should also be evaluated by experts in geology, seismology, meteorology etc.

7.3. Risks to preservation of sandstone cave-temples in Longdong region

Based upon the research on the deterioration of the North Grotto Temple, the representative cave-temple in the Longdong region, it implies that the decay of sandstone cave-temples in this region can be summarized as being associated with the following influences (see Figure 7.2):

The first is salt weathering which process leads to slow, but irreversible loss of components of the rock, i.e. mineral grains and matrix, and significant modification of the properties of the remaining sandstone, such as rock

strength, open porosity, water absorption coefficient etc., It also damages the surficial appearance of the cave-temples due to the formation of deterioration patterns, e.g. crust, crack, efflorescence etc., on the outer surface of the rock sculptures and cave structures.

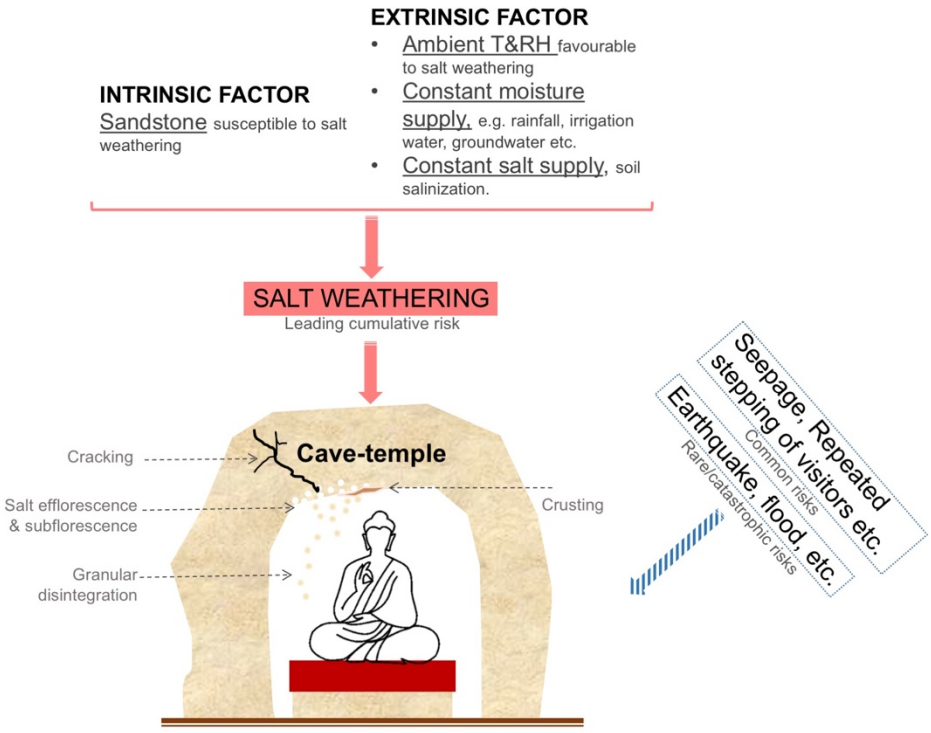

Figure 7.2. Risks threatening the preservation of the sandstone cave temples in Longdong region

The second is natural hazards, such as earthquake and flooding. Such hazards exert destructive power that can destroy the integrity of the rock structure instantaneously, although they occur infrequently. The occurrence of these catastrophic events can promote the development of internal rock fractures, destabilize the structure, and induce rock mass collapse and

structural disintegration (Li, 2006, Parisi and Augenti, 2013, Valente and Milani, 2019). In addition, it may trigger the occurrence of failure on rock cumulatively affected by salt weathering process over the years. For example, heavy rains or flooding may accelerate the dissolution of sandstone that has been severely contaminated with soluble salt.

Finally, it is necessary to pay attention to some situations that constantly occur in daily life, such as water flow over and through the porous sandstone. It will not only soil the rock surface, but also affect the distribution of soluble salt within the rock. The increase in tourists also brings some hidden dangers, such as the compression exerted from tourists during walking on the ground rock which may affect the loose and deteriorated parts of façade due to the vibration caused, and the impact of exhaled carbon dioxide from tourists on the temperature and humidity of the cave environment (Nuryanti, 1996, Brimblecombe and Grossi, 2007, Belsoy et al., 2012).

In a real scenario, the cumulative risk (the first one), catastrophic risk (the second one) and the common risk (the final one) are mutually influential. Common risk determines the rate and distribution of cumulative risk. The occurrence of catastrophic risk may maximize the destructive effect of cumulative weathering in a short time. Furthermore, previous conservation practices are also influential to the preservation of cave-temples. It would be worthwhile to acquire further information regarding the conservation history,

particularly the applied materials and treated locations, and evaluate their effectiveness and impact prior to formulate conservation strategies.

7.4. Implications for the conservation of cave-temples

As a precious components of the world's cultural heritage, rock-hewn cave-temples need proper and sustainable means of conservation to prolong their life. It is, therefore, necessary to carry out a series of scientific and profound studies to obtain comprehensive understanding of the nature of the rock mass, the characteristics of the ancillary environment and the mechanism of the weathering process occurring on the cave-temples. These are important pieces of information to assist site managers and stakeholders manage the risks threatening the site and formulate endurable and feasible conservation strategies.

In accordance with the study on the weathering and deterioration in the North Grotto Temple, a research framework to assess the impact of risks/ weathering agents is summarized below (see Figure 7.3):

First and foremost, surveying the types, distribution and quantity of deterioration phenomena at the heritage site and concluding which are the main actively-forming deterioration phenomena.

As well as field survey, historic documents and daily observations of the site managers and staff are very helpful resources to understand the condition of the cave-temples.

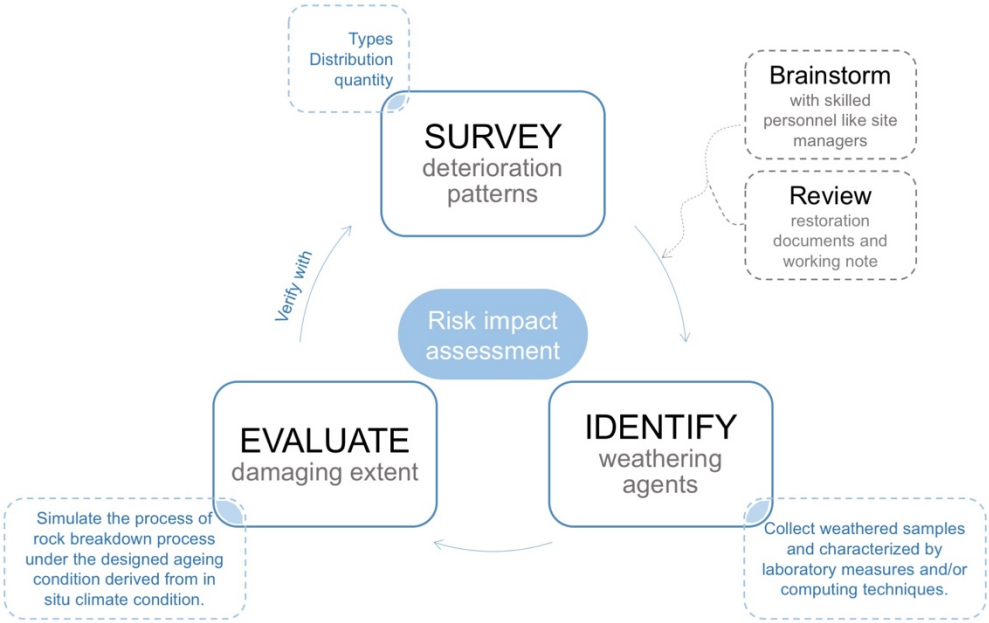

Figure 7.3. Risk impact assessment for study the risks on sandstone cave-temples in Longdong region

Secondly, identifying the possible weathering agents causing the deterioration phenomena found in the field survey. In this step, laboratory characterization techniques and computing modelling are helpful methods to obtain deep understanding of the weathering mechanisms found at the site.

Last but not least, evaluating/quantifying the rate of deterioration caused by the weathering processes by using laboratory simulation ageing tests to mimic the breakdown processes occurring on site.

Ultimately, the evaluation phase results could be compared with findings obtained in the early field survey as well as the evidence from the historical

record (written archives, imagery, oral histories) in order to verify whether the laboratory simulation results reflect the progress of deterioration at the site.

8. CONCLUSIONS

The highly valuable cave-temples in Longdong area, China which represent a high standard of artistic value of Buddhist grotto art in the eastern section of the Silk Road, are under threat from the inevitable processes of weathering synergistically driven by various weathering agents.

From the findings of the research at North Grotto Temple presented in this thesis, salt weathering caused by single and mixed salts appears to play a dominant role in the deterioration of the rock mass in the sandstone cave-temples in the Longdong region. The wide range of fluctuation of humidity and low amounts of precipitation in this region provide favourable climatic conditions for the occurrence of the cycle of crystallization – deliquescence/dissolution/hydration-recrystallization of soluble salt within the pores of the sandstone, leading to damage to the appearance, strength and rock properties of the cave-temples.

As noted at North Grotto Temple, numerous deterioration patterns have formed on the rock mass of the sandstone cave-temples, in which salt-induced deterioration patterns are most evident and prevalent, such as alveolar weathering, salt efflorescence, sanding, granular disintegration, cracking, and crusting. The upper stratum of the sandstone in the cave-temples appears to be the focus of granular disintegration and crack/fissure development derived from more intensive salt weathering there. Because of this, there is a higher risk of collapse of sandstone from these upper layers.

Salt weathering is a leading cumulative risk threatening the long-term preservation of the sandstone cave-temples in Longdong area. However, weathering is a natural, continuous process affecting cave-temples because they are directly carved into the lithosphere and entirely exposed to the atmosphere. It is almost impossible to stop weathering in such a situation and only feasible to mitigate its impacts. Environmental control, therefore, could be a viable method to conserve cave-temples in this region.

Possible environmental control solutions are a) cutting off water/moisture supply to the rock surface, b) reducing fluctuations of ambient temperature and humidity surrounding cave-temples and maintaining them in a constant regime and c) avoiding direct insolation. Other conservation approaches such as d) removing loose salt efflorescence attached on the rock surface, and e) digitalizing the rock Buddha sculptures, inscriptions, niches and cave structures may also be useful.

On the other hand, risk management and site conservation should engage with more disciplines in order to manage all risks to the cave-temples, especially catastrophic risks such as flooding and damaging earthquakes. Their impacts need to be rigorously evaluated considering that they cause rapid, dramatic structural damage as well as triggering effects which can unleash the cumulative impact of stone weathering instantaneously.

In the future, a data base documenting the deterioration extent, petrophysical properties, classification of sandstones from several different

cave-temple sites and salt content of sandstones from a sequence of sedimentary units near the cave-temple could be established.. This would provide a reference for heritage scientists and conservators to evaluate the existing condition of a specific cave-temple.

Study of the hydrogeological conditions of rock-hewn cave-temples would be a very useful direction for future research. The movement and storage of water in the rock masses in which cave-temples are hewn largely determines the extent and speed of deterioration of the cave-temples. Knowledge of the hydrological process and dynamics in the subsurface zone within the rock mass can aid conservation practice. Some well-established computer modesl of ground water flow, such as MIKE SHE (Demetriou and Punthakey, 1998), MODFLOW (McDonald *et al*., 2003) and SPHY (Terink *et al*., 2015), could help address the issue. In addition, many near-surface geophysics measurement techniques, for instance microwave remote sensing, electromagnetic water content sensors etc. can also be supplementary measures to strengthen the predictions gained from computer models (Robinson *et al*., 2008).

In addition, monitoring the weathering rate of different parts of the sandstone cave-temples would provide helpful information, and could be done by measuring the surface recession and detecting the change of the width of fissures every year. Furthermore, it would be important to study the influence of complex modern conservation measures, such as cements, chemical consolidants etc. on the preservation of the sandstone cave-temple.

BIBLIOGRAPHY

Akhurst MC, Monro SK. Excursion 9. 1996. In Stone P (ed.), Geology in south-west Scotland: an excursion guide. Keyworth, Nottingham: British Geological Survey.

Akin M, Özsan A. 2011. Evaluation of the long-term durability of yellow travertine using accelerated weathering tests. Bulletin of Engineering Geology and the Environment 70(1): 101-114.

Alves C, Figueiredo C, Maurício A. 2017. A critical discussion of salt weathering laboratory tests for assessment of petrological features susceptibility. *Procedia Earth and Planetary Science* 17: 324-327.

Angeli M, Bigas JP, Benavente D, Menéndez B, Hébert R, David C. 2007. Salt crystallization in pores: quantification and estimation of damage. *Environmental Geology* 52(2): 205-213.

Aoki H, Matsukura Y. 2007. A new technique for non-destructive field measurement of rock-surface strength: an application of the Equotip hardness tester to weathering studies. *Earth Surface Processes and Landforms* 32(12): 1759-1769.

Aoki H, Matsukura Y. 2008. Estimating the unconfined compressive strength of intact rocks from Equotip hardness. *Bulletin of Engineering Geology and the Environment 67*(1): 23-29.

Archie GE. 1950. Introduction to petrophysics of reservoir rocks. *AAPG Bulletin* 34(5): 943-961.

Arizzi A, Viles H. Cultrone G. 2012. Experimental testing of the durability of lime-based mortars used for rendering historic buildings. *Construction and Building Materials 28*(1): 807-818.

Atakul N, Thaheem MJ, De Marco A. 2014. Risk management for sustainable restoration of immovable cultural heritage, part 1: PRM framework. *Journal of Cultural Heritage Management and Sustainable Development* 4(2): 149-165.

Baker PH, Bailly D, Campbell M, Galbraith GH, McLean RC, Poffa N, Sanders CH. 2007. The application of X-ray absorption to building moisture transport studies. *Measurement* 40(9-10): 951-959.

Bala'awi F, Mustafa MH. 2017. Cultural heritage site under risk: a case study from Petra, Jordan. *Mediterranean Archaeology and Archaeometry* 17(1): 1-14.

Balboni E, Espinosa-Marzal RM, Doehne E, Scherer GW. 2011. Can drying and re-wetting of magnesium sulfate salts lead to damage of stone?. *Environmental Earth Sciences* 63(7-8): 1463-1473.

Baraka-Lokmane S, Main IG, Ngwenya BT, Elphick SC. 2009. Application of complementary methods for more robust characterization of sandstone cores. *Marine and Petroleum Geology* 26(1): 39-56.

Belsoy J, Korir J, Yego J. 2012. Environmental impacts of tourism in protected areas. *Journal of Environment and Earth Science* 2(10): 64-73.

Benavente D, Cueto N, Martínez-Martínez J, Del Cura MG, Cañaveras JC. 2007. The influence of petrophysical properties on the salt weathering of porous building rocks. *Environmental Geology* 52(2): 215-224.

Benavente D, García del Cura MA, Bernabéu A, Ordóñez S. 2001. Quantification of salt weathering in porous stones using an experimental continuous partial immersion method. *Engineering Geology* 59(3-4): 313-325.

Bian JJ, Hao ZX, Zheng Jy., Ge QS, Yin YH 2013. The shift on boundary of climate regionalization in China from 1951 to 2010. *Geographic Research* 32(7): 1179-1187. (in Chinese)

Binda L, Saisi A, Zanzi L. 2003. Sonic tomography and flat-jack tests as complementary investigation procedures for the stone pillars of the temple of S. Nicolò l'Arena (Italy). *NDT & E International 36*(4): 215-227.

Bionda D. 2005. RUNSALT—a graphical user interface to the ECOS thermodynamic model for the prediction of the behaviour of salt mixtures under changing climate conditions. http://science.sdf-eu.org/runsalt/

Bjørlykke K. 2014. Relationships between depositional environments, burial history and rock properties. Some principal aspects of diagenetic process in sedimentary basins. Sedimentary Geology 301: 1-14.

Bosiljkov V, Uranjek M, Žarnić R, Bokan-Bosiljkov V. 2010. An integrated diagnostic approach for the assessment of historic masonry structures. *Journal of Cultural Heritage 11*(3): 239-249.

Breen C, Clegg F, Herron MM, Hild GP, Hillier S, Hughes TL, Jones TGJ, Matteson A, Yarwood J. 2008. Bulk mineralogical characterisation of oilfield reservoir rocks and sandstones using Diffuse Reflectance Infrared Fourier Transform Spectroscopy and Partial Least Squares analysis. *Journal of petroleum science and engineering* 60(1): 1-17.

Brencich A, Campeggio F. 2019. Leeb hardness for yielding stress assessment of steel bars in existing reinforced structures. *Construction and Building Materials 227*: 116570.

Brimblecombe P, Grossi C. 2007. Damage to Buildings from Future Climate and Pollution. *APT Bulletin: The Journal of Preservation Technology* 38(2/3): 13-18.

Bryan K. 1928. Niches and other cavities in sandstone at Chaco Canyon, New Mexico. *Zeitschrift für Geomorphologie* 3: 125-140.

BS EN 12370:1999. Natural stone test methods.Determination of resistance to salt crystallization

BS EN 16302:2013. Conservation of cultural heritage- Test methods- Measurement of water absorption by pipe method.

BS EN 1925:1999. Natural stone test methods- Determination of water absorption coefficient by capillarity. London: British Standards Institution.

BS EN 1936:2006. Natural stone test methods -Determination of real density and apparent density, and of total and open porosity. London: British Standards Institution.

Cabello Briones c. 2013. A methodological approach to evaluate shelter effectiveness for the conservation of archaeological sites. *In Science and Technology for the Conservation of Cultural Heritage* (pp. 53-56). CRC Press.

Cabello-Briones C, Viles HA. 2017. Evaluating the effects of open shelters on limestone deterioration at archaeological sites in different climatic locations. *International Journal of Architectural Heritage 11*(6): 816-828.

Canadian Conservation Institute (CCI), ICCROM. 2016. A Guide to Risk Management of Cultural Heritage. [online] Available at https://www.iccrom.org/sites/default/files/2017-12/risk_management_guide_english_web.pdf

Cardell C, Rivas T, Mosquera MJ, Birginie JM, Moropoulou A, Prieto B, Van Grieken R. 2003. Patterns of damage in igneous and sedimentary rocks under conditions simulating sea-salt weathering. *Earth Surface Processes and Landforms 28*(1): 1-14.

Cassar M, Brimblecombe P, Nixon T, Price C, Sabbioni C, Saiz Jimenez C, Van Balen K. 2001. Technological Requirements for Solutions in the Conservation and Protection of Historic Monuments and Archaeological Remains, Final Study, Working paper for the for the Scientific and Technological Options Assessment (STOA) Unit, European Parliament, PE 303.120/Fin. St. Luxembourg.

Çelik MY, Aygün A. 2019. The effect of salt crystallization on degradation of volcanic building stones by sodium sulfates and sodium chlorides. Bulletin of Engineering Geology and the Environment 78(5): 3509-3529.

Çelik SB. 2019. Prediction of uniaxial compressive strength of carbonate rocks from nondestructive tests using multivariate regression and LS-SVM methods. *Arabian Journal of Geosciences* 12(6): 193.

Ceniceros RP, Martínez JP, Marín MH, Lozano JÁO, Tapia EEO. 2019. Internal Geometrical Characterization of Stone Masonry Walls Using Electrical Resistivity Tomography. In *Structural Analysis of Historical Constructions* (pp. 644-651). Springer, Cham.

Chan WT. 1957. Transformation of Buddhism in China. *Philosophy East and West* 7(3/4): 107-116.

Charola AE. 2000. Salts in the deterioration of porous materials: an overview. *Journal of the American institute for conservation* 39(3): 327-343.

Chen J. 2012. The third national general investigation of cultural heritages was successfully completed, [online] Available at http://www.ncha.gov.cn/art/2012/7/24/art_722_107377.html (in Chinese)

Chen W, Liao R, Wang N, Zhang J. 2019. Effects of experimental frost–thaw cycles on sandstones with different weathering degrees: a case from the

Bingling Temple Grottoes, China. *Bulletin of Engineering Geology and the Environment* 78(7): 5311-5326.

China National Petroleum Corporation (CNPC), n.d. Ordos Basin (Brochure), https://www.cnpc.com.cn/en/brochures/brochures_index.shtml

Cooke RU, Smalley IJ. 1968. Salt weathering in deserts. *Nature 220*(5173): 1226-1227.

Cooke RU. 1979. Laboratory simulation of salt weathering processes in arid environments. *Earth Surface Processes 4*(4): 347-359.

Corvo F, Reyes J, Valdes C, Villaseñor F, Cuesta O, Aguilar D, Quintana P. 2010. Influence of air pollution and humidity on limestone materials degradation in historical buildings located in cities under tropical coastal climates. *Water, air, and soil pollution 205*(1-4): 359.

Cui H. 2012. Study on the current state of rock leakage in the North Grotto Temple. *The Silk Road* (12): 58-59. (In Chinese)

Cutler NA, Viles HA, Ahmad S, McCabe S, Smith BJ. 2013. Algal 'greening'and the conservation of stone heritage structures. *Science of the Total Environment 442*: 152-164.

Demetriou C, Punthakey JF. 1998. Evaluating sustainable groundwater management options using the MIKE SHE integrated hydrogeological modelling package. *Environmental Modelling & Software* 14(2-3): 129-140.

Desarnaud J, Kiriyama K, Bicer Simsir B, Wilhelm K, Viles H. 2019. A laboratory study of Equotip surface hardness measurements on a range

of sandstones: What influences the values and what do they mean?. *Earth Surface Processes and Landforms 44*(7): 1419-1429.

Doehne E. 2002. Salt weathering: a selective review. *In Siegesmund S, Weiss T, Vollbrecht A (Eds), Natural stone, weathering phenomena, conservation strategies and case studies, Geological Society, London, Special Publications 205*(1): 51-64.

Dragovich D, Egan M. 2011. Salt weathering and experimental desalination treatment of building sandstone, Sydney (Australia). *Environmental Earth Sciences 62*(2): 277-288.

Du J, Guo Sh, Chen Sh, Guo Q, Chen J, Yu Sh. 2017. Experimental study of crack initiation in wall-paintings of Mogao Grottoes, *Rock and Soil Mechanics* 38(1): 11-25. (in Chinese)

Duan Y, Wang CY, Zheng CY, Wu BX, Zheng GD. 2008. Geochemical study of crude oils from the Xifeng oilfield of the Ordos basin, China. *Journal of Asian Earth Sciences* 31(4-6): 341-356.

Dullien FA, Batra VK. 1970. Determination of the structure of porous media. *Industrial & Engineering Chemistry* 62(10): 25-53.

Dunhuang Research Academy (DRA), Gansu Cultural Heritage Administration (GCHA). 2011. Gansu cave-temples, Gansu Education Publishing house, Lanzhou, China. (in Chinese)

Dunhuang Research Academy (DRA), Gansu Cultural Heritage Administration (GCHA). 2011. Gansu cave-temples, Gansu Education Publishing house, Lanzhou, China. (in Chinese)

Egartner I, Sass O. 2016, April. Investigation of salt distribution in porous stone material using paper pulp poultices under laboratory condititions and on site. In EGU General Assembly Conference Abstracts (Vol. 18).

EN 12370:1999, Natural stone test methods: Resistance to salt crystallization, 1999.

English Stone Forum (ESF). 2018. The building stone industry in Britain past and present. https://englishstone.org.uk/Dimension_stone.html (accessed 09 Oct 2020).

Erić S, Matović V, Kremenović A, Colomban P, Batoćanin DS, Nešković M, Jelikić A. 2015. The origin of Mg sulphate and other salts formed on pure calcium carbonate substrate–Tufa stone blocks built into the Gradac Monastery, Serbia. *Construction and Building Materials* 98: 25-34.

Favero-Longo SE, Viles HA. 2020. A review of the nature, role and control of lithobionts on stone cultural heritage: weighing-up and managing biodeterioration and bioprotection. *World Journal of Microbiology and Biotechnology* 36(7): 1-18.

Fearnsides WG, Bisat WS, Edwards W, Lewis HP, Wilcockson WH. 1932. The geology of the eastern part of the Peak District. Proceedings of the Geologists' Association 43(2): 153-I81.

Fick SE, Hijmans RJ. 2017. WorldClim 2: new 1-km spatial resolution climate surfaces for global land areas. *International journal of climatology 37*(12): 4302-4315.

Fitzner B, Heinrichs K, La Bouchardiere D. 2003. Weathering damage on Pharaonic sandstone monuments in Luxor-Egypt. *Building and Environment 38*(9-10): 1089-1103.

Flatt RJ, Aly Mohamed N, Caruso F, Derluyn H, Desarnaud J, Lubelli B, Espinosa-Marzal RM, Pel L, Rodriguez-Navarro C, Scherer GW, Shahidzadeh N. 2017. Predicting salt damage in practice: a theoretical insight into laboratory tests. *RILEM Technical Letters* 2: 108-118.

Flatt RJ, Caruso F, Sanchez AMA, Scherer GW. 2014. Chemo-mechanics of salt damage in stone. *Nature communications 5*: 4823.

Fort R, de Buergo MA, Perez-Monserrat E, Varas MJ. 2010. Characterisation of monzogranitic batholiths as a supply source for heritage construction in the northwest of Madrid. *Engineering Geology 115*(3-4): 149-157.

Fort R, de Buergo MA, Perez-Monserrat EM. 2013. Non-destructive testing for the assessment of granite decay in heritage structures compared to quarry stone. *International Journal of Rock Mechanics and Mining Sciences 61*: 296-305.

Franzen C, Mirwald PW. 2009. Moisture sorption behaviour of salt mixtures in porous stone. *Geochemistry 69*(1): 91-98.

Franzoni E. 2014. Rising damp removal from historical masonries: A still open challenge. *Construction and Building Materials* 54: 123-136.

Fu Z, Sun Y. 2019. Investigation of deterioration patterns and conservation strategies of Diaoluosi Grottoes, Datong, Shanxi province. *Industrial Architecture* 3: 24-35. (in Chinese)

Garzanti E. 2019. Petrographic classification of sand and sandstone. *Earth-Science Reviews* 192: 545-563.

Gibeaux S, Vázquez P, De Kock T, Cnudde V, Thomachot-Schneider C. 2018. Weathering assessment under X-ray tomography of building stones exposed to acid atmospheres at current pollution rate. *Construction and Building Materials* 168:187-198.

Girard F, Antoni M, Faure S, Steinchen A. 2008. Influence of heating temperature and relative humidity in the evaporation of pinned droplets. *Colloids and Surfaces A: Physicochemical and Engineering Aspects 323*(1-3): 36-49

Godts S, Hayen R, De Clercq H. 2017. Investigating salt decay of stone materials related to the environment, a case study in the St. James church in Liège, Belgium. *Studies in Conservation* 62(6): 329-342.

Gomez-Heras M, Fort R. 2007. Patterns of halite (NaCl) crystallisation in building stone conditioned by laboratory heating regimes. Environmental geology, 52(2): 259-267.

Gómez-Pujol L, Fornós JJ, Swantesson JO. 2006. Rock surface millimetre-scale roughness and weathering of supratidal Mallorcan carbonate coasts (Balearic Islands). *Earth Surface Processes and Landforms 31*(14): 1792-1801.

Gonçalves TD, Rodrigues JD, Abreu MM. 2006. Evaluating the salt content of salt-contaminated samples on the basis of their hygroscopic

behaviour: Part II: experiments with nine common soluble salts. *Journal of Cultural Heritage* 7(3):193-200.

Gonzalez IJ, Scherer GW. 2004. Effect of swelling inhibitors on the swelling and stress relaxation of clay bearing stones. *Environmental Geology* 46(3-4): 364-377.

Goudie AS, Cooke R, Evans I. 1970. Experimental investigation of rock weathering by salts. *Area 2*(4): 42-48.

Goudie AS, Viles HA, Parker AG. 1997. Monitoring of rapid salt weathering in the central Namib Desert using limestone blocks. *Journal of Arid Environments 37*(4): 581-598.

Goudie AS, Viles HA. 1997. Salt weathering hazards. Wiley.

Goudie AS. 1977. Sodium sulphate weathering and the disintegration of Mohenjo-Daro, Pakistan. *Earth Surface Processes and Landforms 2*(1): 75-86.

Goudie AS. 1986. Laboratory simulation of 'the wick effect'in salt weathering of rock. *Earth Surface Processes and Landforms* 11(3): 275-285.

Guo F, Chen LQ, Xu H, Liu X. 2018. Origin of beaded tafoni in cliffs of Danxia landscapes, Longhushan Global Geopark, South China. *Journal of Mountain Science* 15(11): 2398-2408.

Guo F, Jiang G. 2015. Investigation into rock moisture and salinity regimes: implications of sandstone weathering in Yungang Grottoes, China. *Carbonates and Evaporites* 30(1): 1-11.

Guo F, Jiang G. 2015. Investigation into rock moisture and salinity regimes: implications of sandstone weathering in Yungang Grottoes, China. *Carbonates and Evaporites* 30(1): 1-11.

Guo F. 1989. Chinese Tradition and the Theory of Buddhism Imagery. *Journal of Liaoning University (Philosophy and Social Sciences Edition)*: 94-97. (in Chinese)

Guo H, Zhao J, Suo A, Yang X, Huang B, Ge J. 2006. Response of Agricultural phenospectrum to global climate change in Loess plateau of East Gansu Province, *Journal of Natural Resources* 21(4): 608-614. (in Chinese)

Guo QN, Wang YQ, Guo TW, Liu J, Nan LL, 2008. Relationship between environment factors and topsoil salt accumulation in semi-arid regions in China. *Acta Pedologica Sinica* 45(5): 957-963.

Hall C, Hoff WD, Nixon MR. 1984. Water movement in porous building materials—VI. Evaporation and drying in brick and block materials. *Building and Environment* 19(1): 13-20.

He L, Ma T, Snethlage R, Wendler E. 1997. Investigations of the deterioration and conservation of the Dafosi grotto. *In Conservation of ancient sites on the Silk Road: proceedings of an international conference on the conservation of grotto sites*, Dunhuang, the People's Republic of China, 3-8 October 1993 (pp. 320-328).

He L. 2006. China's provincial administrative divisions in the early days of the founding of the People's Republic of China, *Dangshibocai* 2: 14-20. (in Chinese)

He Z, Gao S, Zheng M. 2015. Regional tectonic framework and evolution of superimposed basins in northwest China, *Earth Science Frontiers* 22(3): 227-240. (in Chinese)

Heinrichs K, 2008. Diagnosis of weathering damage on rock-cut monuments in Petra, Jordan. *Environmental Geology 56*(3-4): 643-675.

Heinrichs K, Azzam R. 2015. Quantitative Analysis of Salt Crystallization–Dissolution Processes on Rock-Cut Monuments in Petra/Jordan. *Engineering Geology for Society and Territory 8:* 507-510.

Hendrickx R. 2013. Using the Karsten tube to estimate water transport parameters of porous building materials. *Materials and structures* 46(8): 1309-1320.

Huang D , Huang RQ. 2010. Physical model test on deformation failure and crack propagation evolvement of fissured rocks under unloading. *Chinese Journal of Rock Mechanics and Engineering* 29(3): 502-512 (in Chinese)

Huang J, Wang J, Gao F, Wang F, Qi Y, Liu S. 2018. Recent Progresses in Sandstone Cave Temples Conservation: A Case Study of Yungang Grottoes, *Southeast Culture* 1: 15-19. (in Chinese)

Huang JZ, Yuan DX. 2004. The impact of water and salt on the stone carvings of the Yungang Grottoes, *Cultural heritage world* 5: 11-15.(In Chinese)

Huang K. 1984. Weathering problem of the sandstone sculptures in Yungang Grottoes. *Hydrogeology & Engineering Geology* 3: 12-15. (in Chinese)

Huang K. 1997. An overview of protection of grottoes in China. *In Conservation of ancient sites on the Silk Road: proceedings of an*

international conference on the conservation of grotto sites, Dunhuang, the People's Republic of China, 3-8 October 1993 (pp. 4-11).

Huang K. 2018. Considering the issues about the conservation of stone heritages. *China Cultural Heritage* 4: 2. (in Chinese)

Huang KZ. 1984. Weathering problem of sandstone sculptures in Yungang Grottoes. *Hydrogeology & Engineering Geology* 3: 10-20. (in Chinese)

Huang WH, Keller WD. 1970. Dissolution of rock-forming silicate minerals in organic acids: simulated first-stage weathering of fresh mineral surfaces. *American Mineralogist: Journal of Earth and Planetary Materials* 55(11-12): 2076-2094.

Hyslop EK, Albornoz-Parra LJ, Fisher LC, Hamilton SL. 2006. Safeguarding Glasgow's stone built heritage skills and materials requirements: facade surveys and building stone analysis. British geological survey geology and landscape northern Britain commissioned report CR/06/077 (issue 1.0).

ICOMOS China. 2015. Principles for the conservation of heritage sites in China, Cultural Relic Press, Beijing.

ICOMOS-China. 2005. Principles for the conservation of heritage sites in China.

ICOMOS-ISCS. 2008. Illustrated glossary on stone deterioration patterns.

ICOMOS. 2011.Guidance on Heritage Impact Assessments for Cultural World Heritage Properties. Paris, France: ICOMOS.

Idema W, Zürcher E, Hulsewé A. 1990. Thought and Law in Qin and Han China: Studies Dedicated to Anthony Hulsewé on the Occasion of His Eightieth Birthday. *Leiden*: 159-162.

Institute for Conservation of Gansu North Grotto Temple (ICGNGT). 2016. Zhang Luzhang Cultural Relics Work Notes, Gansu People's Publishing House, Lanzhou, China (In Chinese)

ISO 31000:2009. Risk Management—Principles and Guidelines. Geneva: International Standards Organisation.

Jaynes SM, Cooke RU. 1987. Stone weathering in southeast England. *Atmospheric Environment* 21(7): 1601-1622.

Jiang G, Guo F, Polk JS. 2015. Salt transport and weathering processes in a sandstone cultural relic, North China. *Carbonates and Evaporites* 30(1): 69-76.

Jiang H, Feng L. 1993. Main problems and their treatment of Xinjiang Grottoes. *Sciences of Conservation and Archaeology* 2: 41-48. (in Chinese)

Kahraman S, Yeken T. 2008. Determination of physical properties of carbonate rocks from P-wave velocity. *Bulletin of Engineering Geology and the Environment 67*(2): 277-281.

Kuchitsu N, Ishizaki T, Nishiura T. 2000. Salt weathering of the brick monuments in Ayutthaya, Thailand. *Engineering Geology* 55(1-2): 91-99.

La Iglesia A, González V, López-Acevedo V, Viedma C. 1997. Salt crystallization in porous construction materials I Estimation of crystallization pressure. *Journal of Crystal Growth* 177(1-2): 111-118.

Labus M, Bochen J. 2012. Sandstone degradation: an experimental study of accelerated weathering. *Environmental Earth Sciences* 67(7): 2027-2042.

Lai WWL, Derobert X, Annan P. 2018. A review of Ground Penetrating Radar application in civil engineering: A 30-year journey from Locating and Testing to Imaging and Diagnosis. *Ndt & E International 96*: 58-78.

Lander R H, Walderhaug O. 1999. Predicting porosity through simulating sandstone compaction and quartz cementation. *AAPG bulletin* 83(3): 433-449.

Leucci G. 2018. *Nondestructive testing for archaeology and cultural heritage: A practical guide and new perspectives*. Springer.

Li B, Pan B, Cheng W, Han J, Qi D, Zhu Ch. 2013. Research on Geomorphological regionalization of China, *ACTA Geographica Sinica*, 68(3): 291-306. (in Chinese)

Li Ch. 1997. A comparative study of Sina-Indian caityagrha. *Buddhist studies* 00: 01-19. (in Chinese)

Li H. 1999. Cradle of North Grotto Temple——the evolution of the establishment and historical events in the upper reaches of the Jinghe River, *Proceedings of North Grotto Temple*, Qingyang Press. (in Chinese)

Li L, Wang SJ, Tanimoto C. 2008. Study of weathering characteristics of sandstone at Longyou grottoes. *Chinese Journal of Rock Mechanics and Engineering* 27(6): 1217-1222. (in Chinese)

Li L, Zhao L. 2014. A kind of hydraulicity oyster ash of restoration and protection stone cultural artifact, CN103880303B. (in Chinese)

Li T, Wang J. 2002. The red sedimentary rock in China and geomorphological type. *Journal of Sichuan Normal University (Natural Science)* 25(4): 427-431. (in Chinese)

Li W. 2006. The relationship between groundwater in North Grotto Temple and the seepage in rock mass of the grotto as well as the groundwater treatment measures, *Dunhuang studies* 4: 109-114. (in Chinese)

Li Wenjun. 2006, Relationship between groundwater in the Northern Grotto Temple and wet seepage of rock mass in the cave and groundwater control measures, *Dunhuang Research* 4: 109-114. (in Chinese)

Li WJ. 2006. The relationship between underground water in the north grotto temple and water permeability of the rock as well as the underground water treatment, *Dunhuang Research* 4: 109-114. (in Chinese)

Li Z. 1992. Preliminary research on investigation of deterioration patterns in Hongqingsi Grottoes and its conservation. *Sciences of Conservation and Archaeology* 1: 9.

Li ZX, Wang X. 2005. Soil site reinforcement agent and reinforcement process, CN1693588A. (In Chinese)

Li ZX. 1985. Application of PS-C on consolidating weathered sandstone sculptures. *Dunhuang Research* 3: 156-168. (in Chinese)

Li ZX. 2010, August. Deterioration and treatment of wall paintings in grottoes along the Silk Road in China and related conservation efforts. In *Conservation of Ancient Sites on the Silk Road: The second International Conference on the Conservation of Grotto Sites*, Magao grottoes, Dunhuang (pp. 46-55).

Li ZY. 1966. Application of polymethacrylate materials to protect stone cultural relics. *Wenwu Cultural Relics* (2): 51-55. (in Chinese)

Lin CY, Wang WG, Dong CM, Zhang XG, Ren LH, Lin JL. 2020. Status Quo of Sandstone Compaction Research and Its Advancement, *Acta Sedimentologica Sinica* 38(3): 538-553. (in Chinese)

Lindström N, Heitmann N, Linnow K, Steiger M. 2015. Crystallization behavior of NaNO3–Na2SO4 salt mixtures in sandstone and comparison to single salt behavior. *Applied Geochemistry* 63: 116-132.

Lindström N, Talreja T, Linnow K, Stahlbuhk A, Steiger M. 2016. Crystallization behavior of Na2SO4–MgSO4 salt mixtures in sandstone and comparison to single salt behavior. *Applied Geochemistry* 69: 50-70.

Linnow K, Zeunert A, Steiger M. 2006. Investigation of sodium sulfate phase transitions in a porous material using humidity-and temperature-controlled X-ray diffraction. *Analytical Chemistry* 78(13): 4683-4689.

Liu F, Huang W. 2014. Geological features of Grottoes in Gansu Province. *Gansu Geology* 23(2): 91-93. (in Chinese)

Liu LC, Dong XF, Wang JH. 2007. Dynamic analysis of eco-environmental changes based on remote sensing and geographic information system: an example in Longdong area of the Chinese Loess Plateau. *Environmental geology* 53(3): 589-598.

Liu M, Liu Z, Liu J, Zhu W, Huang Y, Yao X. 2014. Coupling relationship between sandstone reservoir densification and hydrocarbon accumulation: A case from the Yanchang Formation of the Xifeng and Ansai areas, Ordos Basin. *Petroleum Exploration and Development* 41(2): 185-192.

Liu RZ, Zhang BJ, Zhang H, Shi MF. 2011. Deterioration of Yungang Grottoes: diagnosis and research. *Journal of Cultural Heritage* 12(4): 494-499.

Liu X. 1993. Features of the eastward spread of Buddhism in the period of the Kushan Empire. *South Asian studies* (3): 40-48. (in Chinese)

Lopez-Acevedo V, Viedma C, Gonzalez V, La Iglesia A. 1997. Salt crystallization in porous construction materials. II. Mass transport and crystallization processes. *Journal of Crystal Growth* 182(1-2): 103-110.

López-Arce P, García-Guinea J, Benavente D, Tormo L, Doehne E. 2009. Deterioration of dolostone by magnesium sulphate salt: an example of incompatible building materials at Bonaval Monastery, Spain. *Construction and Building Materials* 23(2): 846-855.

Lu HB, Su DC, Zhang YX, Feng F. 2017. Landform features of salt weathering in different climatic zones in China. *Geological Review* 63(4): 911-926.

Lubelli B, Cnudde V, Diaz-Goncalves T, Franzoni E, van Hees RP, Ioannou I, Menendez B, Nunes C, Siedel H, Stefanidou M, Verges-Belmin V. 2018.

Towards a more effective and reliable salt crystallization test for porous building materials: state of the art. *Materials and Structures* 51(2): 55.

Lubelli B, Van Hees RP. 2010. Desalination of masonry structures: fine tuning of pore size distribution of poultices to substrate properties. *Journal of Cultural Heritage* 11(1): 10-18.

Lubelli B, Van Hees RPJ, Brocken HJP. 2004. Experimental research on hygroscopic behaviour of porous specimens contaminated with salts. *Construction and Building Materials 18*(5): 339-348.

Ludovico-Marques M, Chastre C. 2016. Effect of artificial accelerated salt weathering on physical and mechanical behavior of sandstone samples from surface reservoirs. In *Handbook of Materials Failure Analysis With Case Studies from the Oil and Gas Industry* (pp. 215-233). Butterworth-Heinemann.

Ma Qian. 1994. Main problems in the protection of Maijishan Grottoes and corresponding measures. *Proceedings of the 2005 Yungang International Conference (Conservation Volume)*: 421-429. (in Chinese)

Ma X. 2011. Research on Air Fungus Ecology at Mogao Grottoes in Dunhuang (master's dissertation). Lanzhou University, Lanzhou, China.

Magara K. 1980. Comparison of porosity-depth relationships of shale and sandstone. *Journal of Petroleum Geology* 3(2): 175-185.

Manley EP, Evans LJ. 1986. Dissolution of feldspars by low-molecular-weight aliphatic and aromatic acids. *Soil Science* 141: 106-112.

Matsukura Y, Oguchi CT, Kuchitsu N. 2004. Salt damage to brick kiln walls in Japan: spatial and seasonal variation of efflorescence and moisture content. *Bulletin of Engineering Geology and the Environment* 63(2): 167-176.

Matsuoka N, Murton J. 2008. Frost weathering: recent advances and future directions. *Permafrost and Periglacial Processes* 19(2): 195-210.

McCabe S, Smith BJ, McAlister JJ, Gomez-Heras M, McAllister D, Warke PA, Basheer PAM. 2013. Changing climate, changing process: implications for salt transportation and weathering within building sandstones in the UK. *Environmental Earth Sciences 69*(4): 1225-1235.

McDonald MG, Harbaugh AW. 2003. The history of MODFLOW. *Groundwater* 41(2): 280-283.

Menéndez B, Petráňová V. 2016. Effect of mixed vs single brine composition on salt weathering in porous carbonate building stones for different environmental conditions. *Engineering Geology* 210: 124-139.

Menéndez B. 2017. Estimation of salt mixture damage on built cultural heritage from environmental conditions using ECOS-RUNSALT model. *Journal of Cultural Heritage* 24: 22-30.

Meng TH, Yang CQ, Lu YH, Zhao GZ. 2011. Spectroscopy study of Yungang Grottoes weathered material in terahertz range. *In International Symposium on Photoelectronic Detection and Imaging 2011: Terahertz Wave Technologies and Applications* 8195: 81951C. International Society for Optics and Photonics.

Meybeck M. 1987. Global chemical weathering of surficial rocks estimated from river dissolved loads. *American journal of science* 287(5): 401-428.

Mol L, Gomez-Heras M. 2018. Bullet impacts and built heritage damage 1640–1939. *Heritage Science 6*(1): 35.

Mol L, Viles H. 2013. Exposing drying patterns: using electrical resistivity tomography to monitor capillary rise in sandstone under varying drying conditions. *Environmental earth sciences 68*(6): 1647-1659.

Mol L, Viles HA. 2010. Geoelectric investigations into sandstone moisture regimes: implications for rock weathering and the deterioration of San Rock Art in the Golden Gate Reserve, South Africa. *Geomorphology* 118(3-4): 280-287.

Morillas H, de Mendonça Filho FF, Derluyn H, Maguregui M, Grégoire D, Madariaga JM. 2020. Decay processes in buildings close to the sea induced by marine aerosol: Salt depositions inside construction materials. *Science of The Total Environment* 137687: 1-9.

Mustoe GE. 1983. Cavernous weathering in the Capitol Reef desert, Utah. *Earth surface processes and landforms* 8(6): 517-526.

North Grotto Temple Conservation Institute (NGTCI). 2013. The contents of North Grotto Temple, Cultural Relics Publishing House, Beijing. (in Chinese)

North Grotto Temple Conservation Institute (NGTCI). 2016. Zhang Luzhang's Cultural relics work note. Gansu People's Publishing House. (in Chinese)

Nuryanti W. 1996. Heritage and postmodern tourism. *Annals of tourism research* 23(2): 249-260.

Orkoula MG, Koutsoukos PG. 2001. Dissolution effects on specific surface area, particle size, and porosity of Pentelic marble. *Journal of colloid and interface science* 239(2): 483-488.

Orr SA, Young M, Stelfox D, Leslie A, Curran J, Viles H. 2019. An 'isolated diffusion'gravimetric calibration procedure for radar and microwave moisture measurement in porous building stone. *Journal of Applied Geophysics 163*: 1-12.

Pan Y, Lu D. 2003. Digital Protection and Restoration of Dunhuang Mural. *Journal of System Simulation* 15(3): 310-314.

Pandey SC, Pollard AM, Viles HA, Tellam JH. 2014. Influence of ion exchange processes on salt transport and distribution in historic sandstone buildings. *Applied geochemistry* 48: 176-183.

Pandey SC, Pollard AM, Viles HA. 2017. A simulation study of capillary transport, preferential retention and distribution of salts in historic sandstone buildings. *Environmental Earth Sciences 76*(12): 434.

Paradise TR. 2005. Petra revisited: An examination of sandstone weathering research in Petra, Jordan. *Special Papers-Geological Society of America* 390: 39.

Parisi F, Augenti N. 2013. Earthquake damages to cultural heritage constructions and simplified assessment of artworks. *Engineering Failure Analysis* 34: 735-760.

Peel MC, Finlayson BL, McMahon TA. 2007. Updated world map of the Köppen-Geiger climate classification. *Hydrology and Earth System Sciences* 11: 1633-1644.

Pel L, Sawdy A, Voronina V. 2010. Physical principles and efficiency of salt extraction by poulticing. *Journal of Cultural Heritage* 11(1): 59-67.

Philip JR. 1957. The theory of infiltration: 4. Sorptivity and algebraic infiltration equations. *Soil science 84*(3): 257-264.

Price CA. (Ed.). 2000. An expert chemical model for determining the environmental conditions needed to prevent salt damage in porous materials. European Commission Research Report No 11, (Protection and Conservation of European Cultural Heritage). Archetype Publications, London.

Price CA. 2007. Predicting environmental conditions to minimise salt damage at the Tower of London: a comparison of two approaches. *Environmental Geology* 52(2): 369-374.

Přikryl R, Lokajíček T, Svobodová J, Weishauptová Z. 2003. Experimental weathering of marlstone from Přední Kopanina (Czech Republic)—historical building stone of Prague. *Building and Environment* 38(9-10): 1163-1171.

Proceq SA. 2007. equotip® 3 portable hardness tester operating instructions. Proceq SA, Zurich, Switzerland.

Proceq SA. 2014. Pundit lab/Pundit lab+ ultrasonic instrument operating instructions. Proceq SA, Zurich.

Proceq SA. 2017. equotip® 550 portable hardness tester operating instructions. Proceq SA, Zurich, Switzerland.

Proceq SA. 2019. Portable Hardness Testing Leeb, Portable Rockwell and UCI, Proceq SA, Zurich, Switzerland

Qu JJ, Zhang MQ, Zhang WM. 1995. A preliminary study of weathering process of salt in rock body at Mogao Grottes, Dunhuang. *Geographica Sinica* 15(2): 182-187. (In Chinese)

Rabat Á, Tomás R, Cano M. 2020. Evaluation of mechanical weakening of calcarenite building stones due to environmental relative humidity using the vapour equilibrium technique. *Engineering Geology* 278: 105849.

RILEM TC 127-MS. 1998. MS-A.1—Determination of the resistance of wallettes against sulphates and chlorides. Materials and Structures 31:2–9

RILEM. 1980. Recommended tests to measure the deterioration of stone and to assess the effectiveness of treatment methods, Test V.1a—crystallization test by total immersion (for untreated stone); Test V.1b—crystallization test by total immersion (for treated stone); Test V.2—crystallization test by partial immersion. Materials and Structures 13(75):175–253.

RILEM. 1987. Measurement of Water Absorption Under Low Pressure. RILEM Test Method No. 11.4.

Rivas T, Prieto B, Silva B, Birginie JM. 2003. Weathering of granitic rocks by chlorides: effect of the nature of the solution on weathering morphology. *Earth Surface Processes and Landforms* 28(4): 425-436.

Robinson DA, Binley A, Crook N, Day-Lewis FD, Ferré T PA, Grauch VJS, Slater L. 2008. Advancing process-based watershed hydrological research using near-surface geophysics: A vision for, and review of, electrical and magnetic geophysical methods. *Hydrological Processes: An International Journal* 22(18): 3604-3635.

Rodriguez-Navarro C, Doehne E, Sebastian E. 2000. How does sodium sulfate crystallize? Implications for the decay and testing of building materials. *Cement and concrete research* 30(10): 1527-1534.

Rodriguez-Navarro C, Doehne E. 1999. Salt weathering: influence of evaporation rate, supersaturation and crystallization pattern. *Earth Surface Processes and Landforms* 24(3): 191-209.

Rörig-Dalgaard I. 2014. Determination of the deliquesce point in double salts and in in-situ multicomponent salts with DVS equipment. *In 3rd International Conference on Salt Weathering of Buildings and Stone Sculptures*. KIK-IRPA.

Rosina E, Sansonetti A, Erba S. 2017. Focus on soluble salts transport phenomena: The study cases of Leonardo mural paintings at Sala delle Asse (Milan). *Construction and Building Materials* 136: 643-652.

Rothert E, Eggers T, Cassar J, Ruedrich J, Fitzner B, Siegesmund S. 2007. Stone properties and weathering induced by salt crystallization of Maltese

Globigerina Limestone. *Geological Society, London, Special Publications 271*(1): 189-198.

Ruiz-Agudo E, Mees F, Jacobs P, Rodriguez-Navarro C. 2007. The role of saline solution properties on porous limestone salt weathering by magnesium and sodium sulfates. *Environmental Geology* 52(2): 269-281.

Salmon LG, Christoforou CS, Gerk TJ, Cass GR, Casuccio GS, Cooke GA, Olmez I. 1995. Source contributions to airborne particle deposition at the Yungang Grottoes, China. *Science of the total environment* 167(1-3): 33-47.

Sancho C, Fort R, Belmonte A. 2003. Weathering rates of historic sandstone structures in semiarid environments (Ebro basin, NE Spain). *Catena* 53(1): 53-64.

Sato M, Hattanji T. 2018. A laboratory experiment on salt weathering by humidity change: salt damage induced by deliquescence and hydration. *Progress in Earth and Planetary Science 5*(1): 1-10.

Schaffer RJ. 2016. The weathering of natural building stones. Routledge.

Scherer GW. 2004. Stress from crystallization of salt. *Cement and concrete research* 34(9): 1613-1624.

Shahidzadeh-Bonn N, Rafaı S, Bonn D, Wegdam G. 2008. Salt crystallization during evaporation: impact of interfacial properties. *Langmuir* 24(16): 8599-8605.

Shen Y, Linnow K, Steiger M. 2020. Crystallization behavior and damage potential of Na2SO4–NaCl mixtures in porous building materials. Crystal Growth & Design 20(9): 5974-5985.

Siehr KG. 2014. Immovable cultural heritage at risk: past–present–future*. International Journal of Cultural Property* 21(3): 267-279.

Smith BJ, Gomez-Heras M, McCabe S. 2008. Understanding the decay of stone-built cultural heritage. *Progress in Physical Geography: Earth and Environment* 32(4): 439-461.

Smith BJ, Warke PA, McGreevy JP, Kane HL. 2005. Salt-weathering simulations under hot desert conditions: agents of enlightenment or perpetuators of preconceptions?. *Geomorphology* 67(1-2): 211-227.

Song W. 2006. Decay analysis and preventive treatment of the North Grotto Temple, Qingyang, Gansu, *Proceeding of the International Conference of Yungang, conservation* 1: 116-121. (in Chinese)

Song W. 2006. Decay analysis and preventive treatment of the North Grotto Temple, Qingyang, Gansu*, Proceeding of the International Conference of Yungang, conservation volume*: 116-121. (in Chinese)

Song W. 2009. Consolidation and conservation of 165 cave in North Grotto Temple. Proceedings of North Grotto Temple, Qingyang Press. (in Chinese)

Song WY. 1998. Introduction of North Cave-temple Complex, *Proceedings of North Cave-temple Complex*: 17-27.

Sousa LM. 2014. Petrophysical properties and durability of granites employed as building stone: a comprehensive evaluation. *Bulletin of Engineering Geology and the Environment* 73(2): 569-588.

Sperling CHB, Cooke RU. 1985. Laboratory simulation of rock weathering by salt crystallization and hydration processes in hot, arid environments. *Earth Surface Processes and Landforms 10*(6): 541-555.

Steiger M, Asmussen S. 2008. Crystallization of sodium sulfate phases in porous materials: the phase diagram Na_2SO_4–H_2O and the generation of stress. *Geochimica et Cosmochimica Acta* 72(17): 4291-4306.

Steiger M, Charola AE, Sterflinger K. 2011. Weathering and deterioration. *In Stone in architecture* (pp. 227-316). Springer, Berlin, Heidelberg.

Steiger M, Heritage A. 2012. Modelling the crystallization behaviour of mixed salt systems: input data requirements. In *Proceedings of the 12th International Congress on the Deterioration and Conservation of Stone*. New York, USA. pp.1-13.

Steiger M, Linnow K, Juling H, Gülker G, Jarad AE, Brüggerhoff S, Kirchner D. 2008. Hydration of $MgSO_4 \cdot H_2O$ and generation of stress in porous materials. *Crystal Growth and Design* 8(1): 336-343.

Steiger M. 2005. Crystal growth in porous materials—I: The crystallization pressure of large crystals. *Journal of crystal growth* 282(3-4): 455-469.

Stubbs M. 2004. Heritage-sustainability: developing a methodology for the sustainable appraisal of the historic environment. *Planning Practice & Research* 19(3): 285-305.

Stück H, Koch R, Siegesmund S. 2013. Petrographical and petrophysical properties of sandstones: statistical analysis as an approach to predict material behaviour and construction suitability. *Environmental earth sciences* 69(4): 1299-1332.

Su B. 1978. Periodization research of Yungang Grottoes. *Acta Archaeological Sinica* 1: 25-38. (In Chinese)

Su B. 2019. Studies of Chinese Cave-temple. SDX Joint Publishing Company, Beijing.

Sun D. 2015. A brief history of Chinese ancient architecture. Beijing: Tsinghua University Press. (in Chinese)

Sun Q, Zhang Y. 2019. Combined effects of salt, cyclic wetting and drying cycles on the physical and mechanical properties of sandstone. *Engineering Geology* 248: 70-79.

Svahn H. 2006. Final report for the research and development project non-destructive field tests in stone conservation, literature study, rapport från riksantikvarieämbetet 2006: 3. Riksantikvarieämbetet, Stockholm.

Terink W, Lutz AF, Simons GWH, Immerzeel WW, Droogers P. 2015. SPHY v2. 0: Spatial processes in Hydrology. *Geoscientific Model Development* 8(7): 2009-2034.

The Archaeological Team of Gansu province, CPAM The North Grotto Temple at Qingyang.1985. The North Grotto Temple at Qingyang, Cultural Relics Publishing House, Beijing. (in Chinese)

Tingstad A. 2008. Simulation of salt weathering in a closely replicated coastal environment. *Geografiska Annaler: Series A*, *Physical Geography* 90(2): 165-171.

Tsui N, Flatt RJ, Scherer GW. 2003. Crystallization damage by sodium sulfate. *Journal of Cultural Heritage* 4(2): 109-115.

Tugrul A. 2004. The effect of weathering on pore geometry and compressive strength of selected rock types from Turkey, *Engineering Geology* 75 (3-4): 215–227.

Turkington AV, Paradise TR. 2005. Sandstone weathering: a century of research and innovation. *Geomorphology* 67(1-2): 229-253.

UNESCO 1972. Convention for the protection of the world cultural and natural heritage. General Conference, Seventeenth session, Paris, France. [online] Available at https://whc.unesco.org/en/conventiontext/.

Urzi CE, Krumbein WE, Warscheid T. 1992. On the question of biogenic colour changes of Mediterranean monuments (coating, crust, microstromatolite, patina, scialbatura, skin, rock varnish). The conservation of monuments in the Mediterranean Basin. *Proceedings of the 2nd international symposium*. Genève, 19-21 Novembre 1991 (pp. 397-420).

Valente M, Milani G. 2019. Damage survey, simplified assessment, and advanced seismic analyses of two masonry churches after the 2012 Emilia earthquake*. International Journal of Architectural Heritage* 13(6): 901-924.

Vandevoorde D, Cnudde V, Dewanckele J, Boone M, de Bouw M, Meynen V, Lehmann E, Verhaeven E. 2012. Comparison of non-destructive techniques for analysis of the water absorbing behavior of stone. In *12th International congress on the Deterioration and Conservation of Stone*. New York, USA.

Vergès-Belmin V, Heritage A, Bourgès A. 2011. Powdered cellulose poultices in stone and wall painting conservation-myths and realities. *Studies in conservation* 56(4): 281-297.

Verwaal W, Mulder A. 1993, December. Estimating rock strength with the Equotip hardness tester. In *International Journal of Rock Mechanics and Mining Sciences and Geomechanics Abstracts* 30 (6): 659-662).

Viles HA, Goudie A, Grab S, Lalley J. 2011. The use of the Schmidt Hammer and Equotip for rock hardness assessment in geomorphology and heritage science: a comparative analysis. *Earth Surface Processes and Landforms* 36(3): 320-333.

Viles HA, Goudie AS. 2004. Biofilms and case hardening on sandstones from Al-Quwayra, Jordan. *Earth Surface Processes and Landforms* 29(12): 1473-1485.

Viles HA, Goudie AS. 2007. Rapid salt weathering in the coastal Namib desert: Implications for landscape development. *Geomorphology* 85(1-2): 49-62.

Wang DP, Zhou YY, Ma PG, Tian TH. 2005, Vector properties and calculation model for directional rock permeability, *Rock and Soil Mechanics* 26(8): 1294-1297. (in Chinese)

Wang H. 2002. Analysis of deterioration patterns of North Grotto Temple, *Longyou Wenbo*: 91-92. (in Chinese)

Wang JH, Chen JQ. 2018. Current status and future development of cave temples protection in China. *South Culture* 1: 6-14. (in Chinese)

Wang X, Li Z, Zhao H. 2005. Conservation of the grottoes and earthen architectures on the Silk Road in China. In *15th ICOMOS General Assembly and International Symposium: 'Monuments and sites in their setting - conserving cultural heritage in changing townscapes and landscapes*', 17 – 21 oct 2005, Xi'an, China.

Wang Y. 2018. Notice of the General Office of the CPC Central Committee and the General Office of the State Council on Issuing the opinions on Enhancing the Reform of the Conservation and Utilization of Cultural Heritage, [online] Available at http://www.gov.cn/zhengce/2018-10/08/content_5328558.htm. (in Chinese)

Warke PA, McKinley J, Smith B J. 2006. Variable weathering response in sandstone: factors controlling decay sequences. *Earth Surface Processes and Landforms* 31(6): 715-735.

Warke PA. 2007. Complex weathering in drylands: Implications of 'stress' history for rock debris breakdown and sediment release. *Geomorphology* 85(1-2): 30-48.

Warscheid T, Braams J. 2000. Biodeterioration of stone: a review. *International Biodeterioration & Biodegradation* 46(4): 343-368.

Watt D, Colston B. 2000. Investigating the effects of humidity and salt crystallisation on medieval masonry. *Building and Environment 35*(8): 737-749.

Wedekind W, Ruedrich J. 2006. Salt-weathering, conservation techniques and strategies to protect the rock cut facades in Petra/Jordan. In *Heritage, Weathering and Conservation. Proceedings of the International Heritage, Weathering and Conservation Conference* (pp. 261-268). Taylor & Francis, London.

Wedekind W, Ruedrich J. 2006. Salt-weathering, conservation techniques and strategies to protect the rock cut facades in Petra/Jordan. In: Fort R, Alvarez de Buergo M, Gomez-Heras M, Vazquez-Calvo C (eds) Heritage, Weathering and Conservation. In *Proceedings of the International Heritage, Weathering and Conservation Conference* (pp. 261-268) Taylor & Francis, London.

Weiss T, Rasolofosaon PNJ, Siegesmund S. 2002. Ultrasonic wave velocities as a diagnostic tool for the quality assessment of marble. *Geological Society, London, Special Publications* 205(1): 149-164.

Weiss T, Siegesmund S, Kirchner DT, Sippel J. 2004. Insolation weathering and hygric dilatation: two competitive factors in stone degradation. *Environmental Geology* 46(3-4): 402-413.

Wilhelm K, Viles H, Burke O, Mayaud J. 2016. Surface hardness as a proxy for weathering behaviour of limestone heritage: a case study on dated

headstones on the Isle of Portland, UK. *Environmental Earth Sciences 75*(10): 931.

Wilhelm K, Viles H, Burke Ó. 2016. Low impact surface hardness testing (Equotip) on porous surfaces–advances in methodology with implications for rock weathering and stone deterioration research. *Earth Surface Processes and Landforms 41*(8): 1027-1038.

Wirilander H. 2012. Preventive conservation: A key method to ensure cultural heritage s authenticity and integrity in preservation process. *E-conservation Magazine* 6(24). Retrieved from http://www.e-conservationline.com/content/view/1081

World Commission on Environment and Development (WCED). 1987. Our Common Future, Oxford, Oxford University Press.

Wu Z. 1985. The time when Buddhism was introduced into the Western Regions from the perspective of archaeological remains. *Journal of Dunhuang Studies* 2: 47. (in Chinese)

Yaalon DH. 1982. Salt weathering. In: *Beaches and Coastal Geology. Encyclopedia of Earth Science*. Springer, Boston, MA

Yang Y, Li W, Ma L. 2005. Tectonic and stratigraphic controls of hydrocarbon systems in the Ordos basin: A multicycle cratonic basin in central China. *AAPG bulletin* 89(2): 255-269.

Yu S, Oguchi CT. 2009. Complex relationships between salt type and rock properties in a durability experiment of multiple salt–rock treatments. *Earth Surface Processes and Landforms* 34(15): 2096-2110.

Yuan J, Shi M, Wen X. 2007. Conservation of Yungang Grotto, *China Cultural Heritage* 5(1): 100. (in Chinese)

Zhang B, Wei G, Yang F, Wang X. 2010. Issues and development trend of conservation materials for immovable cultural heritage. *Sciences of Conservation and Archaeology* 22(4): 102-109. (in Chinese)

Zhang C. 2019. Seventy years of the conservation of the cave-temples, [online] Available at http://www.ncha.gov.cn/art/2019/10/23/art_723_157150.html

Zhang J, Huang J, Liu J, Jiang S, Li L, Shao M. 2019. Surface weathering characteristics and degree of Niche of Sakyamuni Entering Nirvana at Dazu Rock Carvings, China. *Bulletin of Engineering Geology and the Environment* 78(6): 3891-3899.

Zhang Sh, Huang K. 2004. Using geophysical technology to explore great stone statue Buddha in Leshan, *Chinese Journal of Engineering Geophysics* 1(3): 226-230. (in Chinese)

Zhang Sh. 1987. Longdong Grottoes, Proceedings of North Grotto Temple, Qingyang Press. (in Chinese)

Zhang W, Wang T, Xue X, Wang W, Guo Y, Liu J. 2000. The Discuss of Comprehensively Preventing Blown-Sand System in Mogao Grottoes, Dunhuang, *Journal of Desert Research* 20(4): 409-414. (In Chinese)

Zhang Z, Liu X. 2013. General Survey of Chinese Regional Culture (Gansu volume), Zhonghua Book Company, Beijing, China. (In Chinese)

Zhang Z, Liu X. 2013. General Survey of Chinese Regional Culture (Gansu volume), Zhonghua Book Company, Beijing, China. (In Chinese)

Zhao L. 2001. Looking back and studying the Kizil Grottoes in the century, Anthology of Dunhuang Studies and Chinese History Studies: Commemorating Mr. Sun Xiushen, Gansu People's Publishing House, Lanzhou, China. (in Chinese).

Zheng J, Yin Y, Li B. 2010. A New Scheme for Climate Regionalization in China. *Acta Geographica Sinica* 65(1): 3-12. (in Chinese)

'Heritage Conservation Defined', Historic England, https://historicengland.org.uk/advice/hpg/generalintro/heritage-conservation-defined/

'SEAHA centre for doctoral training (SEAHA CDT)', University College London (UCL), https://www.ucl.ac.uk/seaha-cdt/about

'World heritage list', United Nations Educational, Scientific and Cultural Organization, World Heritage Convention, https://whc.unesco.org/en/list.

APPENDIX I: Protocol of the laboratory salt ageing test

This experiment protocol was applied in the phase (c) of the research.

a. *Sample and salt solution preparation:*

1. Cutting sandstone samples.

Sandstone types	Size	Amount
NGT sandstone	3 cm × 3 cm × 1.5 cm	12
Locharbriggs sandstone	2.5 cm × 2.5 cm × 2.5 cm	16
Stoke Hall sandstone	2.5 cm × 2.5 cm × 2.5 cm	16

2. Salt solution preparation

- Preparing 100ml saturated **$NaSO_4$ solution** at room temperature

  Solubility of anhydrous $NaSO_4$ at 20 °C: 0.963 mol/kg,

- Preparing 100ml saturated **$MgSO_4$ solution** at room temperature

  Solubility of anhydrous $MgSO_4$ at 20 °C: 2.9 mol/kg.

- Preparing 100ml saturated **mixed Na_2SO_4 - $MgSO_4$ solution**: at 20.7 °C

  Solubility mixed Na_2SO_4 - $MgSO_4$ solution at 20.7 °C :1.50 mol/kg for $NaSO_4$ and 2.49 mol/kg for $MgSO_4$.

b. *Experiment steps:*

Step 1: Drying samples in oven at 60 Celsius until the weight unchanged,

Step 2: Marking each samples and recording their weight,

Step 2: Soluble salt impregnation: Placing samples in respective solution with their bottom side surface until the solution reaching the top surface by capillary sorption.

Step 3: weighting samples and wrapping samples with aluminum foil to left only one face open for evaporation,

Step 4: placing samples into the environmental cabinet (Sanyo-MLR-351, OxRBL, Oxford University)

T&RH settings:

(1) Dehumidification stage: 22 °C, 60% RH, 7 hours;

(2) Deliquescence stage: 16 °C, 85% RH, 15 hours.

Step 5: Monitoring weigh changes after 30 ageing cycles and 90 ageing cycles.

Step 6: Taking out all samples after 90 ageing cycles.

APPENDIX II: Summarized protocol of BS EN1925:1999

Natural stone test Method- Determination of water absorption coefficient by capillarity

a. Experimental steps:

Step 1. Dry rock samples to an accuracy of 0,01 g,

Step 2. Weigh the rock samples (m_d),

Step 3. Calculate the area of the base to be immersed (A),

Step 4. Place the rock samples in the tank on the thin supports *(provided such that they only rest partially on their base)*,

Step 5. Immerse the base of the rock samples in the water to a depth of 1 mm, *(Note: maintain the water level constant throughout the test by adding water as necessary, and close the container with a lid to avoid evaporation of the damp samples.)*

Step 6. Start the timer device,

Step 7. Remove rock samples in succession after 1 minute,

Step 8. Lightly dry the immersed part by using a damp cloth to remove all water droplets,

Step 9. Weigh immediately to the nearest 0.01 g (m_i),

Step 10. Replace in the container and repeat the step 7 to step 10 with time intervals of 3, 5, 10, 15, 30, 60, 120, 180, 240, 480 and 1 440 min.

b. Expression of results

*'Show as a graph the mass of water absorbed in gram divided by the area of the immersed base of the specimen in square metres as a function of the square root of time expressed in seconds' (*BS EN1925:1999*, p. 4)*.

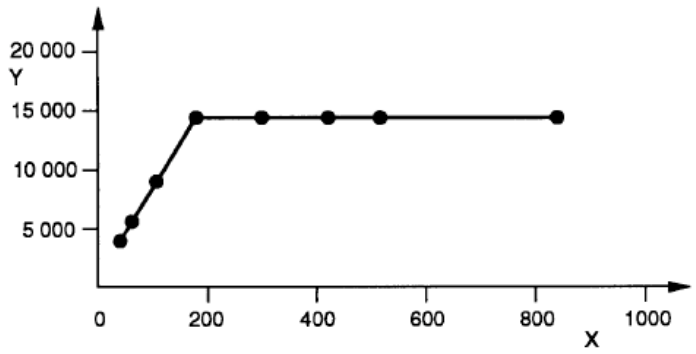

Legend
Y is the water absorption in g/m^2
X is the square root of time in s^{0,5}

Graph **Water absorption by capillarity perpendicular to the planes of anisotropy as a function of the square root of time for a specimen with a low water absorption coefficient (C_1 = 86,0 g/m^2 s^{0,5})**

The coefficient of water absorption by capillarity C ($g/m^2s^{0.5}$) is represented by the slope of the C regression line.

It can be calculated using following formula:

$$C = \frac{m_i - m_d}{A \cdot \sqrt{t}}$$

C: water absorption coefficient by capillary ($g/m^2s^{0.5}$),

m_i: successive masses of the samples during testing (g),

m_d: dry mass (g)

A: area of the immersed face in water (m^2)

t: times elapsed from the beginning of the test (s)

APPENDIX III: Summarized protocol of BS EN 1936:2006

Natural stone test method —Determination of real density and apparent density, and of total and open porosity

a. Experimental steps

Step 1. Weigh dry rock samples (m_d),

Step 2. Put the samples into an evacuation vessel and lower the pressure gradually to (2,0 ± 0,7) kPa = (15 ± 5) mm Hg,

Step 3. Maintain the pressure in the step 2 for (2 ± 0,2) h to eliminate the air contained in the open pores of the rock samples.

Step 4. Slowly introduce demineralized water at (20 ± 5) °C into the vessel until the rock samples completely being immersed (more than 15 min), *Note: maintain the pressure of (2,0 ± 0,7) kPa when introducing water.*

Step 5. Return the vessel to atmospheric pressure While all the rock samples are immersed,

Step 6. Leave the rock samples under water for another (24 ± 2) h at atmospheric pressure,

Step 7. Weigh the rock samples under water (m_h),

Step 8. Lightly wipe the rock samples with a damp cloth and weight the mass of the rock samples saturated with moisture (m_s).

b. Expression of results

The open porosity (p_o) is calculated by the equation:

$$p_o = \frac{m_s - m_d}{m_s - m_h} \times 100$$

The apparent density (ρ_b) is calculated by the equations:

$$\rho_b = \frac{m_d}{m_s - m_h} \times \rho_{rh}$$

p_o: open porosity of the rock sample (%),

m_s: mass of the saturated sample (g),

m_d: mass of the dry sample (g),

m_h: mass of the sample immersed in water (g),

ρ_b: apparent density of the sample (kg/m^3),

ρ_{rh}: density of water (998 kg/m^3, at 20 °C)

APPENDIX IX: Co-authors' statements

These statements act as confirmation by the co-authors involved in each of the three papers contained within this thesis (reproduced as chapters 4, 5 and 6) that the bulk of the work within these papers has been carried out by the author of this thesis.

As a co-author of the following publication (published and/or submitted) I confirm that the first author Yinghong Wang has made a substantive contribution, which includes conceptualisation of the research project, data collection, data analysis, writing and revising the manuscript.

Wang Y, Pei Q, Yang S, Guo Q, Viles H. 2020. Evaluating the Condition of Sandstone Rock-Hewn Cave-Temple Façade Using in Situ Non-invasive Techniques. *Rock Mechanics and Rock Engineering* 53(6):2915-2920.

NAME: Heather Viles, Professor of Biogeomorphology and Heritage Conservation

SIGNATURE:  DATE: 24/9/2020

As a co-author of the following publication (published and/or submitted) I confirm that the first author Yinghong Wang has made a substantive contribution, which includes conceptualisation of the research project, data collection, data analysis, writing and revising the manuscript.

Wang Y, Yang S, Yu Z, Guo Q, Viles H. 2020. Evaluation of the impact of salts on the deterioration of a sandstone rock-hewn cave-temple in NW china through the combination of in situ salt extraction and salt behaviour modelling. *In the proceeding of the 14th International Congress on the Deterioration and Conservation of Stone (*pp.355-360), Göttingen, Germany.

NAME: Heather Viles, Professor of Biogeomorphology and Heritage Conservation

SIGNATURE:  DATE: 24/9/2020

As a co-author of the following publication (published and/or submitted) I confirm that the first author Yinghong Wang has made a substantive contribution, which includes conceptualisation of the research project, data collection, data analysis, writing and revising the manuscript.

Wang Y, Vile H, Desarnaud J, Yang S, Guo Q. 2020. Laboratory simulation of salt weathering under moderate ageing conditions: implications for the deterioration of sandstone heritage in the temperate climates. *Earth Surface Processes and Landforms*, under review.

NAME: Heather Viles, Professor of Biogeomorphology and Heritage Conservation

SIGNATURE:  DATE: 24/9/2020

As a co-author of the following publications (published and/or submitted) I confirm that the first author Yinghong Wang has made a substantive contribution to each of the publications, which includes conceptualisation of the research project, data collection, data analysis, writing and revising the manuscript.

Wang Y, Pei Q, Yang S, Guo Q, Viles H. 2020. Evaluating the Condition of Sandstone Rock-Hewn Cave-Temple Façade Using in Situ Non-invasive Techniques. *Rock Mechanics and Rock Engineering* 53(6):2915-2920.

NAME: Shanlong Yang, Associate research fellow, Dunhuang Research Academy

SIGNATURE: DATE: 19 September 2020

As a co-author of the following publications (published and/or submitted) I confirm that the first author Yinghong Wang has made a substantive contribution to each of the publications, which includes conceptualisation of the research project, data collection, data analysis, writing and revising the manuscript.

Wang Y, Yang S, Yu Z, Guo Q, Viles H. 2020. Evaluation of the impact of salts on the deterioration of a sandstone rock-hewn cave-temple in NW china through the combination of in situ salt extraction and salt behaviour modelling. *In the proceeding of the 14th International Congress on the Deterioration and Conservation of Stone (*pp.355-360), Göttingen, Germany.

NAME: Shanlong Yang, Associate research fellow, Dunhuang research Academy

SIGNATURE: DATE:19 September 2020

As a co-author of the following publications (published and/or submitted) I confirm that the first author Yinghong Wang has made a substantive contribution to each of the publications, which includes conceptualisation of the research project, data collection, data analysis, writing and revising the manuscript.

Wang Y, Viles H, Desarnaud J, Yang S, Guo Q. 2020. Laboratory simulation of salt weathering under moderate ageing conditions: implications for the deterioration of sandstone heritage in the temperate climates. *Earth Surface Processes and Landforms*, under review.

NAME: Shanlong Yang, Associate research fellow, Dunhuang research Academy

SIGNATURE: DATE: 19 September 2020

As a co-author of the following publication (published and/or submitted) I confirm that the first author Yinghong Wang has made a substantive contribution, which includes conceptualisation of the research project, data collection, data analysis, writing and revising the manuscript.

Wang Y, Pei Q, Yang S, Guo Q, Viles H. 2020. Evaluating the Condition of Sandstone Rock-Hewn Cave-Temple Façade Using in Situ Non-invasive Techniques. *Rock Mechanics and Rock Engineering* 53(6):2915-2920.

NAME: Qinglin Guo, Director, Conservation Institute of Dunhuang Academy

SIGNATURE: Qinglin Guo DATE: September 22, 2020

As a co-author of the following publication (published and/or submitted) I confirm that the first author Yinghong Wang has made a substantive contribution, which includes conceptualisation of the research project, data collection, data analysis, writing and revising the manuscript.

Wang Y, Yang S, Yu Z, Guo Q, Viles H. 2020. Evaluation of the impact of salts on the deterioration of a sandstone rock-hewn cave-temple in NW china through the combination of in situ salt extraction and salt behaviour modelling. *In the proceeding of the 14th International Congress on the Deterioration and Conservation of Stone (*pp.355-360), Göttingen, Germany.

NAME: Qinglin Guo, Director, Conservation Institute of Dunhuang Academy

SIGNATURE: Qinglin Guo DATE: September 22, 2020

As a co-author of the following publication (published and/or submitted) I confirm that the first author Yinghong Wang has made a substantive contribution, which includes conceptualisation of the research project, data collection, data analysis, writing and revising the manuscript.

Wang Y, Viles H, Desarnaud J, Yang S, Guo Q. 2020. Laboratory simulation of salt weathering under moderate ageing conditions: implications for the deterioration of sandstone heritage in the temperate climates. *Earth Surface Processes and Landforms*, under review

NAME: Qinglin Guo, Director, Conservation Institute of Dunhuang Academy

SIGNATURE: Qinglin Guo DATE: September 22, 2020

As a co-author of the following publication (published and/or submitted) I confirm that the first author Yinghong Wang has made a substantive contribution, which includes conceptualisation of the research project, data collection, data analysis, writing and revising the manuscript.

Wang Y, Viles H, Desarnaud J, Yang S, Guo Q. 2020. Laboratory simulation of salt weathering under moderate ageing conditions: implications for the deterioration of sandstone heritage in the temperate climates. *Earth Surface Processes and Landforms*, under review.

NAME: Julie Desarnaud, (Please fill in your position and company here)

Post doc manager; Royal Institute for Cultural heritage (KIK-IRPA)

SIGNATURE: DATE: 21/09/2020.

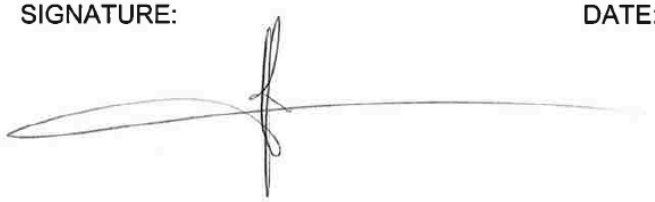

As a co-author of the following publication (published and/or submitted) I confirm that the first author Yinghong Wang has made a substantive contribution, which includes conceptualisation of the research project, data collection, data analysis, writing and revising the manuscript.

Wang Y, Pei Q, Yang S, Guo Q, Viles H. 2020. Evaluating the Condition of Sandstone Rock-Hewn Cave-Temple Façade Using in Situ Non-invasive Techniques. *Rock Mechanics and Rock Engineering* 53(6):2915-2920.

NAME: Qiangqiang Pei, Professor, Conservation Institute, Dunhuang Academy

SIGNATURE: Qiangqiang Pei DATE: October 28 2020.

As a co-author of the following publications (published and/or submitted) I confirm that the first author Yinghong Wang has made a substantive contribution to each of the publications, which includes conceptualisation of the research project, data collection, data analysis, writing and revising the manuscript.

Wang, Y., Yang, S., Yu, Z., Guo, Q., Viles, H., 2020. 'Evaluation of the impact of salts on the deterioration of a sandstone rock-hewn cave-temple in NW china through the combination of in situ salt extraction and salt behaviour modelling', *Proceeding of the 14th International Congress on the Deterioration and Conservation of Stone*, Göttingen, Germany. pp.355-360.

NAME: Zongren Yu, (associate director, Conservation Institute of Dunhuang Academy)

SIGNATURE: Zongren Yu DATE: 27/10/2020